Reviews in Mineralogy & Geochemistry
Vol. 81 pp. 239-304, 2015

Distribution and Processing of Highly Siderophile Elements in Cratonic Mantle Lithosphere

Sonja Aulbach

Facheinheit Mineralogie
Institut für Geowissenschaften
Johann Wolfgang Goethe-Universität Frankfurt am Main
Altenhöferallee 1
Frankfurt am Main
Germany

s.aulbach@em.uni-frankfurt.de

James E. Mungall

Department of Earth Sciences
University of Toronto
22 Russell St
Toronto, ON, M5S 3B1
Canada

mungall@es.utoronto.ca

D. Graham Pearson

Department of Earth and Atmospheric Sciences
University of Alberta
Edmonton AB, T6G 2R3
Canada

gdpearso@ualberta.ca

INTRODUCTION

Cratonic lithospheric mantle is composed of predominantly refractory materials that formed at higher mantle potential temperatures (T_P) than recorded in non-cratonic peridotites. It also shows stronger depletion and fractionation of Pd and Pt from Ru, Os and Ir than oceanic, supra-subduction zone or off-cratonic lithospheric mantle, as well as some of the lowest Se and Te contents. The varied response of the highly siderophile elements (HSE: Os, Ir, Ru, Rh, Pt, Pd, Re, Au), and their embedded radioactive decay systems, to changes in oxygen fugacity (f_{O_2}), sulfur fugacity (f_{S_2}) and pressure (P)—in particular through the impact of these parameters on the stability of the main HSE-bearing sulfide and alloy phases makes them potentially powerful tracers of their melting environment. Therefore, investigation of the HSE systematics of cratonic mantle peridotites, in combination with information from Re–Os isotopes on time-integrated enrichment or depletion, can help us to understand processes leading to mantle differentiation and continental lithosphere formation in the Archean, which are controversial subjects despite decades of research.

The longevity of the cratonic lithosphere implies that there was ample opportunity for secondary overprint, obscuring our view of earlier processes. For example, destabilization of platinum-group element (PGE: Os, Ir, Ru, Rh, Pt, Pd) alloy leading to depletions in the

1529-6466/16/0081-0005$10.00 http://dx.doi.org/10.2138/rmg.2016.81.5

compatible PGE, and perhaps Pt, in some cratonic mantle samples may occur in an oxidizing mantle wedge or through interaction with oxidizing small-volume, volatile-rich melts that typically invade cratonic roots. Such melts may eventually deposit S, Pd, Pt and Re and also capture remaining PGE alloys, consistent with the anomalous S-rich character of many kimberlite-borne xenoliths. Their basalt-borne counterparts show additional late effects of subaerial degassing that can deplete volatile elements (S, Re, Os). Basaltic melts can also scavenge PGE alloys at depth, while still sulfide-undersaturated. Such melts, may, on ascent, add sulfides when they become sulfur-saturated and, during the process, refertilize the mantle and modify major-element and modal compositions. The investigation of minor lithologies in the cratonic lithosphere, such as eclogites and pyroxenites, which are expressions of tectonothermal events ranging from subduction to melt infiltration, can enhance our understanding of the effects of these processes on HSE redistribution.

Thus, three major topics will be discussed, using HSE systematics in cratonic mantle samples: (1) How did the HSE behave during the (in part) extreme degrees of partial melt extraction experienced by cratonic lithospheric mantle; (2) What were the effects of the secular metasomatic overprint of the cratonic mantle; (3) What was the composition of the Archean convecting mantle, for which cratonic mantle samples may afford better insight than modern samples, provided, of course, that we have an accurate grasp of how HSE are redistributed during partial melting and metasomatism. Models based on experiments done under controlled pressure (P), temperature (T), f_{O_2} and f_{S_2} conditions can help place the data in context and to distinguish between melt- and metasomatism-related processes. Disentangling the various primary and secondary effects is only possible when HSE are studied in combination with lithophile elements, with due attention to petrography and mineralogy. This adds many layers of complexity, but ultimately allows a more complete understanding of the variegated processes that have shaped the cratonic lithosphere through time.

In this review, we commence by discussing the peculiarities and complexities of continental lithospheric mantle origin, evolution and current state. We then introduce the database used in this contribution, followed by a brief review of the mineral hosts of HSE in peridotite and of the diverse approaches to isolate the HSE for measurement. We examine the behavior of the HSE during the formation of cratonic lithospheric mantle under non-uniformitarian conditions, where the application of the Re–Os isotope system has afforded particularly useful information on the timing of initial melt depletion and the stabilization of cratonic roots. We then turn to the effects of mantle metasomatism, both during intra-plate and craton-margin processes (see also Gannoun et al. 2016, this volume), on HSE systematics in cratonic mantle. We also discuss the data in the context of melt extraction modelling that shed light on the primary versus secondary HSE signatures in cratonic mantle rocks. Finally, we evaluate the possibility that the HSE in cratonic mantle retain a memory of core formation and subsequent accretionary processes.

THE CRATONIC MANTLE SAMPLE: PECULIARITIES, OPPORTUNITIES AND PITFALLS

Cratons are usually taken to represent the ancient (≥ 2.5 Ga) cores of stable continental regions that are commonly, but not always, underlain by broadly coeval and possibly cogenetic lithospheric roots, and where voluminous tectonomagmatic activity is confined to the margin (Bleeker 2003). Their areal extent has been mostly defined based on outcropping Archean basement (Fig. 1). Some cratonic entities were themselves formed from continental nuclei that were amalgamated and "stabilized" predominantly during the NeoArchean, and welded together to form larger landmasses (composite cratons) during Proterozoic collisions (Bleeker 2003). The resultant mobile belts provided protection against later tectonothermal overprint and helped ensure craton longevity (Lenardic et al. 2000).

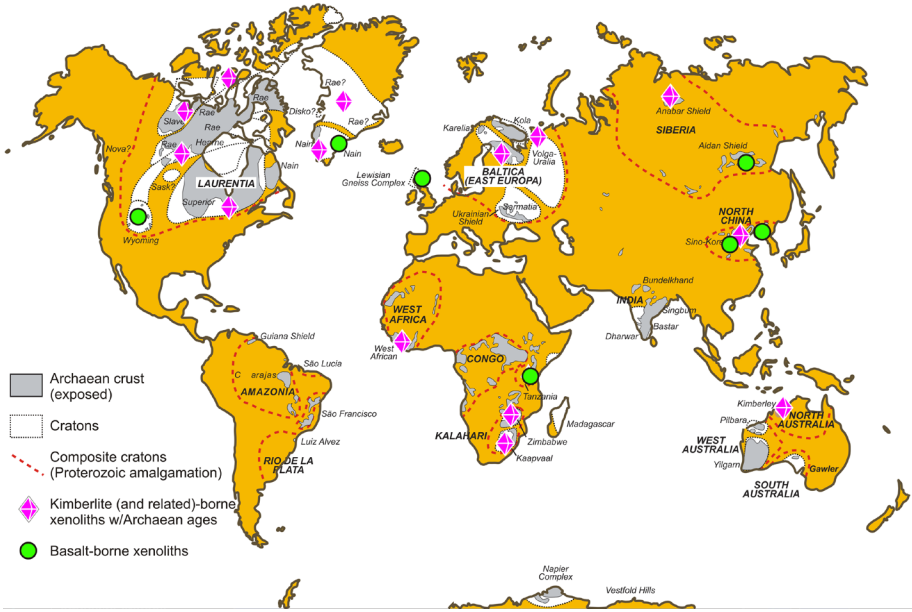

Figure 1. Global distribution of cratonic regions of crust ≥2.5 Ga old, modified after Bleeker (2003) and Pearson and Wittig (2008). Grey = outcropping Archean crustal rocks, white with dotted border = other definable fragments of composite cratons. Question marks indicate uncertain boundaries. Dashed lines encompass Archean cratonic bocks amalgamated during the Proterozoic. Diamonds show examples of localities where kimberlites and related rocks carried mantle xenoliths with Archean ages to the surface, circles show localities where basalt-borne xenoliths sample thinned cratonic lithosphere. For a more extensive list of mantle xenolith localities see Nixon (1987).

Cratonic lithosphere generally extends to a maximum of 200–250 km depth (Artemieva and Mooney 2001; Priestley and McKenzie 2006). The mechanism(s) by which this depth was attained—in collisional settings or during plume tectonics or both—remains a controversial issue (Arndt et al. 2002, 2009; Griffin et al. 2003a, 2009; Lee 2006; Aulbach et al. 2007; Pearson and Wittig 2008, 2014; Lee et al. 2011; Aulbach 2012; Herzberg and Rudnick 2012). Peculiar properties of cratonic lithosphere include not only its greater thickness compared to average younger lithosphere, but also its higher average degree of melt depletion, viscosity and seismic velocity and cooler geothermal gradients (e.g., O'Reilly et al. 2001) that can be linked to the secular evolution of T_P. While the details of this evolution are debated, higher T_P in the Archean is generally advocated (e.g., Korenaga 2008; Davies 2009). The exceptional depletion of incompatible FeO and H_2O that were possible at higher Archean T_P and the resultant increased buoyancy and viscosity are thought to be pivotal in the long-term stability of cratonic lithosphere. The relative importance of these two physical parameters for craton stability has been modeled by various authors and remains debated (Jordan 1988; Abbott et al. 1997; Lenardic et al. 2003; Afonso and Schutt 2012; Wang et al. 2014), but it is clear that metasomatic modification appears to be a pre-requisite for weakening and generating negative buoyancy in the craton root (Wang et al. 2015) that can lead to its destruction in some instances.

The thick and cool cratonic lithospheric lid exceeds the depth where dry fertile convecting mantle crosses its solidus and reaches not much shallower depths than that of mantle with moderate volatile contents (e.g., Dasgupta et al. 2013), preventing large degrees of partial melting in upwelling mantle at current ambient T_P (1310–1460 °C; e.g., Dalton et al. 2014). Consequently, intact cratonic mantle is typically sampled by deep-seated (>250 km)

low-volume carbonate-rich melts, such as kimberlites (e.g., Nixon 1987; Tappe et al. 2006). These melts entrain fragments (xenoliths) or their disaggregation products (xenocrysts including diamond and its inclusions) from the conduit wall consisting predominantly of variably depleted and metasomatized peridotite, the petrology of which reflects the sum of processes that occurred during cratonic lithosphere formation and evolution. Cratonic mantle that has lost a portion of its deep root due to erosion or delamination is occasionally sampled by higher-volume basaltic melts, as is the case for the North China craton (Gao et al. 2002) and the Tanzanian craton (Burton et al. 2000).

Besides peridotites, pyroxenites and eclogites form a generally subordinate, though in some cases locally dominant constituent of mantle xenolith and diamond inclusion suites (Schulze 1989). In particular cratonic mantle eclogites having elemental and isotopic compositions consistent with a crustal origin document the emplacement of crustal components into the cratonic lithosphere (Macgregor and Manton 1986; Jacob 2004). The presence of such lithologies has been argued to attest to the relevance of accretionary processes in the construction or evolution of cratons (e.g., Helmstaedt and Schulze 1989; Pearson et al. 1995a, 1998; Shirey et al. 2001; Shirey and Richardson 2011). Regardless of interpretation, it is important to bear in mind that magma-entrained material depicts the state of the cratonic lithosphere not at the present day, but at the time of magma emplacement, which encompasses Cenozoic to rare Proterozoic and Neo-Archean kimberlites, lamproites and ultramafic lamprophyres (summarized in Gurney et al. 2010).

Several potential pitfalls are associated with the accidental mode of lithospheric mantle sampling by xenoliths, which have to be taken into account in an evaluation of constraints that can be obtained from these samples: (1) It is likely that the mantle material entrained in kimberlites is not representative of cratonic lithospheric mantle as a whole because kimberlites are thought to erupt through reactivated lithospheric weak zones that were altered by the passage of fluids and melts (e.g., Poudjom-Djomani et al. 2005; Afonso et al. 2008) and because the entire lithosphere column is rarely equally sampled by the rising kimberlite magma (e.g., Finnerty and Boyd 1987; Lee et al. 2011). (2) Kimberlite infiltration into entrained xenoliths is ubiquitous (e.g., Schmidberger and Francis 2001; Jacob 2004) and its effects range from the deposition of host magma-derived material at grain boundaries and in grain fractures, to the formation of melt pools (e.g., Barth et al. 2001; Dawson 2002). Chemical data from the measurement of whole rocks are therefore mixtures of the pre-entrainment compositions and fractionated kimberlite magma (e.g., Pearson and Wittig 2014). (3) Although occasionally very large xenoliths are entrained (>25 cm; e.g., Bell et al. 2005), the sample size is limited by the loading capacity of the host magma and dike width (e.g., Sparks et al. 2006), and by access to often small specimens (≤3 cm) that have passed the processing stage from modern-day diamond exploration and mining companies. This makes accurate estimates of representative bulk composition and relationships between different lithologies difficult, and the definition of structural relationships impossible. On the other hand, xenoliths are brought to the surface quickly, in a matter of hours or days (e.g., Canil and Fedortchouk 1999; Sparks et al. 2006) and, as such, there are no complications from slow exhumation, retrogression and re-equilibration that plague slowly exhumed orogenic mantle slices (e.g., Ernst and Liou 2008).

The above illustrates that the longevity of cratons simultaneously offers great benefits and drawbacks. Cratons provide the only rock archive of the Earth's earliest lithosphere and its interaction with the emerging hydrosphere, atmosphere and biosphere, and of mantle dynamics that eventually resulted in the face of the planet we inhabit today (e.g., Santosh 2013). This archive may hold clues to the earliest planetary differentiation processes, such as core formation, mixing of late accreted material into the mantle and magmatic differentiation, which are particularly sensitively monitored by HSE (e.g., Shirey and Walker 1998; Lorand et al. 2013; Day et al. 2016, this volume). Furthermore, cratons are unique hosts to specific

deposits, such as world-class magmatic PGE–Ni ores and gem-quality diamonds (de Wit and Thiart 2005; Gurney et al. 2010). Because cratonic mantle is often sampled during multiple magma emplacement episodes at different times, as is the case for the Kaapvaal, North China, Siberia, Wyoming and Slave cratons (Smith 1983; Menzies et al. 1993; Mitchell 1995; Heaman et al. 2004; Pernet-Fisher et al. 2015; Sarkar et al. 2015), several "snapshots" of the state of the mantle lithosphere at different times are sometimes available. This temporally punctuated view can be augmented by information from inclusions in diamond (typically 10–300 μm), which are shielded from post-entrapment chemical modification by their inert and often ancient hosts (reviewed in Gurney et al. 2010). On the other hand, this antiquity ensures that over the course of eons, cratonic roots were multiply affected by passing melts and fluids (Fig. 2), and hence unmodified depleted material may be all but non-existent (e.g., Pearson and Wittig 2014). Cooling and subsolidus re-equilibration subsequent to craton formation leads to element redistribution and modal changes, further adding to the complexity of present-day compositions (Cox et al. 1987; Canil 1991).

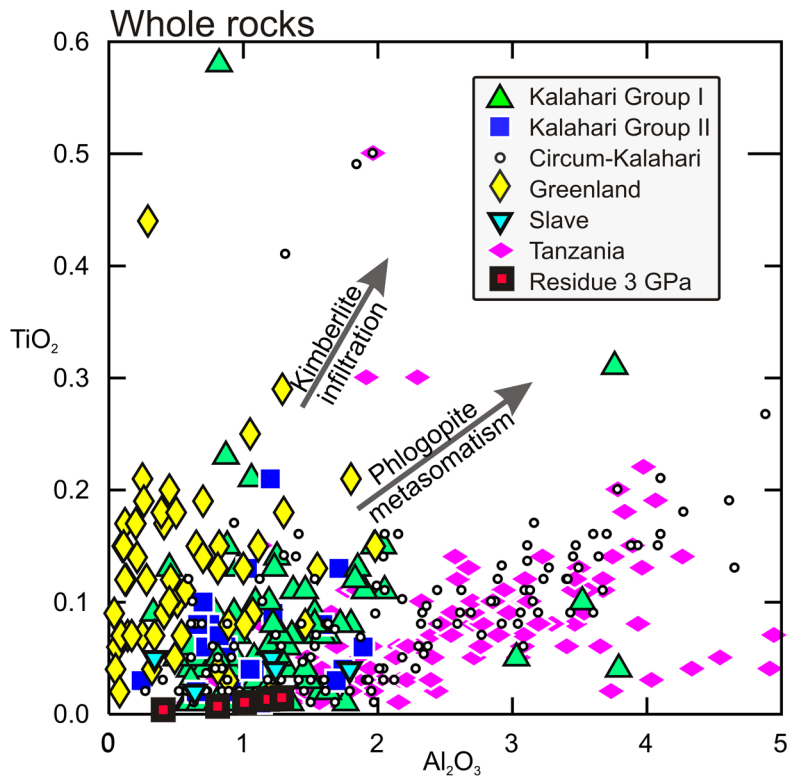

Figure 2. Whole-rock Al_2O_3 vs. TiO_2 for some kimberlite-borne (Kalahari, Circum-Kalahari, Slave, Greenland) and basalt-borne (Tanzania) mantle xenolith suites used in this study (references in caption to Figure 3). Shown for comparison are the compositions of model equilibrium residues from partial melting of fertile peridotite at 3 GPa, for melt fractions of 0.10, 0.12, 0.15, 0.19, and 0.31 (from Herzberg 2004). Note that at the scale depicted, different choices of pressure or melting model will not significantly change the position of the model data-points. Qualitative trends for phlogopite-accompanied metasomatism and host rock infiltration, which may explain some of the elevated and scattered contents in measured whole rocks, are also shown.

Despite the caveats outlined above, cratonic mantle xenolith and xenocryst samples are an invaluable resource with which we can study the formation and evolution of cratonic mantle roots, and interrogate the early state of the convecting mantle. A significant contribution to our understanding of early mantle geodynamics, the nascence of continents and the subsequent evolution of the lithospheric mantle has come from the investigation of the HSE systematics of cratonic mantle-derived rocks (Walker et al. 1989; Reisberg et al. 1991; Carlson and Irving 1994; Pearson et al. 1995b,c, 2004; Pearson 1999; Carlson et al. 2008; Shirey and Richardson 2011; Maier et al. 2012). In particular, the Re–Os isotope system has become the tool of choice to date lithosphere stabilization, to identify the presence of cratonic mantle and to investigate the relationship between cratonic mantle and overlying crust (e.g., Pearson et al. 2007; Griffin et al. 2014; Pearson and Wittig 2014), using peridotite and eclogite whole rocks, their mineral separates, single sub-mm-sized sulfide (e.g., Griffin et al. 2002, 2004; Aulbach et al. 2004; Luguet et al. 2008), and even sulfide inclusions in diamond (e.g., Pearson et al. 1998, 1999; Richardson et al. 2001, 2004; Aulbach et al. 2009a, 2011).

DATABASE

This contribution builds on published data for mantle xenoliths from ten cratons (i.e., ≥ 2.5 Ga: Kalahari comprising Kaapvaal and Zimbabwe, Tanzania, Karelia, Siberia, Slave, Rae, North American with Greeland, Wyoming, and North China; Fig. 1), mostly entrained in kimberlites and related rocks of various ages. The data cover not only the "classic" HSE composed of PGE plus Re and Au, but also the chalcogens, S, Se, and Te, which partition into sulfides and tellurides (Hattori et al. 2002; Lorand and Luguet 2016, this volume). Selenium and Te display highly siderophile element character at conditions relevant to core formation (Rose-Weston et al. 2009) and the database on cratonic peridotites is expanding through high-precision analyses obtained by isotope dilution techniques (reviewed in Lorand and Luguet 2016, this volume). Lithologically, the featured samples encompass peridotites ranging from chemically depleted to enriched varieties, and minor lithologies where only limited data are available. In addition, there is a sizable database for Re and Os concentrations in sulfides, where grains occurring in peridotite and eclogite xenoliths are distinguished from those included in diamonds. With regard to sample digestion and analytical strategies, the data include whole rocks and mineral separates, as well as single grains of amenable minerals, as further reviewed below.

Within the cratonic database, we distinguish a sub-group of "disturbed" cratonic root samples, where the xenoliths are not hosted in kimberlites, but are erupted by less deeply derived magmas such as lamprophyres and alkali basalts. Such samples are typified by certain localities in the Wyoming, Tanzanian and North China cratons where the xenoliths have been erupted following variably severe thermo-tectonic processes that have led to thinning and removal of a portion of lithospheric mantle roots. We further consider regions where cratonic mantle was identified beneath Proterozoic crust (e.g., Western Australia: Luguet et al. 2009; Western Greenland: Wittig et al. 2010a) and circum-cratonic Paleoproterozoic areas, some of which are underlain by mantle showing geochemical, microstructural, thermal or geophysical affinities with their Archean neigbors (Table 1), such as the Rehoboth terrane in Namibia (west of the Kaapvaal craton; Luchs et al. 2013, and references therein). To illustrate the secular evolution of the lithospheric mantle and the effects of various processes on PGE systematics, we compare data from cratonic peridotites to those from younger circum- and off-cratonic areas, typically sampled by basalts, to orogenic peridotites, which have been affected by melt percolation and strong refertilization processes, and to Phanerozoic supra-subduction zone (SSZ) peridotites and ophiolites (see also Luguet and Reisberg 2016, this volume and Becker and Dale 2016, this volume), which have interacted with slab-related melts and fluids, the latter also affected by PGE mineralization, for example associated with chromitites.

Table 1. Statistical results for HSE concentrations and ratios in peridotites, eclogites and sulfides from various tectonic settings.

	Crat-k	Crat-b	Circ-crat	Off-crat	Orogenic	SSZ	Ophiolite	Crat-k	Crat-b	Circ-crat	Off-crat	Orogenic	SSZ	Ophiolite
				Ir ppb							Pt/Ir			
Points	258	150	40	111	109	26	42	254	108	38	105	102	26	23
Minimum	0.1	0.1	0.4	0.1	0.2	0.4	1.5	0	0	0.1	0.3	0.5	0.6	0.4
Maximum	9.9	7.9	9.2	9.1	29.1	6.8	12	9.7	6.5	2.5	26.5	7.8	44.8	2
Mean	3.3	2.4	3.1	2.6	3.6	3.1	3.7	0.6	0.8	0.8	1.1	1.2	4.1	0.9
Median	3.1	2.4	2.9	2.5	3.5	3.4	3.5	0.4	0.7	0.6	0.8	0.9	1.3	0.9
Std Deviation	1.7	1.3	1.6	1.2	2.7	1.6	1.5	0.9	0.7	0.6	2.5	1.1	9	0.3
				Os ppb							Pd/Ir			
Points	428	344	107	311	228	99	116	240	109	36	99	109	26	23
Minimum	0	0	0.3	0.1	0.1	0	0.4	0	0	0	0	0	0	0.3
Maximum	18.4	20.4	10.4	14.4	56.2	8.2	41.7	6.4	5	1.1	1.8	38.2	11.5	1
Mean	3.4	2.3	3.4	2.1	4	2.1	4.3	0.4	0.5	0.3	0.5	1.3	1.4	0.6
Median	3.1	2.2	3.3	1.9	3.8	1.8	3.9	0.2	0.3	0.2	0.5	0.8	0.7	0.6
Std Deviation	2.2	1.8	1.8	1.4	3.9	1.7	3.8	0.8	0.6	0.2	0.3	3.8	2.3	0.2
				Pd ppb							Os/Ir			
Points	241	147	36	99	110	27	42	193	107	30	87	100	25	23
Minimum	0	0	0.3	0	0.4	0.1	1.5	0	0.1	0.2	0.1	0.2	0.3	0.5
Maximum	10.8	12	6.1	8.4	84.5	96	27	3	2.2	1.5	2.3	3.3	7.6	1.2
Mean	1.8	2.5	1.4	2.7	6.4	8.3	5.6	1	0.7	0.8	0.7	1	1.8	1
Median	1.2	1.5	1.2	2.2	5.7	3	4.6	0.9	0.8	0.9	0.7	1	1	1
Std Deviation	2	2.5	1.1	1.8	8.4	18	4	0.3	0.3	0.3	0.3	0.3	2	0.1
				Pt ppb							Pt/Pd			
Points	255	146	38	104	103	27	42	240	105	36	97	103	27	23
Minimum	0	0	0.5	0.2	3.4	2	1	0.1	0.2	0.5	0.4	0.2	0.3	1
Maximum	18.3	19.2	13.5	13.5	39	126.6	34	230.7	30	14.7	35.6	14.6	107.5	3.3
Mean	3.4	4.6	4.5	4.8	7.3	16.2	7.6	7.8	3	3.9	2.6	1.9	7.8	1.5
Median	2.8	3.8	4.6	4.2	6.9	9.1	6.9	2	2.1	2.8	1.7	1.2	1.9	1.4
Std Deviation	2.8	3.6	2.7	2.5	3.6	24.4	5	22.8	3.6	3.2	3.8	2.4	20.7	0.5

Notes: Crat-k kimberlite-borne, Crat-b basalt-borne, Circ-crat circum-cratonic Off-crat off-craton, SSZ supra-subduction zone, E- eclogitic, P- peridotitic, WR whole rocks, Diamond-Inc. inclusions in diamond; for references see caption to Figure 2.

Table 1 (cont'd). Statistical results for HSE concentrations and ratios in peridotites, eclogites and sulfides from various tectonic settings.

	Cratonic					Orogenic
	E-sulfides	**E-sulfides**	**P-sulfides**	**P-sulfides**	**Eclogites**	**Eclogites**
	Xenoliths	Diamond Inclusions	Xenoliths	Diamond Inclusions	Whole-rock	Whole-rock
	Os ppm	Os ppm	Os ppm	Os ppm	Os ppb	Os ppb
Points	62	82	280	54	73	35
Minimum	0.01	0.0018	0.3	0.022	0.026	0.002
Maximum	11.31	1.8	20000	3805	2.2	0.9
Mean	0.35	0.098	230	200	0.33	0.05
Median	0.04	0.034	17	42	0.3	0.011
Std Deviation	1.47	0.274	1263	590	0.35	0.15

The minimum, maximum, mean and median concentrations and ratios of some PGE in the various peridotite groups and in eclogites are given in Table 1, along with their standard deviation. In general, median concentrations will be presented as a more robust measure of central tendency, due to the often non-normal nature of the data and due to their robustness to the biasing affects of outliers, of which there are many (Fig. 3). Compared to orogenic peridotites (median Ir = 3.5 ng g^{-1}, Os = 3.8 ppb, Pt = 6.9 ppb, and Pd = 5.7 ppb), which represent the modern convecting upper mantle, kimberlite-borne xenoliths have low median concentrations of all PGE (Ir = 3.1 ppb, Os = 3.1 ppb, Pt = 2.8 ppb, and Pd = 1.2 ppb, respectively; Fig. 3 and Table 1). This is true also for circum-cratonic peridotites (Ir = 2.9 ppb, Os = 3.3 ppb, Pt = 4.6 ppb, Pd = 1.2 ppb). Basalt-borne cratonic xenoliths show even lower concentrations of the Ir-group PGE (Ru, Os, Ir: IPGE) (Medians: Ir = 2.4 ppb, Os = 2.2 ppb, Pt = 3.8 ppb, Pd = 1.5 ppb), similar to younger off-cratonic xenoliths, which are also basalt-borne (2.5 ppb, 1.9 ppb, 4.2 ppb, and 2.2 ppb). By comparison, supra-subduction zone peridotites have strikingly higher Pt abundances (Ir = 3.4 ppb, Os = 1.8 ppb, Pt = 9.1 ppb, Pd = 3.0 ppb). Ophiolites, the majority of which are subduction-related (Dilek and Furnes 2011), have concentrations similar to orogenic peridotites (Ir = 3.5 ppb, Os = 3.9 ppb, Pt = 6.9 ppb, Pd = 4.6 ppb). The processes leading to these observed differences in HSE systematics of peridotites of different ages and from different tectonic settings will be explored below.

As mentioned above, with the exception of Re and Os, few data are reported for minor lithologies occurring in cratonic lithosphere and for sulfides. As meta-basaltic or -gabbroic rocks, cratonic eclogites are characterized by a significantly lower median Os concentration (0.30 ppb, $n = 73$) compared to peridotite which is, however, significantly higher than that observed for orogenic eclogites (0.011 ppb, $n = 35$). Median S, Se, and Te contents in 27 eclogite xenoliths from Roberts Victor (Kaapvaal) are 260 ppm, 73 ppb, and 9 ppb, respectively (Gréau et al. 2013), compared with 360 ppm S, 115 ppb Se, and 0.8 ppb Te in cratonic peridotite xenoliths. Exotic lithologies, such as Mica–Amphibole–Rutile–Ilmenite–Diopside rocks (MARID) and Phlogopite–Ilmenite–Clinopyroxene (PIC) occur mainly in the Kaapvaal craton where they are associated with different types of kimberlite magmatism, as is true for the megacryst suite (Grégoire et al. 2002). The PGE systematics of six MARID samples were investigated by Maier et al. (2012), in addition to a few pyroxenites, wehrlites and megacrysts of metasomatic origin. MARID xenoliths have low HSE concentrations (average Ir = 0.3 ppb, Ru = 0.92 ppb, Pt = 2.0 ppb, Pd = 2.1 ppb, Os not available), which is true also for the megacrysts (average Os = 0.5 ppb, Ir = 0.1 ppb, Ru = 1.1 ppb, Pt = 1.0 ppb, Pd not available). The reason for the paucity of data for these minor metasomatic lithologies may be that most efforts of using Re–Os isotope systematics

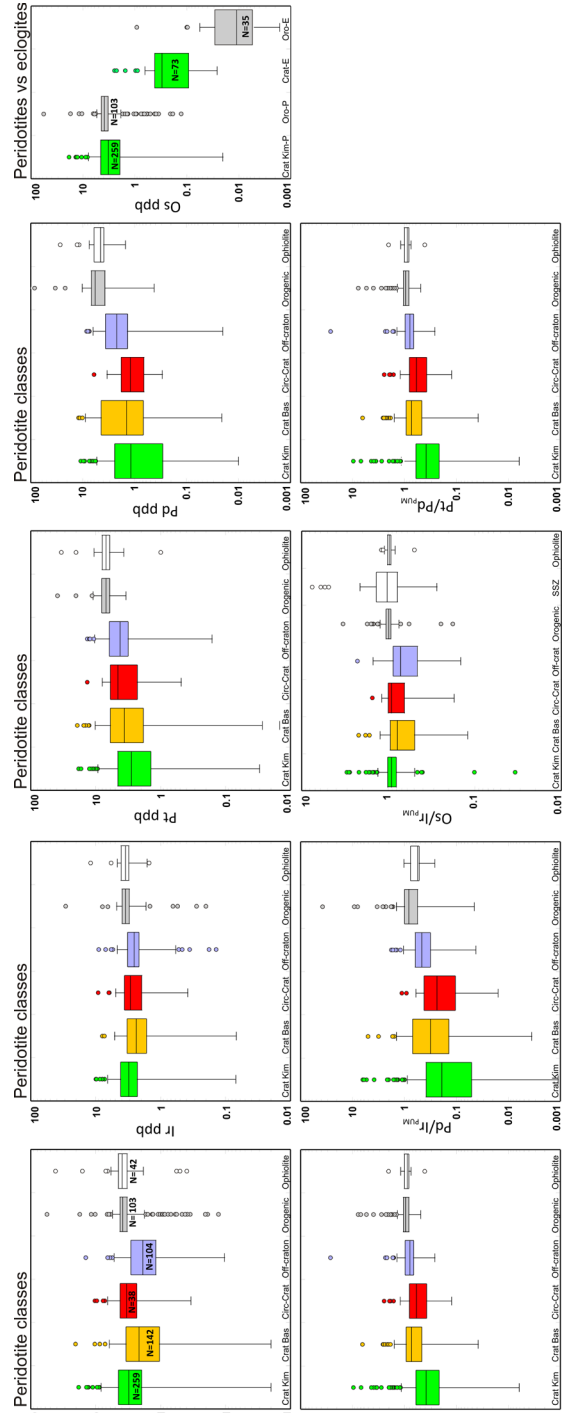

Figure 3. "Box-and-whiskers" plots for various peridotite and eclogite groups for some whole-rock PGE concentrations and ratios given in Table 1 (Peridotites: Walker et al. 1989; Reisberg et al. 1991, 2005; Carlson and Irving 1994; Reisberg and Lorand 1995; Snow and Reisberg 1995; Pearson et al. 1995b,c, 2002, 2004; Pearson et al. unpubl.; Roy-Barman et al. 1996; Brandon et al. 1996; McBride et al. 1996; Meisel et al. 1996, 2001; Melcher and Meisel 2004; Garuti et al. 1997; Handler et al. 1997, 1999, 2003; Rehkämper et al. 1997, 1999; Burnham et al. 1998; Parkinson et al. 1998; Burton et al. 1999; Widom et al. 1999, 2003; Carlson et al. 1999a,b; Chesley et al. 1999; McInnes et al. 1999; Menzies et al. 1999; Lee et al. 2000, 2001; Peslier et al. 2000a,b; Schmidt et al. 2000, 2003; Hanghøj et al. 2001, 2010; Irvine et al. 2001, 2003; Irvine unpubl.; Lorand and Alard 2001; Lorand et al. 2003b, 2008, 2010; Saal et al. 2001; Gao et al. 2002; Kepezhinskas et al. 2002; Lee 2002; N.J. Pearson et al. 2002; Luguet et al. 2003, 2004, 2007; Sen et al. 2003; Wu et al. 2003, 2006; Büchl et al. 2002, 2004; Carlson and Moore 2004; Griffin et al. 2004; Yongbin et al. 2004; Becker et al. 2006; Harvey et al. 2006, 2010; Ionov et al. 2006; Lee and Walker 2006; Peltonen and Brügmann 2006; Westerlund et al. 2006; Bizimis et al. 2007; Powell and O'Reilly 2007; HF Zhang et al. 2008, 2009; Batanova et al. 2008; Ackerman et al. 2009; Chu et al. 2009; O'Driscoll et al. 2009; Schulte et al. 2009; Smith et al. 2009; Dijkstra et al. 2010; Janney et al. 2010; Wittig et al. 2010a,b; Fischer-Gödde et al. 2011; Ishikawa et al. 2011; Liu et al. 2011; Maier et al. 2012; Sun et al. 2012; Wang et al. 2013; Wang and Becker 2013; Armytage et al. 2014; Aulbach et al. 2014; König et al. 2014; Pernet-Fisher et al. 2015; Eclogites: Pearson et al. 1995a; Barth et al. 2002; Menzies et al. 2003; Aulbach et al. 2009b). The median lies in a box that comprises 50% of the data (i.e., the inter-quartile range IQR). The whiskers on each side reach to 1.5 times the IQR outside of the edge of the box. Note that the group of kimberlite-borne xenoliths encompasses alkaline ultramafic rocks (e.g., ultramafic lamprophyres—Western Greenland), which are more similar to Group I kimberlites than to basalts. Eclogite xenoliths are all kimberlite-borne, no bulk-rock PGE data other than Os are available for this rock type.

in combination with HSE abundances are directed towards obtaining lithosphere stabilization ages, for which the least visibly metasomatized samples are targeted. Further analyses of both bulk rock and in-situ mineral HSE systematics in these rocks would be a welcome addition to furthering our understanding of the metasomatic evolution of the cratonic mantle.

Sulfides, which concentrate the HSE, have higher concentrations than their corresponding whole rocks (Table 1), which is true for sulfides in xenoliths (median peridotitic sulfide Os = 17000 ppb, $n = 280$; eclogitic sulfide Os = 40 ppb, $n = 62$), and for corresponding sulfide populations occurring as inclusions in diamond (median peridotitic sulfide Os = 42000 ppb, $n = 54$; eclogitic sulfide Os = 34 ppb, $n = 82$). Few additional data are available for these minerals, which have been targeted mostly for single-mineral Re–Os dating (e.g., Pearson et al. 1998, 1999; Richardson et al. 2001, 2004). Nickel-rich peridotitic monosulfides tend to exsolve to a low-temperature assemblage upon cooling, accompanied by fractionation of HSE between the low-temperature minerals (pyrrhotite, pendlandite, chalcopyrite), which complicates acquisition of representative trace-element concentrations (Richardson et al. 2001; Dale et al. 2009; van Acken et al. 2010). Nickel-poor sulfides in eclogitic rocks are little affected by exsolutions; sulfide inclusions in eclogitic diamonds ($n = 41$) have median concentrations of 41 ppb Ir, 140 ppb Ru, 315 ppb Pt and 340 ppb Pd (Aulbach et al. 2012).

MINERALOGY AND HSE HOSTS IN CRATONIC MANTLE PERIDOTITES

Depending on degree of depletion and metasomatic re-enrichment, mantle peridotites are composed of olivine, orthopyroxene, clinopyroxene, an Al-phase (plagioclase, spinel or garnet, with increasing pressure) plus accessory sulfides (base metal sulfides, BMS: Fe–Ni–Cu sulfides) or trace platinum-group minerals (PGM) (Lorand and Luguet, 2016 this volume). Here we define PGM as any phase in which PGE are major or stoichiometric components; these can be sulfides (e.g., the erlichmanite–laurite series; Bockrath et al. 2004a), arsenides, sulfarsenides, bismutho-tellurides (Lorand et al. 2010), alloys or intermetallic compounds, depending on sulfur fugacity and temperature (Fonseca et al. 2012; also see O'Driscoll and González-Jiménez 2016, this volume). Typically metasomatic minerals, such as amphibole, phlogopite, ilmenite and diamond are sometimes present, but the primary minerals can be also metasomatically added (and removed) and are then sometimes difficult to distinguish from the original assemblage (O'Reilly and Griffin 2013; Pearson and Wittig 2014).

Olivine and pyroxene separates have yielded variably elevated HSE contents (Pearson et al. 1995c; Burton et al. 2000, 2002; Luguet et al. 2009; Wittig et al. 2010a; Aulbach et al. 2014; Smit et al. 2014a; Pernet-Fisher et al. 2015). With the exception of Re, which has been suggested to be compatible in silicate minerals including garnet, especially under oxidizing conditions after sulfide break-down (Righter and Hauri 1998; Burton et al. 2002; Mallmann and O'Neill 2007; Righter et al. 2008), such enrichments may in part be due to inclusions of PGE alloys and/or sulfides that were trapped during formation or recrystallization (e.g., Walker et al. 1991; Ballhaus and Sylvester 2000; Mungall and Brenan 2014). This is also evident from the considerably higher Os concentrations in visibly inclusion-bearing mineral separates compared to inclusions-free separates from the same sample (Burton et al. 2000). Nonetheless, the compatibility of the IPGE and Rh in olivine has also been inferred from inter-element relationships in komatiites (e.g., Brügmann et al. 1987) and confirmed in several experimental studies where care was taken to avoid inclusions of PGE-rich trace phases during the analysis of the run-products (Brenan et al. 2003, 2005).

Pearson et al. (1995c) found that olivine in a dunite from Udachnaya (Siberian craton) contains ~ 400 ppt Os and less radiogenic $^{187}Os/^{188}Os$ than the whole rock. In contrast, a fertile lherzolite (whole rock) from the same locality yielded only 2 ppt Os. Work on mantle xenoliths

from the Tanzanian craton has shown that olivine, inclusion-bearing or inclusion-free, has higher $^{187}Os/^{188}Os$ than sulfide or the bulk rock, which is thought to be dominated by accessory HSE hosts (Burton et al. 2000). In xenoliths from western Greenland, lower $^{187}Os/^{188}Os$, lower IPGE and Pt concentrations but similar chondrite-normalized HSE patterns have been determined in olivine separates compared with whole rocks (Wittig et al. 2010a). Olivine separated from peridotite xenoliths from the Superior craton have HSE patterns similar to sulfide, but at lower concentrations, due to a dilution effect. Such systematics are consistent with a signature of sulfide inclusions diluted by olivine, whereas other olivine separates from different peridotites have patterns mimicking those of highly depleted, S-poor whole-rock peridotites, suggestive of PGEs being hosted within olivine by alloy inclusions (Smit et al. 2014a).

Chromite is a typical spinel present within the deep cratonic lithosphere and has been discussed as a potential host for PGE based on the observation that chromite-rich cumulates in basalts and komatiites, chromite xenocrysts and chromite in some cratonic mantle peridotites have elevated contents of the IPGE (e.g., Mitchell and Keays 1981; Barnes and Picard 1993; Hart and Ravizza 1996; Chesley et al. 1999; Graham et al. 1999, 2004; Walker et al. 2002; Luguet et al. 2009). Both the compatibility of the IPGE in the chromite crystal lattice (Capobianco and Drake 1990; Righter et al. 2004; Brenan et al. 2012) and the presence of minute PGE alloy inclusions (Ballhaus and Sylvester 2000; Sattari et al. 2002; Finnigan et al. 2008; Godel et al. 2010) have been discussed as reasons for elevated PGE in chromite. Under reducing conditions that may be applicable to the cratonic mantle, Ru most strongly partitions into chromite, whereas Ir and Rh are mildly incompatible to compatible and Re, Au, Pt, and Pd are strongly incompatible (Righter et al. 2004; Brenan et al. 2012; Park et al. 2013). Several chromite generations in peridotite xenoliths from the Argyle lamproites (just off the Kimberley craton margin, Western Australia) were identified, separated and measured for Re–Os isotopes by Luguet et al (2009). These authors found that a primary chromite generation preserved extremely unradiogenic $^{187}Os/^{188}Os$ giving Archean ages, but likely experienced (late) Re gain, whereas a late, symplectite-derived generation (from the break-down of garnet) gave Mesoproterozoic T_{RD} similar to the age of the host lamproite (Luguet et al. 2009).

Given the siderophile and chalcophile nature of the HSE (Peach et al. 1990; Fleet et al. 1999; Bockrath et al. 2004b), their concentration in PGM (Luguet et al. 2007; Lorand et al. 2010, 2016, this volume; O'Driscoll and Gonzáles Jiménez 2016, this volume) and in BMS is orders of magnitude higher than in whole rocks dominated by silicates (e.g., Pearson et al. 1998, 1999; Lorand et al. 2008, 2010, 2013). This has also been demonstrated experimentally (Brenan et al. 2016, this volume). Consequently, these minerals dominate the bulk-rock budget of mantle rocks, despite having $\ll 1\%$ modal abundances in primitive or depleted mantle, and they are amenable to being analysed by single-grain techniques. The presence of accessory sulfide or alloy in cratonic mantle peridotites has long been postulated based on direct observations on mantle samples (e.g., Frick 1973), the observation of low PGE contents of constituent silicates (Mitchell and Keays 1981) and because the poor reproducibility of PGE and Re in some rocks requires the so-called "nugget-effect", i.e., the irregular distribution of HSE-rich accessory minerals in the sample powder (e.g., Ravizza and Pyle 1997; Pearson and Woodland 2000; Reisberg and Meisel 2002).

In the absence of PGM, HSE are expected to strongly prefer BMS over silicate minerals or melt in mantle rocks (Mitchell and Keays 1981; Lorand 1989; Fleet et al. 1996; Hart and Ravizza 1996; Burton et al. 1999; Alard et al. 2000; Sattari et al. 2002). In particular, within cratonic peridotites, sulfides can contain 1000s of ppm or even % levels of the HSE, either due to the effect of extreme concentration these elements into remaining sulfide during partial melt extraction (Jgaoutz et al. 1979; Alard et al. 2000 Griffin et al. 2002), or because they derive from PGE alloys in a highly refractory residue that was captured by BMS, in which case discrete Pt-rich microphases can be present in the sulfides (Griffin et al. 2002, 2004).

For simplicity, all such secondary PGE-rich sulfide assemblages will be referred to here as "resulfidized PGM". In addition, HSE-rich monosulfides may yield abundant discrete PGM by subsolidus cooling (Lorand and Luguet 2016, this volume).

Pre-metasomatic cratonic mantle sulfides are typically monosulfide solid solutions (mss) that exsolve to low-temperature assemblages of pyrrhotite plus pentlandite and chalcopyrite in the mantle and during transport to the surface (Mitchell and Keays 1981; Lorand and Conquéré 1983). Lorand and Luguet (2016, this volume) review a wide range of exsolved PGM (laurite, Ru–Os–Ir sulfarsenides, Pt–Fe alloys) in cratonic mantle samples. The presence of Pt–Ir–Os alloys embedded in BMS has been inferred by Griffin et al. (2002) due to the irregularities in signal intensity during in-situ laser analysis. The occurrence of such minerals in residual mantle, possibly as micro- or nano-inclusions, has also been inferred from the PGE systematics of basalts and komatiites (Fiorentini et al. 2011; Fonseca et al. 2011) and is expected for peridotites that have been depleted to S exhaustion, based on analytical (e.g., Pearson et al. 2004) and experimental evidence (e.g., Fonseca et al. 2012). The modelling of experimentally derived alloy solubilities and stability at a range of *P, T* and oxygen and sulfur fugacities (f_{O_2}, f_{S_2}) by Mungall & Brenan (2014) indicates that there is no field of mantle stability for Pd alloys in nature but that Pt alloy stability is expected at ambient T_P whereas Ir alloy stability is broader still, suggesting the presence of Os, Ir, and Ru alloys even at very high (50%) levels of melt depletion and excess T_P. This, combined with the possibility that some cratonic mantle roots reach depths where iron-nickel metal saturation is expected, due to falling f_{O_2} with increasing *P* (Ballhaus 1995; Rohrbach et al. 2007; Rohrbach and Schmidt 2011; Stagno et al. 2013), suggests that HSE could be hosted in PGE alloys or in iron-nickel metal in strongly depleted, sulfide-free shallow lithosphere and in the deeper reaches of cratonic mantle, respectively. These minerals may be easy to overlook and even if actively searched for, may be too small to be observed with conventional analytical techniques. Their presence as micro- or nanoinclusions may be responsible for PGE patterns with low Pd/Ir in olivine separates that strongly resemble those of highly depleted, S-poor cratonic xenoliths (Smit et al. 2014a), as outlined above.

ANALYTICAL TECHNIQUES FOR CRATONIC MANTLE PERIDOTITES

Analytical techniques for the accurate and precise determination of HSE concentrations and Re–Os isotopes are reviewed in Meisel and Horan (2016, this volume). The spectrum of possible HSE hosts in peridotites has given rise to various sample digestion and analytical strategies that each has their advantages and drawbacks. Clearly, the best approach is to use a combination of techniques in order to obtain maximum constraints on the origin and evolution of the cratonic lithosphere from a HSE perspective. Here, we focus on those that are particularly usefully applied to cratonic mantle samples. Actual data from various sample types and their implications will be discussed in later sections dealing with signatures of melt depletion and metasomatism.

Whole rocks and mineral separates

Cratonic peridotite xenoliths contain sufficient Re and PGE abundances—mostly concentrated in BMS and PGM—to allow determination of Re–Os isotopes and PGE abundances by routine isotope dilution mass spectrometry techniques (Creaser et al. 1991; Walker et al. 1989). The presence of irregularly distributed accessory HSE-rich minerals poses several challenges to obtaining precise and accurate results from whole rock powders of mantle xenoliths. Firstly, a technique has to be chosen that ensures that refractory minerals are reliably digested. This may be achieved by—and requires—high-temperature and -pressure techniques, such as Carius tube or high-pressure asher digestions at 300 ºC. A drawback of such methods is that in general, sample sizes are limited to 5 g or less (Shirey and Walker 1995; Meisel et al. 2001; Becker et al. 2006), leading to potential problems from sampling errors and the "nugget effect" (Pearson and Woodland 2000). Alternatively,

a Ni–S fire assay can be used (e.g., Pattou et al. 1996; Maier et al. 2012), which allows larger aliquots to be analyzed (therefore not practicable for mineral separates), potentially lessening the impact of the "nugget effect" (e.g., Lorand et al. 2013). This method suffers from larger blank contributions and, unless great care is taken, possible incomplete digestion of refractory phases, producing data with relatively large scatter (Pearson and Woodland 2000; Becker et al. 2006). It is clear amongst practitioners that a Te co-precipitation step is required to ensure best recovery of PGE during Ni–S fire assay (e.g., Gros et al. 2002; Maier et al. 2012). Perhaps the most significant draw-back of this technique, especially for cratonic peridotites, is that obtaining high-quality Os isotope and concentration data is difficult and it is not possible to obtain quantitative Re data, such that combined Re–Os plus PGE studies on the same sample dissolution (Pearson and Woodland 2000) are precluded. Also, while it is desirable for any of the above methods that the sample size be sufficiently large to diminish sampling errors due to the "nugget effect", this is often not achievable for kimberlite-entrained cratonic mantle xenoliths, which—by nature or because of their comminution in diamond processing plants—are limited to hand specimens rarely exceeding 5–10 cm in the longest dimension, especially outside of the historic mines of South Africa, where access and size is controlled by exploration companies and smaller concentrate samples are produced by modern kimberlite processing procedures.

Several instrumental approaches are available for PGE abundance and isotope ratio measurement. Measurement of Os isotopes by N-TIMS remains the most widely used method (Creaser et al. 1991; Völkening et al. 1991). The sparging technique, where Os is volatilized directly from the sample solution and measured online using an ICPMS instrument (Schoenberg et al. 2000; Hassler et al. 2000), suffers from incompletely understood problems (Liu et al. 2010). In contrast, measurement of PGE concentrations by isotope dilution sector-field ICPMS and of Re–Os isotopes by multicollector ICPMS, where the sample solution is aspirated into the torch with a nebulizer/spray chamber (Pearson and Woodland 2000; Day et al. 2003; Nowell et al. 2008), has yielded reproducible and accurate results of sufficient precision to be usefully applied to mantle xenoliths (Sen et al. 2011; Aulbach et al. 2014). In this case, care has to be taken to exclude the severe memory problems that can affect the sample introduction system (Pearson and Woodland 2000).

The potential presence of multiple generations of BMS and/or PGM in a whole-rock sample, described above, implies that a mixed signal is obtained (Alard et al. 2002; Griffin et al. 2002, 2004). In general, for cratonic mantle samples, sulfide-rich rocks and sulfides having Ni/Fe ratios that are inappropriate for residual phases remaining after melting extents exceeding 30% (Lorand and Grégoire 2006) should be avoided in the whole rock approach. Rather, S-poor, refractory samples, in which all the Os resides in laurite/erlichmanite series minerals or alloys that were produced during the melting event that formed the rock should be targeted (Pearson and Wittig 2014). Single sulfide grains measured in some cratonic samples have yielded significantly lower $^{187}Os/^{188}Os$, and therefore older minimum ages, than their corresponding whole rocks (e.g., Griffin et al. 2004; Bragagni et al. 2014).

Several studies report HSE and/or Re–Os isotopes in peridotitic mineral separates that were measured with the aim to identify mineral hosts of the HSE, to obtain information uncorrupted by ubiquitous kimberlite addition during xenolith entrainment or to access a component in xenoliths that is dominated by included and presumably therefore least modified HSE carriers (e.g., Chesley et al. 1999; Burton et al. 2000; Hanghøj et al. 2001; Luguet et al. 2009; Wittig et al. 2010a; Aulbach et al. 2014; Pernet-Fisher et al. 2015). For example, in the case of Smit et al (2014a) the small kimberlite-derived xenoliths were so extensively invaded by kimberlite melt that digestion of a whole-rock sample was not useful; olivine separates were the least compromised part of the rocks. The sample preparation and analytical requirements for peridotitic mineral separates are identical with those of the

whole rocks reviewed above, since complete digestion also of refractory phases is required for meaningful results. Ruthenium analyses by ICPMS in chromites must be evaluated with caution due to the detrimental effects of Cr-based polyatomic interference.

Single-grain techniques

Advancements in analytical techniques over the ~15 years have allowed Re–Os isotope measurement of single sulfide grains (see review by Harvey et al. 2016, this volume). Two approaches have been applied. One measures Re and Os isotopes using Negative Thermal Ionization Mass Spectrometry (NTIMS) after digestion of entire, or close to entire, single grains isolated from mantle xenoliths or diamonds (e.g., Pearson et al. 1998, 1999; Richardson et al. 2001, 2004; Luguet et al. 2008; Aulbach et al. 2009a,b,c, 2011; Harvey et al. 2011). The other uses an *in situ* approach, where the sulfide is analysed using laser ablation microprobe inductively-coupled plasma mass spectrometry (LA-ICPMS); if applied to sectioned rocks, valuable microstructural context is preserved (Alard et al. 2000, 2002; Pearson et al. 2002a; Aulbach et al. 2004; Griffin et al. 2004; Zheng et al. 2007). A hybrid method consists of extracting sulfide remains in polished thick sections, followed by solution and measurement by NTIMS (Bragagni et al. 2014; Luguet et al. 2015). The concentration of the analyte in the sulfide grains dictates the size of the grains that must be processed to achieve satisfactory counting statistics during measurement and useful precision on the concentration and isotope ratio, if measured.

Typically, unless a diamond inclusion study is being performed, sulfide grains < 30–50 μm are not analyzed, meaning that if such a fraction is present in the whole rock, its HSE and isotopic contribution cannot be directly accounted for. These issues limit how representative the analysis of single or multiple sulfide grains per sample is of the whole rock and mantle source region, especially in highly depleted peridotites where melt extraction has proceeded to the level of sulfide exhaustion and PGE such as Os, Ir and Ru are likely hosted in micron to sub-micron phases such as laurite or alloys (Luguet et al. 2007; Lorand et al. 2008, 2010; Kogiso et al. 2008) in addition to olivine (Mungall and Brenan 2014). The *in situ* method additionally requires the correction of ^{187}Os from the isobaric interference of ^{187}Re, which in practice means that accurate Re–Os isotope data can only be confidently obtained for sulfides with low Re/Os (N.J. Pearson et al. 2002b; Nowell et al. 2008), leading to exclusion of unsuitably high-Re/Os grains present in some samples. Given the mostly young emplacement ages of kimberlite, which likely reflect the limited preservation of older kimberlites (e.g., Tappe et al. 2014), the differential distribution of Re and Os associated with sub-solidus exsolution of mss has a limited effect on Os isotopes, but will contribute to uncertainties in model ages and produce scatter on Re–Os isochron diagrams.

Thus, where possible, intact or recombined whole sulfide grains should be analyzed to avoid these complications (Richardson et al. 2001; Rudnick and Walker 2009; Pearson and Wittig 2014). Both solution and in situ techniques have shortcomings in this regard because the former do not always succeed in recovering the entire sulfide (Richardson et al. 2001; A. Wainwright pers. comm. 2014) and the latter may not sample representative portions of grains exposed in sections even if total ablation is attempted (see discussion in Pearson and Wittig 2014). Nevertheless, the single grain technique has led to the recognition that cratonic peridotites—and even single diamonds—can harbor multiple generations of sulfide (Pearson et al. 1998; Alard et al. 2000; Griffin et al. 2002, 2004) and is the only way of demonstrating that some diamonds grow in pulses that may be separated by 1 Ga (Wiggers de Vries et al. 2013). Although PGM lend themselves to in situ or single mineral techniques similar to those described for BMS, large enough grains suitable for in-situ analyses in cratonic mantle samples have not been reported so far.

UTILIZATION OF THE Re–Os ISOTOPE SYSTEM IN CRATONIC MANTLE STUDIES

The development of Re–Os isotope geochemistry has played a pivotal role in dating lithosphere stabilization and exploring links between continental crust and mantle formation (Walker et al. 1989; Carlson and Irving 1994; Pearson et al. 1995b,c, 2007; Pearson 1999; Griffin et al. 2002, 2004; Carlson et al. 2005, 2008). Rudnick and Walker (2009) give a comprehensive general review of the principles and issues of interpreting Re–Os isotope ages, and an assessment specifically with regard to dating cratonic mantle samples is provided by Pearson and Wittig (2014). The salient characteristics and complexities in the application of the Re–Os isotope system are summarized here.

Because Re is mildly incompatible in the absence of sulfide melt (with a distribution coefficient broadly similar to Al, Yb, or Ti), whereas Os is compatible during peridotite partial melting and generation of basalt (e.g., Righter and Hauri 1998; Brenan et al. 2003; Righter et al. 2004; Fonseca et al. 2007; Mallmann and O'Neill 2007), isolation of lithospheric from convecting mantle by melt extraction leads to strong fractionation of the daughter from the parent element, in particular if the degree of melting is great enough to exhaust sulfide from the mantle residue, which occurs after ~25% of partial melting (Keays 1995), but may occur at very low degrees of melting in oxidized mantle (Mungall et al. 2006; Botcharnikov et al. 2013). This results in Os isotope compositions being virtually frozen in at the time of the strong melt depletion inferred for cratonic mantle (Walker et al. 1989; Shirey and Walker 1998). In addition, the high Os concentrations in residual mantle compared to low concentrations in metasomatic melts and fluids confer a high degree of robustness to post-formation overprint (Reisberg and Lorand 1995; Rudnick and Walker 2009). However, no Re–Os isotope study of cratonic peridotites has so far resulted in a meaningful isochron relationship that defines a clear partial melting event, with the possible exception of peridotites from Hannuoba (Gao et al. 2002), which have isochron relationships dating the formation of new lithosphere at ~1.9 Ga. Much of the scatter in Re–Os geochronology results from direct modification of Os isotope compositions and/or from changes Re addition and time-integrated ingrowth of radiogenic Os, e.g., following sulfide breakdown or addition (Rudnick and Walker 2009).

Two types of model age have been formulated for the application of the Re–Os isotope system to mantle samples (Walker et al. 1989; Shirey and Walker 1998): (1) An age for the isolation from the model convecting mantle reservoir (T_{MA}) assuming that all Re is primary—this is analogous to model ages calculated using Sm–Nd (McCulloch and Wasserburg 1978); (2) A Re-depletion age (T_{RD}) assuming that all Re has been extracted during melt depletion and that any Re present was added later—this is a minimum age whereby the measured $^{187}Os/^{188}Os$ is projected to the mantle evolution line assuming Re/Os is zero. A variation on this age is the T_{RD} eruption age (Pearson et al. 1995b) calculated for mantle xenoliths, assuming that all measured Re was added during xenolith transport in the host magma, which is manifested by sub-horizontal arrays in the Re–Os isochron diagram (e.g., Carlson et al. 2005). In this case, the measured $^{187}Os/^{188}Os$ is corrected for the ingrowth of ^{187}Os from Re since kimberlite emplacement and a T_{RD} is calculated for the resultant value (Pearson et al. 1995b; Shirey and Walker 1998; see their Fig. 1 for an illustration of the various model ages).

An initially depleted, but refertilized mantle may have PGE and Re–Os isotope systematics that are difficult to distinguish from initially less depleted mantle. Unless Re addition has occurred quasi-contemporaneously with melt depletion or with emplacement of the host magma, metasomatic Re addition to the cratonic mantle during its long isolation from the convecting mantle will lead to calculated T_{MA} that are too old and T_{RD} that severely underestimate the true age—assuming preservation of original $^{187}Os/^{188}Os$ (Rudnick and Walker 2009). Thus, T_{RD} should not be calculated for moderately to minimally depleted mantle

samples that did not suffer quantitative Re extraction, and T_{MA} may be meaningless for those bulk rocks which likely had a multi-stage Re–Os isotope evolution as inferred from PGE systematics (Pearson and Wittig 2014). Consequently, application of the Re–Os isotope system to whole-rock peridotites requires careful selection of samples that show the highest levels of melt depletion (usually the least diopside- and garnet rich), minimal modal metasomatism and minimal addition of metasomatic sulfides. The use of combined PGE and Re–Os isotopes in whole-rock studies reveals that often the oldest Re depletion ages are obtained from the samples with the most Platinum-group PGE (Pt and Pd: PPGE) depleted normalized PGE patterns (D.G. Pearson et al. 2002), irrespective of their Re enrichment.

Recently, König et al. (2014) and Luguet et al. (2015) have shown that combined S and Se/Te measurements are highly useful in deciphering whole-rock Re–Os and PGE systematics. They find that, within a suite of peridotites from Letlakhane, Botswana, the most depleted rocks that are sulfide-free contain high but variable Se/Te ratios (15–40) and very Pd- and Pt-depleted normalised patterns. Such characteristics are indicative of melting residues. Indeed, these samples yield the oldest, most robust whole-rock Os isotope ages. In the same suite of rocks, only the most metasomatized BMS-rich peridotites experienced enrichment of both $^{187}Os/^{188}Os$ and Pd/Ir at constant Se/Te, such that the Os isotopes yielded unrealistically young T_{RD} eruption ages for mantle root stabilization in this region.

In an effort to isolate the oldest Os isotopic component in mantle xenoliths, sulfide inclusions, or mineral separates, where the Os signature is presumably dominated by primary inclusions, have been targeted. Sulfide inclusions have in some instances been shown to preserve older age information and more residual HSE systematics compared to sulfides occurring in the interstices (Burton et al. 1999; Alard et al. 2002, 2011; Harvey et al. 2011). This has led to the expectation that silicate-hosted sulfide grains, being protected from post-formation modification by their host, will preserve older age information than interstitial grains. However, mantle metasomatism induces recrystallization (Drury and van Roermund 1989), during which metasomatic minerals including sulfides can be trapped in primary minerals. Therefore, inclusions do not necessarily yield Archean or even the most ancient ages in cratonic—or any—mantle xenoliths (e.g., Burton et al. 1999). Detailed recent studies of whole rocks and associated sulfide grains with particular attention to various textural contexts (included versus interstitial or in melt pools) have revealed an almost bewildering lack of correspondence between textural position and Os isotope systematics, and interstitial sulfide grains in strongly metasomatized cratonic and other peridotites can give Archean model ages (Bragagni et al. 2014; González-Jiménez et al. 2014; Wainwright et al. 2015). Nevertheless, because metasomatic sulfur addition sometimes appears to be accompanied by only minor HSE input, in particular the compatible IPGE, previously hosted in residual alloys, can retain their original, unradiogenic $^{187}Os/^{188}Os$ for eons (Marchesi et al. 2010; Fonseca et al. 2012) even if they are now present as sulfides (Griffin et al. 2002, 2004; Lorand et al. 2013). An example of the "resulfidation" of older residual alloys, imparting the ancient signatures of these grains on more recent metasomatic sulfide phases has been documented by Wainwright et al. (2015).

Though rare, meaningful ages have been been obtained from Re–Os isochrons for several peridotitic sulfide suites from the central Slave craton, yielding radiogenic initial $^{187}Os/^{188}Os$ (Aulbach et al. 2004, 2009a, 2011; Westerlund et al. 2006). Consequently, model ages for samples with unradiogenic Os are systematically underestimated when projected back to a primitive mantle evolution curve. This highlights the effect of uncertainty regarding source composition for model age calculations. The uncertain evolution and pronounced heterogeneity of present-day convecting mantle (Brandon et al. 2000; Meibom et al. 2002; Walker et al. 2002; Pearson et al. 2007) further diminish the resolution of Re–Os ages. Despite the smaller isotopic diversity of the early convecting mantle (Rudnick and Walker 2009), an uncertainty of ca. 200 Ma may

still be indicated for model ages calculated for Archean samples, and cratonic mantle lithosphere can only be unambiguously identified if a sufficiently large number of samples yielding Archean ages are analyzed (see also discussion of data presentation in Pearson and Wittig 2014).

Despite the many complications, the Re–Os isotope system has confirmed the presence of Archean mantle beneath many cratonic regions and has provided remarkably detailed information on coupled cratonic crust and mantle evolution. One of the clearest examples of the success of both sulfide and whole rock analytical approaches in defining cratonic mantle lithosphere is given by the multitude of studies performed on and adjacent to the Kaapvaal craton, summarized in Janney et al. (2010) and Pearson and Wittig (2014). The mode in T_{RD} ages given by xenolith suites from all kimberlites erupted within the recognized crustal bounds of the craton is Archean, with the exception of those from the Premier mine, which samples mantle with a major Mesoproterozoic overprint (Shirey et al. 2002). In contrast, while there are signs of Archean heritage in some xenoliths from circum-cratonic kimberlites, their dominant age signature is Mesoproterozoic (Janney et al. 2010; Aulbach et al. 2014). A link between large-scale mantle melt depletion events, gauged by Os isotopes in a variety of mantle materials (BMS, PGM, peridotites), and spurts of continental crust formation are observed no earlier than 3.3 Ga ago, and again at 2.7, 1.9, and 1.2 Ga (Pearson et al. 2007). Accordingly, juvenile crust formation pulses at 4.2 and 3.8 Ga—evidenced by zircon U-Pb ages combined with Hf and O isotopes—were apparently not accompanied by the formation of cratonic lithosphere (at least none that survived to be sampled today). The oldest preserved vestiges of cratonic mantle probably formed ca. 3.5 Ga ago (Griffin et al. 2014). In some instances, cratonic mantle has been discovered beneath younger mobile belts: This applies to the ca. 1.8 Ga Nagssugtoqidian mobile belt in northwestern Greenland (adjacent to Greenlandic part of the North Atlantic craton; Wittig et al. 2010a) and the ca 1.9–1.8 Ga Halls Creek Orogen in northwestern Australia (at the southeastern margin of the Kimberley craton; Luguet et al. 2009). In other instances, Re–Os isotope systematics reveal that deep cratonic keels were lost (by an uncertain mechanism) and replaced by younger mantle (of uncertain origin), the most prominent case being that of the North China craton (Gao et al. 2002), which will be discussed further below. Finally, it is worth noting that crust-mantle links exist not only for the timing of cratonic lithosphere formation, but also for its subsequent tectonothermal evolution, as evidenced by multiple peaks in age spectra for sulfide or peridotite suites from a single mantle section, which may reflect new lithosphere formation or overprint during collisions or rifting subsequent to cratonization (e.g., Pearson et al. 1995c; Pearson 1999; Griffin et al. 2002, 2004; Wittig et al. 2010a).

EFFECT OF MELT DEPLETION DURING CRATONIC LITHOSPHERE STABILIZATION ON SULFUR AND HSE SYSTEMATICS

Partial melting of convecting mantle generates a lithosphere that should be enriched in compatible elements, such as the IPGE and depleted in incompatible elements, such as the PPGE and Re, depending on extent of melting (e.g., Pearson et al. 2004). Because of the extreme compatibility of HSE with sulfide phases, the main effect of partial melt extraction will be through consumption of sulfide; after sulfide has been exhausted, the HSE are dominated by IPGE compatibility in olivine and by possible saturation in alloy (e.g., Mungall and Brenan 2014).

Sulfur and the persistence of sulfides

Komatiites are high-degree melts that have been suggested to be complementary melts to cratonic lithosphere (e.g., Herzberg and O'Hara 1998). Since some komatiite types are sulfide-undersaturated at source (Fiorentini et al. 2011), an absence of primary residual sulfides in highly depleted cratonic mantle could be implied, with the potential exception of sulfide trapped in silicates during the partial melting. This is true, for example, for the Kaapvaal

craton, where petrographic evidence and young Re–Os isotope ages for peridotitic sulfide inclusions in diamond suggest secondary introduction of sulfide into an initially (post-melting) sulfide-barren lithosphere (Lorand and Grégoire 2006; Aulbach et al. 2009a).

Despite the general expectation that the primary cratonic mantle residue is sulfide-free, the thickness of cratonic mantle roots combined with their formation during polybaric melting (e.g., Walter 1998, 2005; Herzberg 2004) warrants the consideration that primary residual sulfide could be present in the deeper, less depleted cratonic mantle regions, although the least depleted, deepest portions may have been lost (Arndt et al. 2009). The presence—or not—of sulfide at the base of the cratonic mantle depends on depth of initiation of melting (P_i) and the depth of any pre-existing lithospheric lid limiting further decompression melting (e.g., Sobolev et al. 2007), and also depends on the f_{O_2} of the convecting mantle, as will be discussed in more detail in a later section. If all PGE are quantitatively retained and little fractionated in the residue, as long as sulfide is stable (Mungall and Brenan 2014), one might expect that the deepest and hence least depleted cratonic mantle residues have relatively high PGE concentrations at near-chondritic ratios of PPGE to IPGE (bearing in mind that during cratonic lithosphere formation all sulfide is molten and hence there is no incongruent melting, during which PGE would be fractionated).

The relatively low PPGE/IPGE, compared to other melts, in Al-depleted komatiites that formed at great depths and relatively small degrees of partial melting (>200 km, $F=0.2$; Arndt et al. 2008) were suggested to indicate the presence of residual sulfide in their source. Figure 4 shows that there are few cratonic samples with high PGE concentrations and high Al_2O_3 contents consistent with extraction of small amounts of partial melt in the presence of sulfide, whereas such systematics are common in orogenic peridotites. Indeed, none of the cratonic peridotites in the dataset should contain primary residual sulfide, which would be exhausted before Al_2O_3 decreases to <1.5 wt% (Pearson et al. 2004), yet most have S concentrations that are vastly too high—even in excess of primitive mantle values—for the degree of depletion gauged from Al_2O_3 concentrations at the conditions considered here (Fig. 5). In contrast, most orogenic and some off-cratonic peridotites, which formed at lower initial pressures, where Al_2O_3 decreases more rapidly compared to S, may have retained primary sulfide.

At decreasing sulfide modes prior to final exhaustion, concentrations of the PGE within the sulfide liquid will increase dramatically and may reach wt% concentrations, possibly leading to the saturation of PGM immediately prior to final exhaustion of sulfide liquid (Mungall and Brenan 2014). This could explain why some sulfides from cratonic peridotites have much higher HSE concentrations than those from younger samples that were generally never depleted to the point of sulfide exhaustion, such as abyssal and orogenic peridotites (Fig. 6).

Alloy saturation

The expectation of PGE alloy saturation during generation of cratonic mantle combined with the presence of BMS, some containing discrete PGM grains, indicates that resulfidation of the mantle may have occurred (Griffin et al. 2002, 2004). The associated capture of residual PGE alloys by BMS melt droplets should lead to formation of composite alloy–BMS grains (Lorand and Luguet 2016, this volume). Alternatively, in the absence of residual IPGE alloy, addition of sulfur to previously melt-depleted mantle may extract IPGE from olivine to form mixtures of BMS and PGE sulfides.

Primary residual sulfides should be distinguishable from resulfidized PGM, which are expected to have low Pd/Os and Re/Os since Pd and Re do not form alloys and are incompatible in olivine, in addition to low Pt/Os for P_i >3 GPa (Mungall and Brenan 2014). There are few complete PGE datasets for sulfide in cratonic mantle samples. Peridotitic sulfide inclusions in diamond, and sulfide grains in peridotite xenoliths from the Kaapvaal and Siberian craton, have Pt/Os from ~0.002 to 20 and show a rough

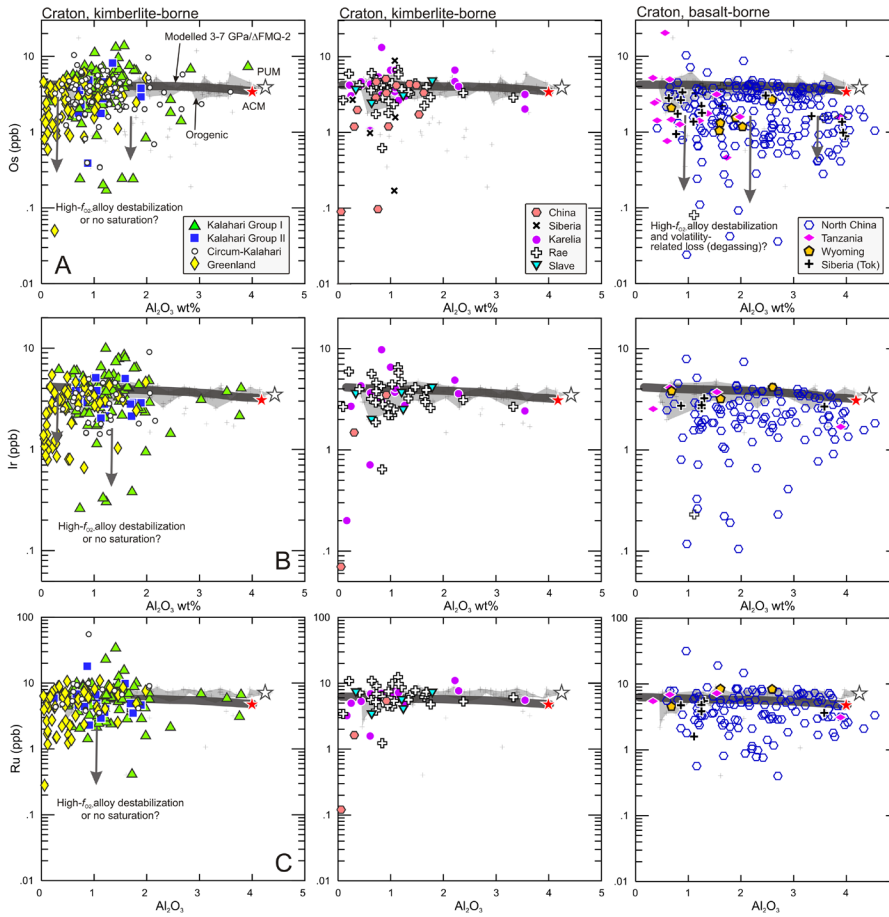

Figure 4. (A–C) Whole-rock HSE concentrations (ppb) in various peridotite classes plotted against Al_2O_3 (wt%) as a melt depletion index, with kimberlite- and basalt-borne xenoliths plotted separately for clarity. Shown for comparison are the residual concentrations in modelled melt depletion residues discussed in the text and displayed in Figure 11. Note that the modelled residual concentrations of Os, Ir, and Ru are very similar at the depicted scale. Also shown are suggested qualitative trends for various melt depletion-related and secondary effects. Grey field roughly encompasses the majority of orogenic peridotites, which are shown as crosses. PUM and ACM refer to the Primitive Upper Mantle and Archean Convecting Mantle reservoirs, respectively, with concentrations and references given in Table 2. "Kalahari Group 2" encompasses both xenoliths from the predominantly older (>110 Ma) micaceous kimberlites emplaced in the Kaapvaal craton and older kimberlites from the Kalahari craton, which entrained xenoliths sampling mantle that was not affected by the pervasive metasomatism observed for samples from the mostly younger, Group I generation of kimberlites (≤95 Ma; Griffin et al. 2003b, and references therein). References as in Figure 3. Continued on next page.

negative correlation with Os concentration (Fig. 6). In time-resolved laser ablation spectra these sulfides display signal intensity spikes indicative of the presence of PGE alloy inclusions, which, combined with their low Pt/Os, is consistent with them being mixtures of BMS and PGM; however, the timing of exsolution of PGM from the BMS is impossible to constrain (Griffin et al. 2002, 2004). Given that most cratonic peridotites apparently gained considerable amounts of secondary S, pervasive resulfidation of the

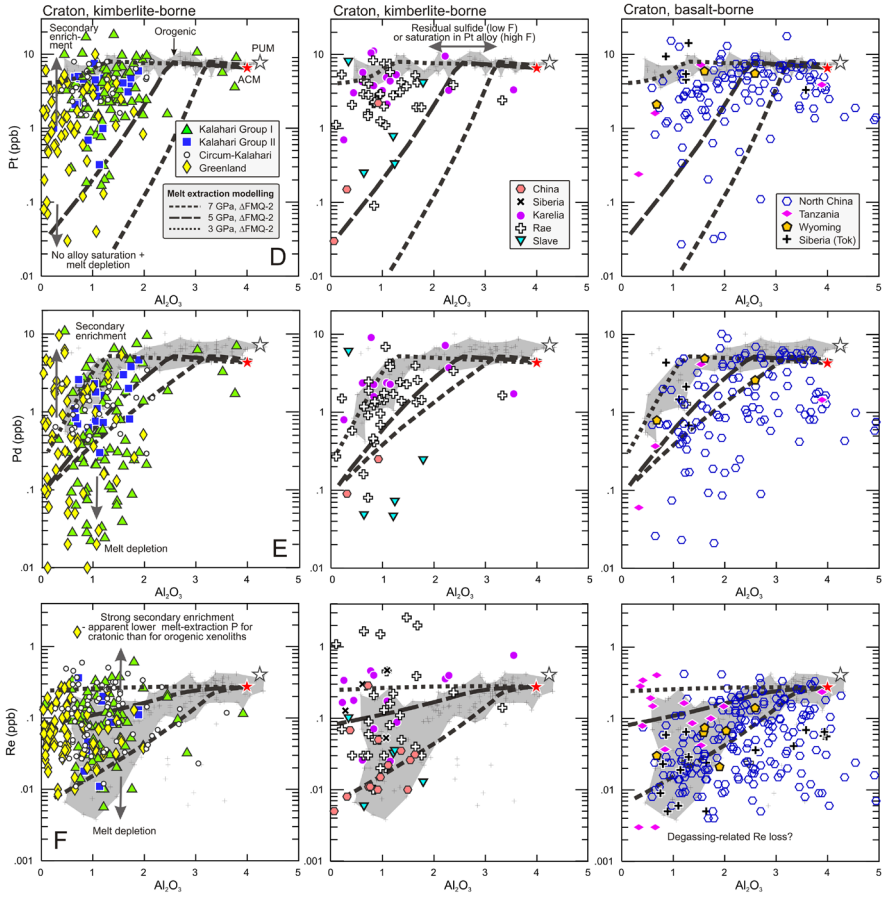

Figure 4 (cont'd). (D–F) Whole-rock HSE concentrations (ppb) in various peridotite classes plotted against Al_2O_3 (wt%) as a melt depletion index, with kimberlite- and basalt-borne xenoliths plotted separately for clarity.

cratonic mantle may help explain why primary alloys, though expected and suspected in many though not all restites, have to date not been directly observed. Nevertheless, little-fractionated Pt/Os and Re/Os at elevated concentrations are observed for sulfide inclusions in diamond and for some sulfide grains in cratonic peridotites (Fig. 6), perhaps consistent with a primary residual sulfide population that is not depleted enough to evolve to unradiogenic Os giving Archean T_{RD}.

A single common PGE host—whether primary sulfide, BMS–PGM mixture or olivine—is indicated for sample suites showing tight correlations of PGE concentrations (Lorand et al. 2013). Such correlations are observed for Os with Ir in all cratonic peridotite suites (Fig. 7A), which may indicate saturation of Os–Ir alloys at high concentrations. In contrast, the less common very low Os and Ir concentrations may indicate failure of alloy to saturate, in which case both elements would be hosted by olivine, or secondary loss of (resulfidized) alloy. Some superposition of secondary effects is particularly evident in the basalt-borne peridotite xenolith variety (Fig. 7A). Ruthenium and Ir are also positively correlated in

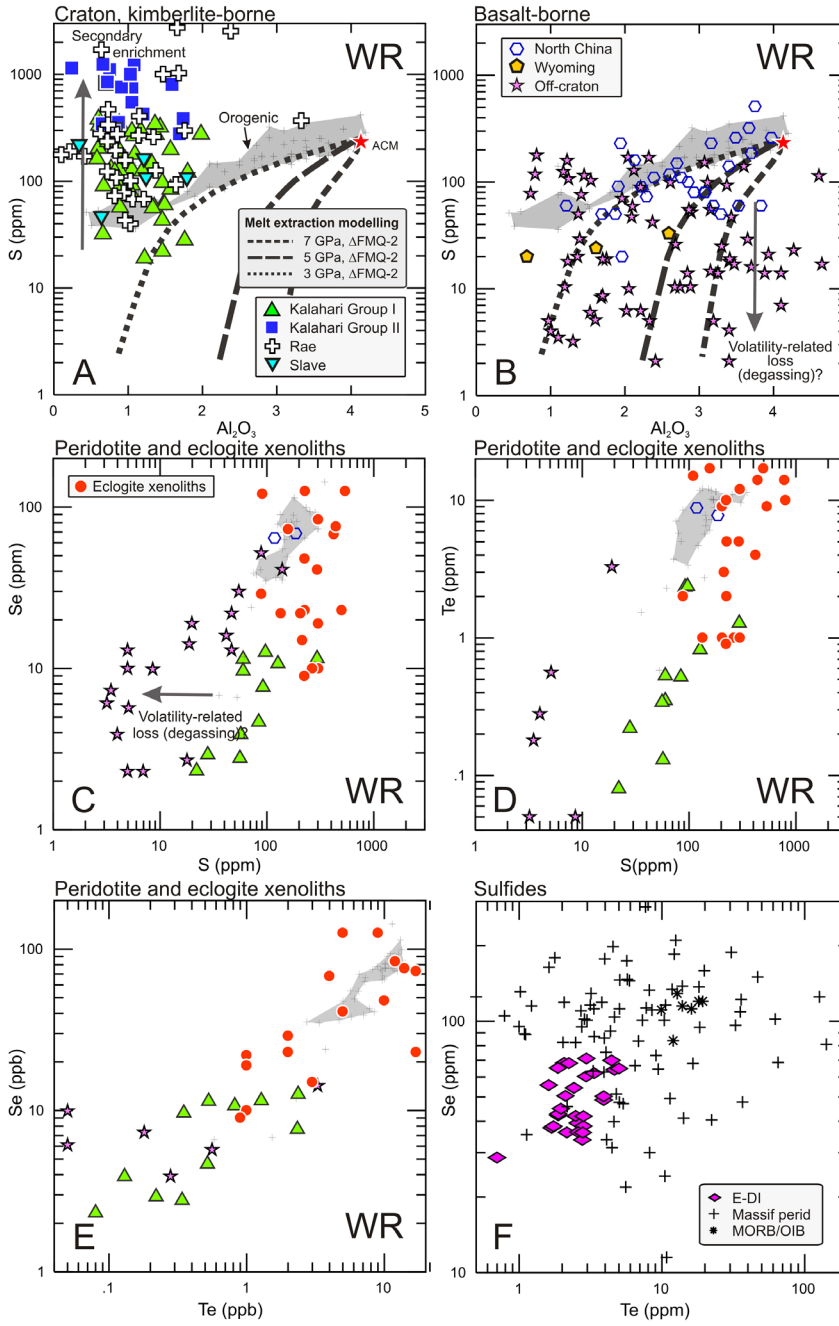

Figure 5. (A–B) Whole-rock S concentrations against Al_2O_3 (as an index of melt depletion), whole-rock (C) Se and (D) Te as a function of S composition, (E) whole-rock and (F) sulfide Te against Se concentrations. Shown in (A) and (B) are melting contours as described in the text and displayed in Figure 11. Other information as in Figures 3, 4, and 6.

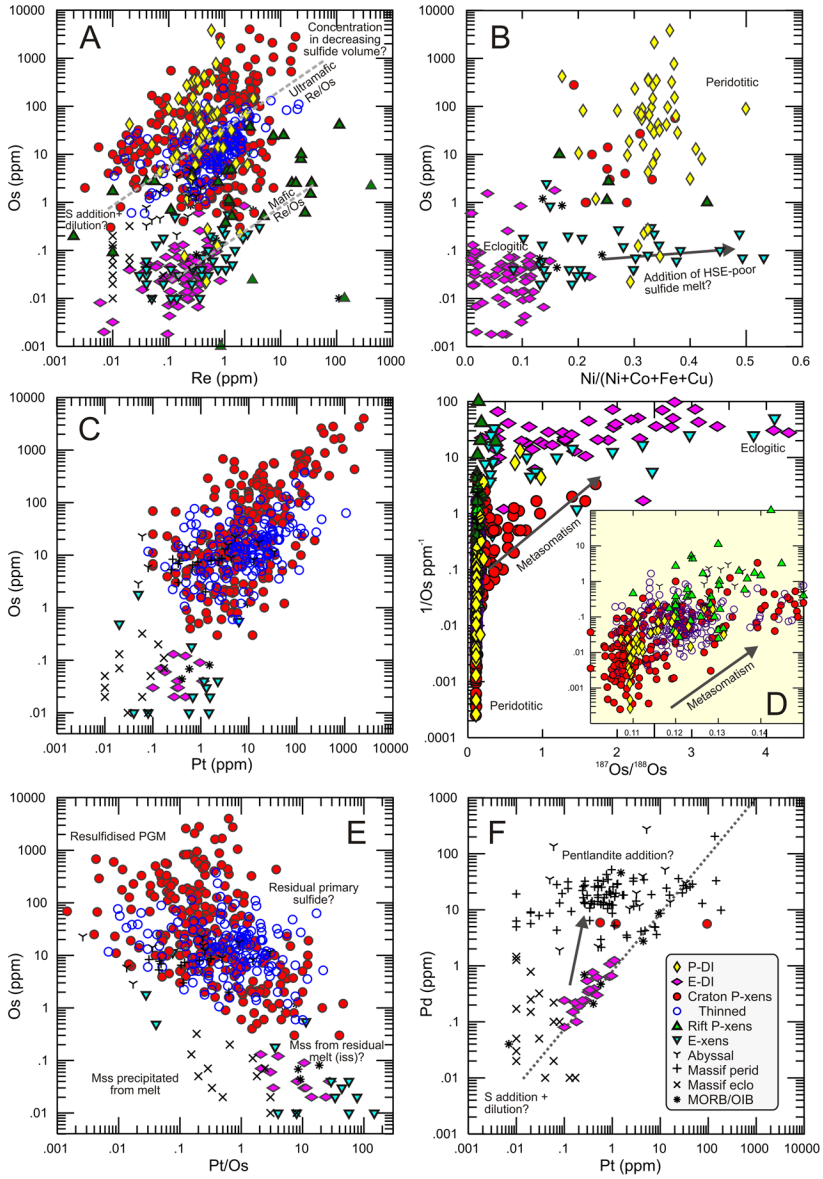

Figure 6. (A–H) Compositional and $^{187}Os/^{188}Os$ relationships for sulfides included in peridotitic (P-DI) and eclogitic (E-DI) diamonds, for sulfides in cratonic peridotite xenoliths (Craton P-xens), sulfides in peridotite xenoliths from thinned continental lithosphere and rifts (Rift P-xens), sulfides in eclogitic xenoliths (E-xens), sulfides in abyssal and massif peridotites, sulfides in massif eclogites and sulfides in oceanic basalts (MORB/OIB; Fleet and Stone 1990; Peach et al. 1990; Roy-Barman and Allègre 1994; Pearson et al. 1998; Roy-Barman et al. 1998; Alard et al. 2000; Luguet et al. 2001, 2008; Richardson et al. 2001, 2004; Griffin et al. 2002, 2004; Aulbach et al. 2004, 2009a,b,c, 2011, 2012; Gannoun et al. 2004, 2007; Westerlund et al. 2004, 2006; Xu et al. 2008; Dale et al. 2009; Harvey et al. 2010, 2011; Lorand et al. 2010; van Acken et al. 2010; Delpech et al. 2012; Warren and Shirey 2012; Patten et al. 2013; Wiggers de Vries et al. 2013; König et al. 2014). Also shown are suggested trends for various secondary effects described in the text.

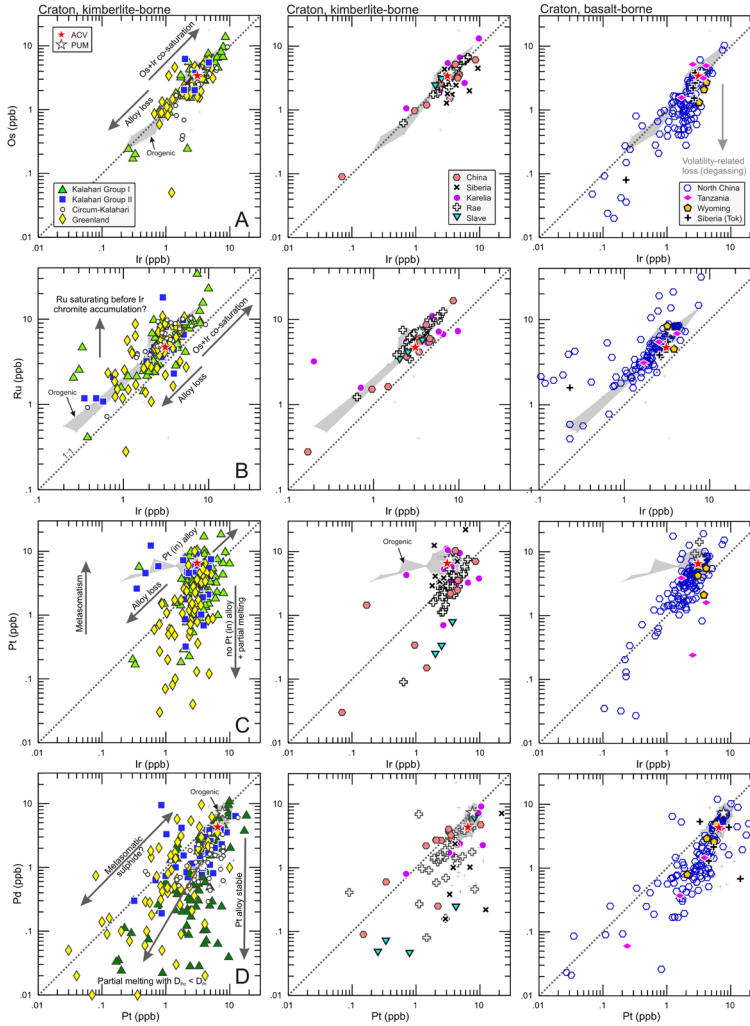

Figure 7. (A–D) Bivariate plots of whole-rock PGE concentrations (ppb) in various peridotite classes. Coherent trends may reflect co-saturation in or loss of PGE alloys, whereas deviation from such trends may reflect differential saturation of the alloy during partial melting (IPGE), different host phases and/or effects of partial melting (Pt vs. IPGE), preferential loss or gain of one element due to volatility (Os) or metasomatism (Pt). Other information as in Figures 3 and 5.

cratonic peridotites (Fig. 7B), probably due to compatibility of both of these IPGE in olivine, but show more scatter to high Ru at a given Ir concentration for the Kalahari and Greenland sections. This could point to a nugget effect from inhomogeneous distribution of chromite, to inhomogeneous distribution of alloys containing Ru or to analytical artefacts due to uncorrected polyatomic interferences involving Cr.

Large scatter is also observed for Pt versus Ir concentrations in some cratonic mantle sections (Kalahari, Greenland; Fig. 7C). Samples with coherent Pt and Ir at the

high concentration end of the array probably indicate the presence of variable amounts of primary sulfide, but coherent behavior at lower concentrations may represent mantle that experienced co-saturation of Pt and Ir alloy at low P_i and f_{O_2} during melt extraction to shallow depths. Offsets to higher Pt at a given Ir concentration may be explained by metasomatic Pt addition, whereas lower Pt may point to the failure of Pt to saturate in the melt at higher P_i and/or f_{O_2} and consequent incompatible behavior during partial melting (Mungall and Brenan 2014). In the absence of primary residual sulfide, roughly equal concentrations of Pt and Pd (Fig. 7D) may be indicative of metasomatic introduction with sulfide, whereas depletions of Pd relative to Pt would be consistent with the stronger incompatibility of Pd during partial melting, as inferred from high-volume melts (e.g., Barnes et al. 1985; Puchtel and Humayun 2000), and/or stabilization of Pt in the residue under reducing conditions and at low pressures.

Chalcogens

The concentrations of both Se and Te in selected cratonic mantle harzburgites are among the lowest of any measured from the Earth's mantle (König et al. 2014) and this is empirically consistent with their melt-depleted character. The relative partitioning behavior of the chalcogens Se and Te has been inferred from studies of various peridotites and sulfides (Hattori et al. 2002; Lorand and Alard 2010; König et al. 2012, 2014, 2015; Wang et al. 2013; Wang and Becker 2013). In peridotites that have suffered sulfide exhaustion, Te has been shown to behave incompatibly—more so than Se—leading to superchondritic Se/Te (>20; König et al. 2014, 2015). In agreement with this, the abundances of these elements in cratonic harzburgites are distinctly lower than in orogenic peridotites, but at highly variable absolute concentrations (Fig. 5). This observation may, in part, be related to a nugget effect caused by accessory sulfide or by PGM that inherited high Se/Te from residual sulfide (Fig. 6), or to secondary overprint (König et al. 2014, 2015). Metasomatic enrichment by high-Te, low-Se metasomatic phases, such as Bi–Pt tellurides, will lower Se/Te ratios at constant Al_2O_3 re-creating "chondritic" Se/Te ratios in samples varying from lherzolite to harzburgite (König et al. 2014). Basalt-borne xenoliths show conspicuous offsets toward lower S concentrations at a given Se or Te, consistent with S loss and Se–Te stability during degassing in subaerially emplaced host basalt (Lorand et al. 2013). While Se and Te are more robust than S to loss during degassing in peridotites, because of metasomatic disturbances, none of these elements is likely to be a faithful recorder of melting conditions in cratonic peridotites.

HSE PROCESSING DURING MANTLE METASOMATISM

Modification of the lithospheric mantle composition during interaction with fluids or melts is known as "mantle metasomatism". This process may be "cryptic", resulting in changes to the trace-element budget usually manifest as strong enrichment of LREE over HREE and addition of LILE introduced by invading volatile-rich fluids or small-volume melts. Alternatively "patent" or "modal" metasomatism is accompanied by major-element enrichment or depletion and modification of the modal mineralogy, including the addition or removal of minerals (e.g., Frey and Green 1974; Harte 1983; Dawson 1984; Menzies and Hawkesworth 1987; Erlank et al. 1987). The large scatter in the PPGE and Re data suggests that such secondary processes have obscured a significant part of the original signatures. The diversity of fluids and melts—reduced or oxidized, poor or rich in volatiles, small or large volumes—that may percolate and interact with the mantle (O'Reilly and Griffin 2013), combined with the antiquity of cratonic lithosphere, gives rise to a wide spectrum of conditions under which HSE can be added, removed and redistributed over the long course of cratonic histories.

The style and intensity of mantle metasomatism have consequences for the long-term survival of cratons, which depends critically on their viscosity and density as a function of H_2O contents and temperature (Jordan 1988; Abbott et al. 1997; Lenardic et al. 2003; Afonso and Schutt 2012; Wang et al. 2015). In extreme cases, intra-plate and subduction processes may lead to tectonic erosion, thermochemical erosion or whole-sale delamination and replacement by convecting mantle. This may be evidenced, *inter alia*, by cratonic mantle xenoliths suites entrained in basalts rather than kimberlites. Because of their varied geochemical behavior, HSE and Re–Os isotope systematics are suited to address the extent of craton survival and disruption beneath thinned cratonic areas. Below, we discuss the effects of various metasomatic styles on HSE abundances and Re–Os isotopes of cratonic mantle, presenting case studies that document various stages of cratonic lithosphere destruction through metasomatism.

Modification during Intraplate Mantle Metasomatism

Silica-undersaturated melts and fluids. During incipient partial melting of a carbonated peridotite source, low-volume, silica-undersaturated melts are generated that form a continuum between carbonatite and carbonated silicate melts, such as kimberlites (Dalton and Presnall 1998). Low-volume, residual melts may also form through reactions during percolation of a silicate melt through the lithosphere (e.g., Vernières et al. 1997) or by immiscibility (e.g., Kogarko et al. 1995). The signatures of the passage of such melts through the cratonic mantle are ubiquitous (Pearson et al. 2005; O'Reilly and Griffin 2013). The contents of HSE in carbonatite and kimberlite melts at depth are presumably initially very low since low-volume melts should leave a sulfide-bearing residue, which effectively retains the HSE (Mungall and Brenan 2014), assuming that the convecting mantle is not highly oxidized. Relatively high PGE and Re contents (>1 ppb) have been measured in some kimberlites and related rocks (e.g., McDonald et al. 1995; Graham et al. 1999, 2004; Chalapathi Rao et al. 2014), but were ascribed to contamination of the kimberlite magma by a high load of lithospheric mantle-derived xenoliths and xenocrysts (e.g., Kopylova et al. 2007). Sub-ppb levels of PGE and Re with fractionated HSE patterns have been determined for carbonatites, with higher concentrations also presumably due to contamination by mantle materials (Widom et al. 1999; Graham et al. 2004; Xu et al. 2008). Indeed, cryptic metasomatism by low-volume melt has been shown to have little effect on the HSE systematics of mantle xenoliths having highly unradiogenic (enriched) Nd and which retained Os with an ancient melt depletion signature (Carlson and Irving 1994; Pearson et al. 1995c; Olive et al. 1997; Aulbach et al. 2014).

Consistent with a predominantly cryptic effect, metasomatic S addition—required to explain the elevated S contents in refractory cratonic peridotites—is not linked to the introduction of a major element, such as Al_2O_3 (Fig. 5; Pearson et al. 2004). Similarly, Se and Te concentrations in harzburgite xenoliths from northern Lesotho (SE margin of the Kaapvaal craton) do not correlate with Al_2O_3 (e.g., Lorand et al. 2003a) (Fig. 5). Metasomatic introduction of sub-micrometric tellurides containing little Os and Re has also been documented (König et al. 2014), but the, on average, distinctly low Se and Te concentrations in cratonic harzburgites indicate that very little of this type of secondary material has been added. Of course, the re-introduction of sulfides (where S is likely sited) or tellurides constitutes a form of modal metasomatism but is rarely treated as such if not also accompanied by changes to silicate mineralogy.

A feature of both cratonic residues and residues from other tectonic settings, is the wide variation of Ir and Os concentrations, far in excess of levels that can be generated by melt depletion for reasonable redox conditions during partial melting of convecting mantle (ΔFMQ $\leq$ 0) (Figs. 4A,B). Metasomatic effects may play a role here, such as (resulfidized) PGE alloy destabilization during post-formation open-system interaction with low-volume oxidizing melts. Indeed, the general assumption of low-volume melt extraction leaving behind sulfide-saturated sources is challenged by the presence of high and unfractionated relative abundances of the HSE in some low-degree melts, and preferential digestion of more fusible

components has been suggested before (Day, 2013). Such characteristics attest to efficient removal of sulfide (and PGE alloy) from their source at low *F*, under relatively oxidizing conditions (Mungall et al. 2006; Botcharnikov et al. 2013).

Kimberlites and carbonatites may form through redox reactions involving oxidizing fluids and deep, initially reducing and diamondiferous cratonic roots (Foley 2011). The imprint of minimally-fractionated, oxidizing silico-carbonatite and its destructive effect on diamond in the deeper lithosphere has been well-documented (e.g., Fedortchouk and Canil 2004; Creighton et al. 2008; Aulbach et al. 2013). As garnet-bearing cratonic mantle has a low oxygen buffering capacity, it is likely to record f_{O_2} related to the last metasomatic overprint prior to entrainment (Luth and Stachel 2014). The fluid-dominated imposition of f_{O_2} on most cratonic mantle roots appears to be reflected by the demonstration that many cratonic mantle sections are more oxidized than expected for depleted or primitive mantle at similar depths, due to melt metasomatism (Foley 2011). Thus, interaction with oxidizing melts may be a plausible mechanism to explain the strong IPGE depletions observed for many cratonic mantle samples, especially because the sampled xenoliths are, by default, the wall-rocks to melt flow channels. Alloy destabilization during elevated f_{O_2} conditions should produce coherent depletions in the IPGE, as observed for most cratonic and circum-cratonic mantle samples (Fig. 7A,B). This also implies that elevated HSE concentrations in carbonatites and kimberlites may be due to redox-driven assimilation of HSE in or near the mantle source region, and cannot be unambiguously ascribed to bulk digestion of entrained mantle fragments.

Sulfur-enrichment. Given the likely exhaustion of sulfide during lithosphere formation, the very high S contents of cratonic mantle xenoliths compared to orogenic and off-cratonic peridotites at similar Al_2O_3 contents, is striking (Fig. 5). This observation invites consideration of the specifically cratonic mantle setting, where the presence of a thick lithospheric lid enables interaction with volatile-rich, silica-undersaturated melts and fluids leading to a cryptic overprint. Evolving oxidized melts that scavenged PGE alloys and sulfides at deeper levels could be efficient metasomatic agents, eventually depositing S and HSE after continued interaction with reducing lithosphere. Deposition of S and HSE may also occur at shallower levels when these melts exsolve volatiles while entraining their wall rocks as xenoliths. Metasomatic precipitation of BMS has been documented in peridotite xenoliths from the Kaapvaal craton that have interacted with low-volume melts prior to and perhaps related to kimberlite magmatism (Lorand and Grégoire 2006; Giuliani et al. 2013) and are manifest as part of the ilmenite–rutile–phlogopite–sulfide (IRPS) group of metasomatic rocks (see review of rock groups in Pearson et al. 2005). Enrichments in the more volatile chalcophile elements (S, Pd, Re, Os, Au) in mantle peridotites, with superchondritic S/Se, Pd/Ir, Pt/Ir and Os/Ir, subchondritic Pt/Pd and variable $^{187}Os/^{188}Os$, were suggested to fingerprint this type of metasomatism (Alard et a. 2011; Lorand et al. 2013). A comparison of S with HSE concentrations in cratonic samples shows no clear co-variations, but some high Re, Pt and Pd concentrations appear to be tied to high S concentrations, especially for the very S-rich group of Kalahari xenoliths entrained in Group II kimberlites (Fig. 8), implying co-enrichment from the same metasomatic agent. High IPGE concentrations at high S contents may point to "resulfidation" of pre-existing PGE alloys, but they may also have been introduced from initially oxidizing, alloy-scavenging small-volume melts. If so, this implies that ancient, unradiogenic Os can be transferred in the cratonic lithosphere along with PGE alloy and deposited with S from the volatile-rich melt. While this may decouple Os isotope signatures from their host rocks, this process would represent a re-distribution of ancient ages within ancient cratonic mantle and would still yield meaningful minimum Re-depletion ages.

Despite elevated Re/Os (Fig. 9A), depleted (unradiogenic) Os isotopic signatures are documented in most cratonic peridotite samples, probably because the Os budget in cratonic mantle is controlled by a residual PGE alloy population or their "resulfidized" equivalents.

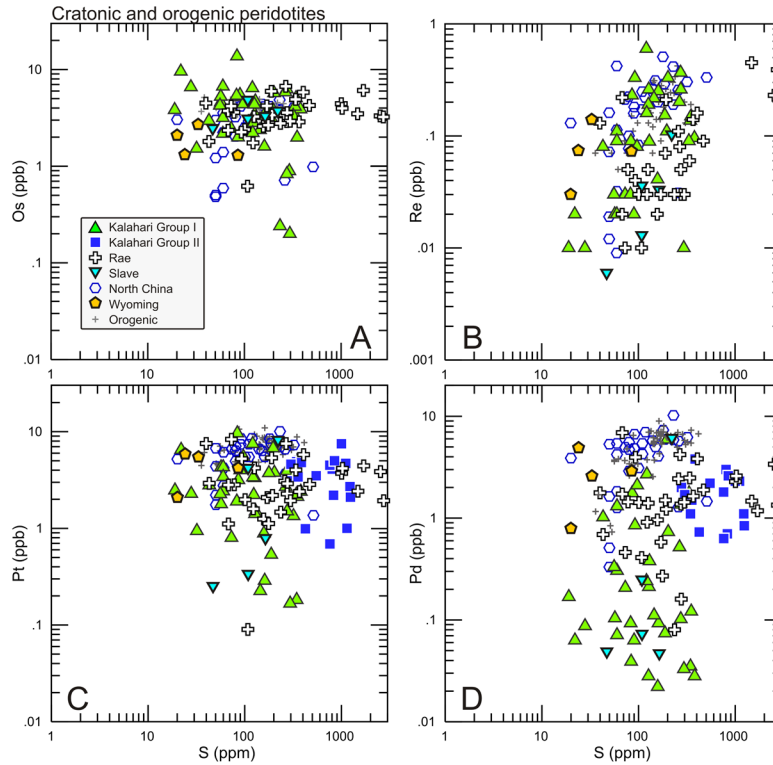

Figure 8. Whole-rock S against HSE concentrations for various peridotite classes. Other information as in Figures 3 and 5.

This is true even for very S-rich samples from Group II kimberlites (Fig. 9B), but requires that the Re addition frequently observed in these samples be a recent event (e.g., Carlson et al. 2005). The notion of late-stage Re enrichment, if not due to contamination with kimberlite in measured whole rocks, is consistent with a frequently recognized metasomatic event that is precursory to kimberlite magmatism, based on trace-element zoning (Smith and Boyd 1992; O'Reilly and Griffin 2013).

In summary, it is plausible that interaction with unfractionated, oxidizing low-volume fluids that typically infiltrate intact cratonic roots, caused loss of part of the HSE budget. Conversely, reaction with evolved low-volume melts may lead to S addition accompanied by increases in Pt, Pd, and Re, but without significant disturbance of the Archean Os isotope signatures.

Effects of mafic (silicate) melt metasomatism. Interaction with melts of basaltic composition is only possible in regions underlain by relatively thin lithospheric roots because such melts typically cannot form beneath the thick (~200 km) lithospheric roots present beneath most cratons. Thinned lithosphere can support a long enough melting column to generate relatively large-degree mafic rather than small-volume volatile-rich melts even at moderate T_P. This scenario applies to cratonic lithosphere where the deep root has been asthenospherized (e.g., the eastern North China craton), where xenoliths are typically entrained in alkali basalts rather than kimberlites. In addition to lithospheric

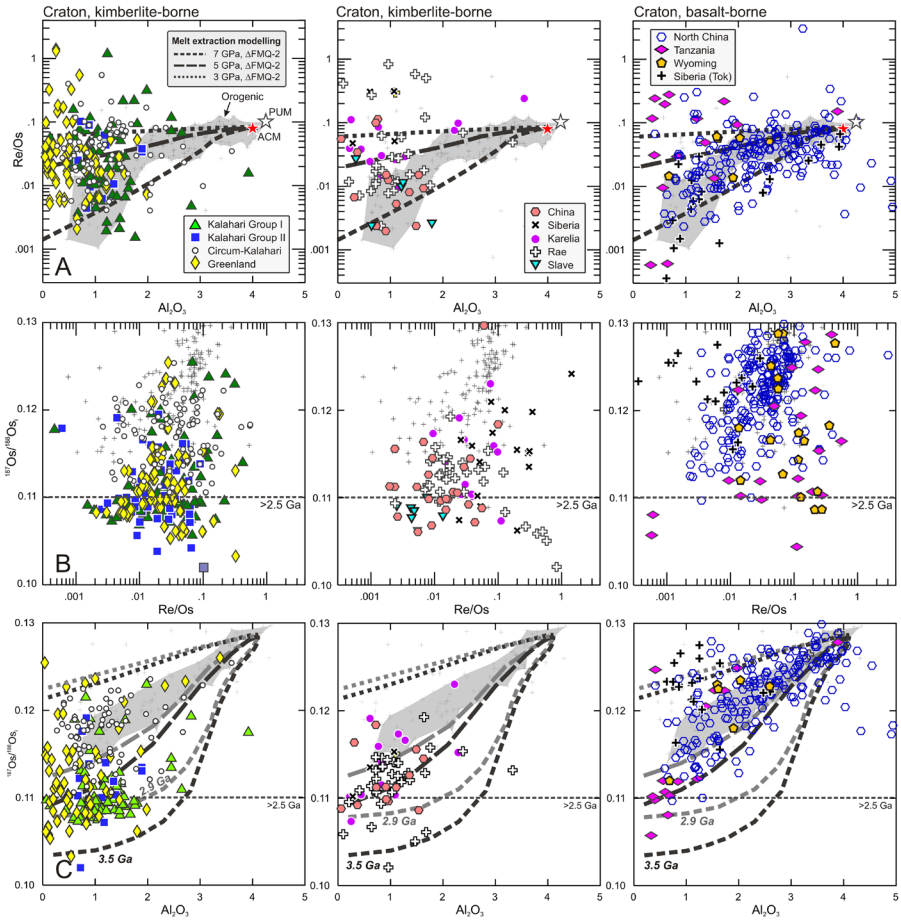

Figure 9. (A) Whole-rock Re/Os in various peridotite classes against Al_2O_3 (wt%), (B) $^{187}Os/^{188}Os$ against Re/Os, and (C) $^{187}Os/^{188}Os$ against Al_2O_3. Light grey thin stippled line labelled "2.5 Ga" shows the $^{187}Os/^{188}Os$ of chondritic mantle at the Archean-Proterozoic boundary. A reference Os isotope ratio of 0.1283 was chosen for the modelling in (C), which is the mean for ordinary chondrites and is intermediate between carbonaceous and enstatite chondrites (Horan et al. 2003), as a compromise that gives conservative results with respect to the PUM model of Meisel et al. (2001) without implying that enstatite chondrites are Earth's main building blocks. Shown for comparison in (C) is the calculated present-day $^{187}Os/^{188}Os$ of mantle formed at 3.5 and 2.9 Ga and evolving at Re/Os of residues after partial melting at P_i of 3, 5, and 7 GPa and $\Delta FMQ = -2$, as determined by melt extraction modelling, and shown in (A). Other information as in Figures 3 and 5.

thinning, unusually high T_P and/or fertile sources can enable the generation of high melt volumes despite the presence of a deep lithospheric lid, as proposed for the 2.05 Ga Bushveld intrusion, which has strongly affected the cratonic mantle—and Re–Os isotope systematics—beneath parts of the Kalahari craton (e.g., Shirey et al. 2002). Most mafic melts penetrating the deep lithosphere represent relatively small melt fractions ($\ll 20\%$) leaving a sulfide-saturated source, where the PGE plus Re will partition into the residual sulfide that is molten at the pressures and temperatures of basalt generation (Mungall and Brenan 2014). Thus, low concentrations of these elements are expected in the silicate melts, unless they contain physically entrained sulfide liquid (Bockrath et al. 2004b; Ballhaus et

al. 2006), a process argued to be highly unlikely by Chung and Mungall (2009) on the grounds that capillary forces would prevent entrainment of immiscible liquids during melt extraction from partially molten peridotite.

Due to the chalcophile behavior of the HSE, the main effects of interaction with mafic melts may be related to the introduction or removal of dissolved sulfur (sulfide). Considering the stronger dependence of sulfur content at sulfide saturation (SCSS) on pressure than on temperature (Wendlandt 1982; Mavrogenes and O'Neill 1999; Holzheid and Grove 2002), two end-member depth-dependent effects on the interaction of such melts with the mantle can be envisaged. First, at high pressure, while the melt is sulfide-saturated, S (and other chalcogens) may be added from the melt to depleted peridotite, and pre-existing PGM may be "resulfidized" (e.g., Griffin et al. 2002, 2004; Lorand and Grégoire 2006). Second, during ascent, as the melt becomes sulfide-undersaturated with decreasing pressure and increasing SCSS, peridotitic sulfide might be dissolved into the melt and stripped from the mantle (e.g., Hart and Ravizza 1996).

However, sulfide can also saturate from a sulfate- or sulfide-bearing silicate melt during ascent if S solubility limits are exceeded due to cooling, fractional crystallization of metasomatic minerals from the percolating liquid (decreasing melt volume), reduction of sulfate-rich magma (Thakurta et al. 2008), or assimilation of pre-existing sulfide in the mantle wall-rock (e.g., Lorand and Alard 2001; Wittig et al. 2010b). Hence, a simple gradient of sulfide/PGE alloy persistence in the deep root and scavenging in the shallow root may not develop, especially if superposed on the effects of interaction with oxidizing silica-undersaturated melts as discussed above. Nevertheless, it is possible that interaction with sulfide-undersaturated silicate melts resulted in the strong IPGE depletions exhibited by basalt-borne cratonic peridotite (e.g., Cenozoic North China craton xenoliths) and off-craton peridotite xenoliths. In particular, percolation at high melt-rock ratios should lead to IPGE depletion, imposition of melt-like $^{187}Os/^{188}Os$ (Lorand et al. 2013; Figs. 4A–C, 8B) and re-fertilization in magmaphile major elements such as Al and Ca. This type of interaction means that such apparently fertile peridotites should not be used in the estimation of Primitive Mantle HSE abundances (e.g., Lorand et al. 2013; König et al. 2014). Indeed, co-saturation of a mafic melt in cpx and sulfide can explain the observed correlation of S or $^{187}Os/^{188}Os$ with Al_2O_3 or cpx mode in orogenic peridotites and some mantle xenolith suites that experienced metasomatism (Lorand 1989; Pearson et al. 2004; Wittig et al. 2010b).

In other off-cratonic suites, such systematics are interpreted as melt extraction trends that did not proceed beyond sulfide and cpx exhaustion (Ionov et al. 2006; Janney et al. 2010). A distinction between these two possibilities is best achieved when considering a highly incompatible element, such as TiO_2, which shows different behavior during melt extraction vs refertilization (Niu 1997). However, xenoliths suites from most cratonic mantle sections show a distinct lack of Al_2O_3–$^{187}Os/^{188}Os$ correlations (Pearson et al. 2004; Maier et al. 2012; Figs. 4, 9C), possibly because sulfide saturation or undersaturation is not coincident with pyroxene saturation. In addition, invasion of the bulk xenolith by late-stage S and Ti-rich kimberlite melt during xenolith eruption and low-*T* contamination during emplacement are superimposed complications (Frick 1973; Lorand and Grégoire 2006).

Effects of incongruent sulfide melting. The conductive geotherm of the continental mantle suggests that once metasomatic fluids infiltrate the lithosphere, HSE redistribution during sulfide addition and removal is governed by mss-sulfide melt partitioning, where sulfide partial melts concentrate Pd, Pt, and Au (in addition to Cu and, under some conditions, Ni), whereas mss partitions Ru, Rh, Ir, Re, and Os (Li et al. 1996; Barnes et al. 1997; Ballhaus et al. 2001; Bockrath et al. 2004b; Mungall et al. 2005; Brenan 2008; Fonseca et al. 2011). This translates to marked HSE fractionation, which is not achieved if sulfide is completely molten.

In a seminal study, Alard et al. (2000) showed that in cratonic and other peridotites, primary sulfides enclosed in silicate minerals have high IPGE concentrations and low Pd/Ir, whereas interstitial metasomatic sulfides have complementary signatures. Later work has demonstrated that often there is no link between textural position and PGE or Re–Os isotopes systematics (Alard et al. 2011; Bragagni et al. 2014; González-Jiménez et al. 2014; Wainwright et al. 2015). Furthermore, Lorand and Grégoire (2006) point out that most mss enclosed in refractory silicate grains have Ni/Fe ratios that are too low to be consistent with equilibration with olivine at magmatic temperatures. Thus, although (re)-introduced sulfides would intuitively occur primarily as interstitial grains, metasomatic sulfides may become occluded in silicate or oxide minerals during recrystallization and therefore, sulfide inclusions cannot be taken as prima-facie evidence of their "primary" residual nature.

The introduction of sulfide melt into peridotite by sulfide-saturated silicate melt should lead to enrichments in Pd, Pt, Cu ± Ni, because they would be stripped from the silicate melt. There are few data from cratonic peridotites, but a trend of Ni enrichment with a weak change to Os concentrations observed for interstitial sulfide in eclogite xenoliths compared to sulfide included in silicates or diamond (Aulbach et al. 2009b; Fig. 6) may attest to metasomatic addition of an IPGE-poor sulfide liquid. High Pt and Pd concentrations at low Pt/Pd are observed in massif peridotites. This signature could be consistent with pentlandite addition, a metasomatic sulfide mineral, which forms from sulfide melts and partitions Pd over Pt, showing strong negative Pt anomalies in chondrite-normalized PGE patterns (Lorand et al. 2013). Thus, addition of a sulfide liquid, as an independently moving melt or precipitating from sulfate-bearing silicates through redox-reactions, should lead to co-enrichment of Pd and Pt, maintaining low Pt/Pd, whereas metasomatism by fluids could be accompanied by enrichment in Pd without enrichment in Pt. Several cratonic samples have both high Pt and Pd concentrations at depleted Al_2O_3 suggestive of sulfide melt addition (Figs. 4D,E). However, for many samples, some degree of secondary Pd and Pt addition is probably hidden in their overall depleted PPGE systematics, leading to apparently lower melt extraction pressures when compared against modelled residues. These superposed effects may be unravelled when bulk-rock HSE systematics are used in concert with sulfide mineralogy and in situ analytical techniques, but such data are seldom reported.

Plume impingement and rifting. Some 40 km of the deep Kaapvaal craton root was strongly refertilized in the Cretaceous during interaction with asthenosphere-derived broadly basaltic to hydrous alkaline melts, perhaps related to impingement of a plume at the base of the lithosphere that ultimately also caused group I kimberlite magmatism (Boyd 1987; Smith and Boyd 1987; Griffin et al. 1996; Grégoire et al. 2003; Le Roex et al. 2003; Becker and Le Roex 2006; Kobussen et al. 2008; O'Reilly and Griffin 2010). Despite this, some sheared garnet peridotites, which sample the deep, hot and more fertile cratonic root, retain unradiogenic Os isotope compositions with Archean minimum ages, precluding wholesale loss of cratonic lithosphere (Walker et al. 1989; Pearson et al. 1995b). The original Os budget was possibly not erased because strong depletion even in the deeper surviving cratonic mantle (assuming that yet deeper, more fertile portions have been lost; Arndt et al. 2009) enables retention of IPGE in alloys and/or olivine, as also evidenced by other peridotite suites that were pervasively percolated by basaltic melts (e.g., Marchesi et al. 2010; Harvey et al. 2011). The retention of Archean and Paleoproterozoic ages in the deeper portions of the Kaapvaal craton, and perhaps also the surrounding mobile belts, are examples of incomplete thermochemical erosion of cratonic subcontinental lithospheric mantle that did not, however, result in observable rifting.

Some xenoliths from Obnazhennaya in the central Siberian craton, which have been entrained after the thermal climax of the Siberian plume, display radiogenic Os-isotope ratios (percent deviation of the sample from chondritic mantle at the time of formation = $\gamma_{Os} > -1$) combined with Pd depletions and high olivine Mg#, consistent with newly formed

residues associated with plume impingement (Pernet-Fisher et al. 2015). Some samples retain Archean T_{RD}, indicating that, as in the case of the Kaapvaal craton, plume impingement did not completely destroy ancient lithospheric signatures. The incomplete removal of cratonic mantle is consistent with dynamic modelling of the combined effects of metasomatism and plume impingement (Wang et al. 2015), and attests to the robustness of cratonic lithosphere even during extreme thermo-mechanical erosion.

Conversely, there are several examples of rift-related, thinned cratonic roots that have been strongly affected by melt infiltration followed by sampling as basalt-borne xenoliths. The mantle keel beneath the central Tanzanian craton appears to remain largely intact, but development of the East African Rift, combined with earlier Proterozoic collision, has led to disruption and thinning of the craton margins. Interaction with dry carbonatitic to basaltic melts caused strong enrichments in CaO and FeO, respectively, and oxidation compared to less overprinted samples (Rudnick et al. 1993, 1994; Ritsema et al. 1998; Lee and Rudnick 1999). Peridotite xenoliths derived from the lithosphere to a depth of ~140 km yield Archean T_{RD}, whereas those derived from greater depth have Os that is more radiogenic, approaching convecting-mantle (plume) Os isotope compositions; modally metasomatized peridotites and replacive dunites experienced recent Re addition and introduction of radiogenic Os, respectively (Chesley et al. 1999; Burton et al. 2000). Basalt-borne xenoliths from Tok (Stavonoy-Aldan Block, SE margin of the Siberian Craton) also comprise a high abundance of Fe-rich peridotites and wehrlites, where alumina and $^{187}Os/^{188}Os$ correlate for the less-metasomatized samples that give an Archean model age, whereas strongly metasomatized xenoliths have more radiogenic Os, in cases associated with elevated Pd and Pt, although the cause of the lithosphere thinning is uncertain (Ionov et al. 2005a,b, 2006). Peridotite xenoliths from the Moroccan Atlas mountains, which may have been underlain by a cratonic root prior to rifting and orogenesis, show evidence for co-precipitation of cpx and sulfide from a melt that led to positive co-variations of Ir with Cu and of $^{187}Os/^{188}Os$, Re, and Ir with Al_2O_3 (Wittig et al. 2010b). Magmatism beneath the Atlas has been ascribed to mantle plume flow, but, alternatively, this region may have been affected by craton-edge driven convection currents (Kaislaniemi and van Hunen 2014).

These examples demonstrate that although the Os isotope signature of lithospheric mantle in rift settings is sometimes impervious to melt percolation (e.g., Massif Central, Central European Volcanic Province; Harvey et al. 2010), the IPGE and Os isotopes are in other cases strongly modified, depending on the severity of the metasomatic overprint. The occasional persistence of strongly unradiogenic Os isotope signatures also in deeper rift-related cratonic xenoliths and/or constituent sulfides appears to indicate the survival of ancient lithosphere and argues against whole-sale loss of cratonic roots. Unfortunately, it is difficult to ascertain whether in any of these examples, xenoliths with mildly unradiogenic to primitive or radiogenic Os are a testament to the replacement of portions of the cratonic lithosphere by isotopically heterogeneous asthenospheric mantle, or whether they represent strongly overprinted, but still intact cratonic lithosphere (Pearson et al. 2004; Rudnick and Walker 2009; Janney et al. 2010; McCoy-West et al. 2013).

Modification during Craton Margin Processes—Subduction

Mantle sources modified by crustal recycling may have yielded boninite-like melts, precipitating mafic–ultramafic cumulates with associated chromitites and in some cases PGE mineralization, as early as the Paleo-Archean (Greenland: Bennett et al. 2002; Polat et al. 2002), Meso-Archean, (Pilbara: van Kranendonk et al. 2010; India: Khatun et al. 2014) and Neo-Archean (Superior: Polat and Kerrich 2001; North China: Polat et al. 2005). Though in some cases contested, the identification of mélange complexes and juxtaposition of contrasting lithotectonic elements in these, and other cratonic, regions have been taken as firm evidence for a transition to Phanerozoic-style plate tectonics (Shervais 2006). Thus, in contrast to the diamond inclusion record, which has been interpreted to reflect the initiation of subduction in the Neo-Archean (Shirey and Richardson 2011), the crustal record suggests that cratonic

mantle may have been affected by plate interactions from the Paleo-Archean onwards, during its amalgamation from early continental nuclei and/or during later collisions, leading to larger cratonic landmasses (e.g., Bleeker 2003). Such continental collisions have been suggested to represent the main mode of cratonic mantle thickening (Jordan 1975; Tainton and Mckenzie, 1994; Canil 2004; Lee 2006; Pearson and Wittig 2008, 2014; Lee et al. 2011).

Radiometric dating of eclogite xenoliths or related inclusions in diamond has yielded ages that can be linked to regional tectonothermal events and accretionary processes during craton amalgamation or at the craton margins. This is true for the Kaapvaal, Slave and Siberian cratons, where the presence of radiogenic initial $^{187}Os/^{188}Os$ in some sample suites (γ_{Os} of +45 for Kaapvaal, +14 for Slave and +2.2 for Siberia) is consistent with ingrowth of ^{187}Os in a high-Re/Os crustal precursor prior to eclogitization (Pearson et al. 1995a; Richardson et al. 2001, 2004; Shirey et al. 2001; Barth et al. 2002; Menzies et al. 2003; Aulbach et al. 2009a,b; Wiggers de Vries et al. 2013). Voluminous fluid emanating from subducting oceanic mantle undergoing serpentinite breakdown has been linked to 1.85 Ga eclogites from the Slave craton, and was proposed induce both eclogitization of the overlying oceanic crust and to generate diamonds entrapping sulfides with nearly homogeneous and radiogenic initial $^{187}Os/^{188}Os$ (Aulbach et al. 2009a). Higher median Os concentrations in ancient mantle eclogite xenoliths (0.3 ppb) compared to young orogenic eclogites (0.011 ppb; Table 1; Fig. 3) are consistent with formation of the former during higher degrees of partial melting, or may in part also be due to metasomatic effects. For example, the secondary deposition of Ni-rich sulfides in mantle eclogite (Aulbach et al. 2009b) is suggested by lower average Os concentrations of sulfides included in diamond (Table 1)

If the mantle wedge is an oxidizing environment, sulfide will be destabilized, giving rise to arc basalts with high Os and Re concentrations compared to melts originating from more reduced mantle due to the lithophile element behavior of Re at high f_{O_2} (Fonseca et al. 2007; Righter et al. 2008). A corollary of this is that lithospheric mantle affected by accretionary processes may be relatively depleted in Re and Os, depending on whether and when mantle wedges became oxidized, as discussed again later. Indeed, lower Os contents coupled with radiogenic Os are observed for peridotite xenoliths from Phanerozoic arc mantle. These peridotites are characterized by high PPGE/IPGE, Pt/Pd and Ru/Ir signatures suggested to be due to interaction with oxidizing, Cl- and ^{187}Os-enriched fluids that scavenged Os and some or all of the sulfide (Brandon et al. 1996, 1999; McInnes et al. 1999; Peslier et al. 2000a,b; Kepezhinskas et al. 2002; Widom et al. 2003; Saha et al. 2005). Such signatures are observed in some cratonic mantle samples (Fig. 10). Interactions between sulfate-rich aqueous subduction fluids and reducing cratonic mantle mineral assemblages might lead to deposition of S as sulfide, with the potential for large increases in S concentration accompanied by increased f_{O_2} up to but not exceeding that of the sulfide-sulfate fence (Mungall 2002; Jugo et al. 2010). Thus, such fluids can also generate bulk rocks with elevated S/Se, as exhibited by cratonic xenoliths (Fig. 5), because of the differential solubility of these elements (Lorand et al. 2003a).

Sulfur concentrations in eclogite xenoliths from the Kaapvaal craton range from 50 to 2000 ppm and although sulfide has been suggested to be of metasomatic origin in the majority of samples (Group I), their average S concentrations are indistinguishable from those in unmetasomatized Group II eclogites (Gréau et al. 2013). The upper limit of S concentrations in eclogite xenoliths is similar to those in basalts and basaltic eclogites with oceanic crust precursors (Dale et al. 2009), whereas the low end of S concentrations may indicate that sulfide that was originally present has been lost, potentially during subduction, along with Se and Te hosted in the sulfides, which control the abundances of these elements in eclogites (Aulbach et al. 2012).

Assuming some form of plate tectonics operated at the time of craton formation and growth, subducting oceanic crust is expected to have more efficiently melted due to higher mantle potential temperatures indicated for the Archean; such melts have been linked to early

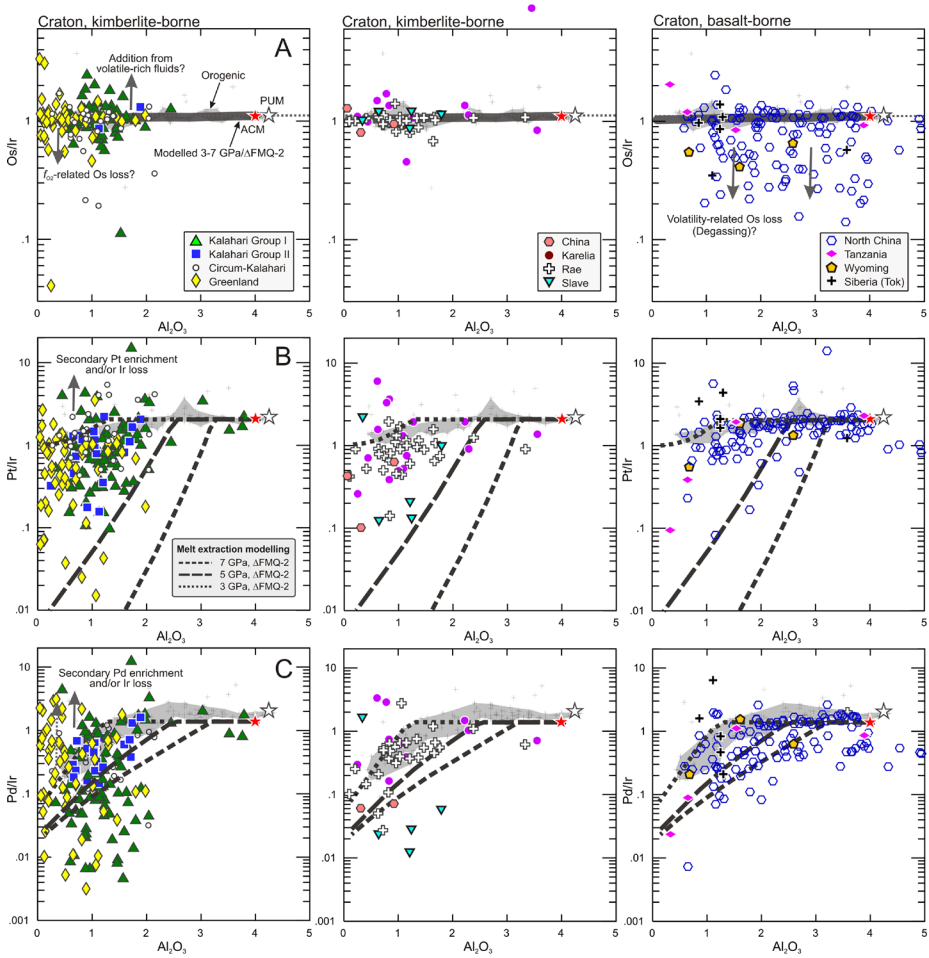

Figure 10. (A-C) Whole-rock PGE/Ir in various peridotite classes against Al_2O_3 (wt%) as a melt depletion index. Shown for comparison are melting contours as described in the text and displayed Figure 11. Other information as in Figures 3 and 5.

continental crust formation (e.g., tonalite–trondhjemite–granodiorite complexes; Martin et al. 2005). However, because slab-derived melts are sulfide-saturated, they are not likely to be efficient carriers of a slab signature with regard to the HSE, which will be largely retained in the sulfide-bearing residue (Chesley et al. 2004; Jégo and Dasgupta 2014; Mungall and Brenan 2014). The interaction of siliceous slab-derived fluid with peridotite would lead to the formation of opx at the expense of olivine and the generation of lithologies ranging from opx-rich harzburgites and lherzolites to websterites to pyroxenites (Rudnick et al. 1994; Kelemen et al. 1998; Yaxley and Green 1998; Rapp et al. 2010). The expected effect on the HSE would be dilution and perhaps mildly increased $^{187}Os/^{188}Os$. A peculiarity of some cratons (Kaapvaal and Siberia) is the opx-rich nature of the shallow lithosphere (Boyd 1989; Boyd et al. 1997), which has been ascribed by some to introduction siliceous, slab-derived fluids (Kesson and Ringwood 1989; Kelemen et al. 1998; Bell et al. 2005). A weak positive correlation between opx modes and $^{187}Os/^{188}Os$ for peridotite xenoliths from the Kaapvaal craton has been

tentatively linked to introduction of a subduction fluid during 2.9 Ga craton amalgamation (Simon et al. 2007), although the expected dilution of HSE contents is not observed for opx-rich xenoliths from the Kaapvaal craton (data-set of Maier et al. 2012). The formation of pyroxenite xenoliths from the Slave and Superior cratons, with compositions intermediate between eclogites and peridotites and initial $^{187}Os/^{188}Os$ ranging from unradiogenic to radiogenic, has been ascribed to reaction of peridotites with slab-derived melts that could be linked to craton-margin processes (Aulbach et al. 2009b; Smit et al. 2014b).

Considering that eclogites and pyroxenites constitute high-Re/Os environments that will very rapidly evolve to radiogenic $^{187}Os/^{188}Os$ (e.g., Shirey and Walker 1998), it is clear that the reaction of these lithologies with cratonic mantle, either by mechanical mingling, melt transfer or isotopic equilibration aided by the percolation of fluids, could lead to mantle regions with elevated $^{187}Os/^{188}Os$, disturbed Re–Os isotope systematics and increases in Pt and Pd. For ancient cratonic peridotites, the disentangling of the signatures of these subduction-related processes from those related to the infiltration of convecting mantle-derived decompression melts is challenging and requires precise Re–Os isotope ages that correlate with known regional collisional events.

Subduction-related hydration, lithosphere weakening and delamination. In recent years, increasing attention has been paid to the role of water in the destabilization of cratons and its link to subduction, either through direct fluid-transfer into the mantle wedge or dehydration from deeply subducted slabs that are stalled in the transition zone (Windley et al. 2010; Kusky et al. 2014; Pearson et al. 2014; Wang et al. 2014). The North China craton (NCC) may be the most prominent example of cratonic lithosphere destruction. The dramatic reduction in lithospheric thickness is evident from a comparison of mantle xenoliths entrained in Paleozoic kimberlites, which attest to the presence of a thick and cool diamondiferous cratonic mantle keel giving Archean to Paleoproterozoic T_{RD} ages, with Cenozoic basalt-borne xenoliths sampling a considerably hotter, thinner mantle root that gives Proterozoic and younger T_{RD} ages (Menzies et al. 1993; Griffin et al. 1998; Fan et al. 2000; Gao et al. 2002, 2009). There are competing hypotheses to account for this striking loss of cratonic lithosphere, including rheological weakening and destabilization by injection of water from multiple subduction zones (e.g., Tang et al. 2013). The deeper mantle beneath the central craton may have been replaced during continental collision at ~1.9 Ga (Gao et al. 2002). Particularly strong tectonic erosion in the Mesozoic is recorded in the eastern NCC, and a wealth of $^{187}Os/^{188}Os$ data now available suggests that the destruction may have been diachronous, occurring earlier in the east and later in the west (Liu et al. 2011). Relatively high Ru/Ir and Pd/Ir, similar to those of orogenic peridotites, are suggestive of the presence of newly accreted, asthenospheric mantle (Zheng et al. 2005; Liu et al. 2010), which was likely affected by melt percolation. This major disruption of the North China Craton means that the compiled Os isotope ratios and resulting T_{RD} ages from this craton show much greater bias towards non-Archean ages than any other craton (Fig. 9B).

The cratonic mantle beneath the western USA, including the Mojavia and Wyoming cratons, which were affected by subduction of the Farallon plate beneath western North America, is unusually thin, fertile and hydrated (as indicated by abundant glimmerite xenoliths), suggesting removal of the deeper lithosphere due to metasomatism (Lee et al. 2001; Lee 2005; Li et al. 2008). The remaining shallow cratonic root persists despite strong refertilization and retains Os isotope evidence for NeoArchean to Paleoproterozoic formation (Lee et al. 2001), as is true also for the North China craton (Sun et al. 2012). Peridotite and websterite xenoliths from the thinned Wyoming craton root also retain some highly unradiogenic Os with Archean T_{RD}, but most samples give younger, overprinted ages (Carlson and Irving 1994).

Thus, as is true for cratons affected by plume impingement leading to melt infiltration due various degrees of stretching (Kaapvaal) up to rifting (Tanzania), interaction with subducted slabs will lead to overprints on Re–Os isotope and HSE systematics that are indistinguishable from those off-cratonic mantle (Figs. 4, 9). The main difference appears to lie in Os isotope

signatures that sometimes preserve a memory of Archean lithosphere formation in the disrupted cratonic roots, due to incomplete thermochemical erosion, but a loss of this signature in deep Archean roots that were affected by subduction-related hydration weakening, delamination and replacement by asthenospheric mantle. All these results are in keeping with recent dynamical modelling that indicates the necessity of metasomatism (probably hydrous) in weakening and removing the lower sections of lithospheric roots and yet still preserving some portion of an original ancient keel (Wang et al. 2015).

MODELLING OF PRIMARY VS. SECONDARY HSE SIGNATURES IN CRATONIC MANTLE

Here, a published model is used to constrain the distribution of Ru, Pd, Ir, and Pt between mantle restite phases and primary silicate melts, where HSE concentrations of residues are determined as a function of P_i (T_P) and f_{O_2} (Mungall and Brenan 2014), with the aims to (1) determine whether HSE systematics are useful indicators of the pressures and f_{O_2} of melt extraction and hence melting environment, (2) determine at which level of depletion Re will be quantitatively removed from the mantle allowing determination of accurate T_{RD} by using proxies less susceptible to overprint and (3) compare natural samples to modelled melting residues in order to distinguish between those that have possibly retained primary residual characteristics from those that have been affected by secondary processes. The Re and Os concentrations were modelled in accordance with the rationale outlined in Mungall and Brenan (2014), with further details given below. For this exercise to be useful, it is first necessary to review the constraints on the initial HSE concentrations, i.e., those of the Archean convecting mantle from which cratonic lithosphere formed.

HSE Concentrations of the Archean convecting mantle (ACM)

Taking modern mantle, as represented by orogenic peridotites, as the benchmark (median Ir = 3.5 ppb, Os = 3.8 ppb, Pt = 6.9 ppb, and Pd = 5.7 ppb), kimberlite-borne xenoliths have strikingly lower median concentrations of all PGE (Ir = 3.1 ppb, Os = 3.1 ppb, Pt = 2.8 ppb, and Pd = 1.2 ppb, respectively; Fig. 3 and Table 1), an observation that has been made before (Maier et al. 2012). Basalt-borne cratonic xenoliths appear to be affected by strong, secondary IPGE depletions, similar to younger off-cratonic xenoliths, which therefore are unlikely to relate to original mantle PGE concentrations, as discussed earlier. The large variability of HSE contents in usually small samples of cratonic peridotite xenoliths may in part reflect control of IPGE by HSE-rich nanometer size nuggets (e.g., Luguet et al., 2007; Lorand et al. 2013) due to melt extraction well beyond sulfide stability. Effects due to inhomogeneous distribution of PGM or to incomplete digestion may be excluded at least for those cratonic mantle xenoliths where low PGE concentrations were reproduced by multiple dissolutions (e.g., Irvine et al. 2003), although the nugget effect can occur at various scales and need not be detected from multiple digestions from the same aliquot powder. At any rate, the median concentrations calculated for kimberlite-borne cratonic peridotites should be robust against such outliers.

Barring artefacts related to the nugget effect, the depletion of cratonic mantle relative to modern convecting mantle may have several causes: (1) It is possible that very low IPGE concentrations in some kimberlite-borne cratonic peridotites relate to secondary, metasomatic effects; (2) The high HSE concentrations in orogenic peridotites are in part caused by secondary refertilization; (3) It may be the signature of a reservoir that was depleted by core formation and was subsequently incompletely mixed with incoming accreted material (Maier et al. 2009, 2012). If we are to successfully model primary residual HSE concentrations in the newly-formed lithosphere and to confidently distinguish them from secondary effects, initial HSE concentrations (C_0) must be better constrained, the rationale for which is laid out in the following.

Knowing the initial concentrations—C_0—of HSE of the undifferentiated "Primitive Upper Mantle (PUM)" is one of the most sought after and yet difficult to define goals of mantle

geochemistry. Much of the problem stems from the fact that almost all samples of mantle that are available have been subject to various types of secondary modification. Notwithstanding this, all parts of the upper mantle have undergone partial melting episodes at some stage during Earth history (e.g., Allègre et al. 1995), so estimating a "primitive" composition necessitates selecting a suite of rocks from which a minimally melted "original" composition can be estimated.

A currently widely used model is based on the Re–Os isotope systematics and HSE concentrations of variably depleted xenoliths and massif peridotites, with suggested concentrations of 3.5 ppb Ir, 3.9 ppb Os, 7.6 ppb Pt, and 7.1 ppb Pd (Table 2) (Meisel et al. 1996; Becker et al. 2006; Fischer-Gödde et al. 2011; Wang et al. 2013). In recent years, it has been cautioned that this PUM model introduces a bias in that orogenic peridotites, from which these estimates are mostly drawn, are variably depleted, strongly melt-metasomatized and refertilized rocks with harzburgite protoliths (Le Roux et al. 2007; Lorand et al. 2009, 2010, 2013; Alard et al. 2011). Similarly, it has been suggested that near chondritic chalcogen ratios in orogenic and xenolithic peridotites reflect ubiquitous refertilization of variably depleted residual mantle containing mss ± PGE alloys plus metasomatic sulfides and tellurides (König et al. 2014, 2015). The effects of mafic melt infiltration are evident in the presence of texturally late spinel and pyroxene clusters, metasomatic pentlandite and ubiquitous pyroxenite dikes, and in linear correlations for incompatible elements with vastly different distribution coefficients, which is inconsistent with simple melt extraction (Lorand et al. 2013).

The refertilized nature of the samples on which PUM is based not only makes them unsuitable for modelling the concentrations of partial melts and their complementary residues, but also raises doubts over suggestions that their non-chondritic relative abundances relate to late accretion of an unknown meteorite component (Pattou et al. 1996; Becker et al. 2006; Fischer-Gödde et al. 2011). In addition, it is problematic that the PUM estimate results in markedly higher Pd/Ir and Ru/Ir than those of various chondrites classes (Horan et al. 2003), which are considered building blocks of Earth and components of the Late Veneer (e.g., Day et al. 2012, 2016, this volume). The non-chondritic ratios in orogenic peridotites, many of which appear to sample supra-subduction zone mantle, may be the result of metasomatic addition of Cu–Ni-rich sulfide melt that later crystallises pentlandite (Alard et al. 2000; Lorand and Grégoire 2006) and chromite accumulation, given the affinity of Ru for Cr-rich spinel (Righter et al. 2004; Brenan et al. 2012).

Table 2. HSE (ppb) and Al_2O_3 (wt%) concentrations in chondrites and models for various terrestrial reservoirs.

	Orgeuil[1]	**DM[2]**	**PUM[3]**	**Orogenic[4]**	**Orogenic/ chondritic[5a,6]**	**ACM[5b,6]**
Ru [Ru/Ir]	627 [1.5]	5.7 [2.0]	7.1 [2.0]	7.2	5.3	4.7
Rh [Rh/Ir]	130 [0.3]	1 [0.3]	1.2 [0.3]	1.1	1.1	0.9
Pd [Pd/Ir]	567 [1.4]	5.2 [1.8]	7.2 [2.1]	6.4	4.8	4.3
Re [Re/Ir]	36.6 [0.1]	0.16 [0.1]	0.4 [0.1]	0.3	0.31	0.27
Os [Os/Ir]	450 [1.1]	3 [1.0]	3.9 [1.1]	3.6	3.8	3.4
Ir	418 [1.0]	2.9 [1.0]	3.5 [1.0]	3.6	3.6	3.1
Pt [Pt/Ir]	872 [2.1]	6.2 [2.1]	7.7 [2.2]	7.4	7.4	6.5
Au [Au/Ir]	149 [0.4]	1 [0.3]	1.7 [0.5]	1.3	1.3	1.2
Al_2O_3	4.28	4.25	3.75–4.0	4	4	

[1]Fischer-Gödde et al. 2010; [2]Depleted Mantle, Salters and Stracke 2004; [3]Becker et al. 2006, Fischer-Gödde et al. 2011; [4]This study, using median concentrations from filtered dataset for orogenic peridotites; [5]This study, using Ir concentration and chondritic relative abundances (Orgeuil) (a) from least depleted orogenic peridotite and (b) from median kimberlite-borne peridotite and suggested to represent the Archean Convecting Mantle ACM (see text for details); [6]Al_2O_3 from Jagoutz et al. (1979) and Hart and Zindler (1986). Values in parentheses are Ir-normalised.

Nevertheless, because orogenic lherzolites are by far the "best-behaved" in terms of producing coherent trends of PGE concentrations versus melting indices such as Al_2O_3 (Reisberg and Lorand 1995; Pearson et al. 2004; Fig. 4), they might be considered the most suitable samples from which to extract convecting mantle compositions. We derived an estimate after careful examination and exclusion ("filtering") of samples showing evidence for secondary effects related to refertilization discussed above, to incomplete digestion/recovery, to analytical artefacts or having statistically anomalous abundances. A median was taken from the resulting subset of samples that have Al_2O_3 contents in the interval between 3.5% and 4.06%, i.e., up to the value suggested for PUM (Jagoutz et al. 1979; Hart and Zindler 1986). The results from this exercise (Table 2; Os = 3.6 ppb, Ir = 3.6, ppb, Ru = 7.2 ppb, Rh = 1.1 ppb, Pt = 7.4 ppb, Pd = 6.4 ppb) show that even in a judiciously filtered data-set, Pd and Ru appear to be implausibly high relative to a chondritic starting material and may be compromised by melt refertilization.

Sub-PUM PGE concentrations (Ir = 2.9 ppb, Os = 3.0 ppb, Pt = 6.2 ppb, and Pd = 5.2 ppb) have been presented for the depleted mantle (DM), based on average concentrations in ophiolites, abyssal peridotites and orogenic peridotites (Salters and Stracke 2004), which likely also include samples affected by melt percolation. If the DM composition reflects extraction of 2–3% partial melt from the primitive mantle (Workman and Hart 2005), then the effect on the PGE and Re should be negligible because the presence of residual sulfide at such low degrees of melt depletion would effectively prevent depletion of all HSE except Au (e.g., Keays, 1995; Mungall and Brenan 2014). Despite this, based on relatively constant Re/Yb in MORB, a Re concentration of 0.157 ppb is provided by Salters and Stracke (2004), which generates subchondritic and sub-PUM $^{187}Os/^{188}Os$ for the present-day DM.

Can C_0 be better constrained, at least for the Archean mantle? Assuming that the IPGE concentrations in kimberlite-borne cratonic xenoliths are least affected by secondary enrichment (as evidenced by the retention of depleted Os isotope signatures), and since the concentrations of compatible elements weakly increase with increasing degree of depletion, a maximum concentration for the HSE can be estimated using the median Ir of 3.1 ppb for this peridotite class (Table 1). The concentrations of the other HSE are calculated assuming chondritic relative abundances, resulting in Os = 3.3 ppb, Pd = 3.7 ppb and Pt = 6.9 ppb (Table 2). Iridium was chosen because it appears to be less affected by secondary processes than Os, as evidenced by much lower variance of Ir in the kimberlite-borne peridotite dataset. Modelling presented below shows that Ir remains compatible with combinations of alloy and olivine in the restite throughout the melting interval responsible for generating cratonic mantle. Uncertainties remain regarding the nature of the late accreted material, as different chondrite classes show significant differences in HSE abundances (Horan et al. 2003; Day et al. 2016, this volume). Nonetheless, we feel that this initial estimate of the ACM starting composition may be the one that is the least compromised by metasomatism and secondary alteration. For the modelling that follows, these new values will be combined with an Al_2O_3 concentration of 4 wt% in keeping with suggested values of 3.97 wt% (Jagoutz et al. 1979) and 4.06 wt% (Hart and Zindler 1986), which are based on the least depleted specimens in a suite of ultramafic xenoliths and comparison of chondritic and mantle peridotitic fractionation trends.

Modelling Rationale

In order to use the HSE to constrain conditions of formation and modification of the cratonic lithosphere, not only must the HSE composition of the Archean mantle source be well constrained, but HSE fractionation(s) related to partial melting must be defined and HSE carriers in such restitic peridotites must be correctly and unambiguously identified. We address the behavior of HSE during partial melting by considering their distribution between sulfide melt, silicate melt, and solid restite phases including silicates and alloys using equilibrium partition coefficients. This approach is complemented by a consideration of alloy solubility, which takes into account that PGE are major elements in alloys, for which the use of a limiting metal solubility is more

appropriate than a simple Nernst partition coefficient (Mungall and Brenan 2014). The model assumes a dry, primitive mantle (PM) source with initial HSE concentrations for "primitive" ACM discussed above. This ignores the possibility of mantle source heterogeneities, such as the presence of pyroxenites or early-depleted mantle portions, which have been inferred from the trace-element and isotopic composition of komatiites and cratonic mantle (e.g., Sobolev et al. 2007; Arndt et al. 2008; Aulbach et al. 2011; Fiorentini et al. 2011). We note, however, that the extent and abundance of such heterogeneity in the Archean mantle should be considerably smaller than that evident in today's mantle following 3 Ga of subduction processing.

The behavior of the HSE during partial melting depends on a range of parameters including bulk composition, oxygen and sulfur fugacity, as well as pressure and temperature (Mungall and Brenan 2014, and references therein). Assuming the shallow portion of the cratonic mantle to be the result of picritic melt extraction at hot ridges (T_P 1500–1600 ºC according to the T_P evolution of Korenaga 2008), with average melt fractions (F) of ~0.3 and initial and final melting pressures of 3–5 GPa and 1–2 GPa, respectively, a mantle lithosphere of 85–135 km is formed, in addition to the crust (Herzberg et al. 2010). Plume subcretion beneath a pre-existing shallow cratonic nucleus or melting to shallow pressures is assumed to occur at excess T_P of 1600–1900 ºC and pressures of up to 10 GPa, whereby the plume would exhibit an internal temperature structure with a hot conduit and cooler periphery (Herzberg and O'Hara 1998; Herzberg et al. 2007, 2010). Komatiites representing ca. 30–50% partial melts (Al-undepleted komatiites) would only be extracted from the shallower portion of the melting column that experienced large melting intervals, leaving a residue of harzburgite to dunite at 100–150 km depth. Basalts and picrites would be extracted either at lower T_P (ambient or cool plume), from the cooler periphery of buoyantly upwelling mantle or from the deeper portions of the melting column, leaving a residue that changes from lherzolite to harzburgite to dunite as F increases (Herzberg et al. 2010).

Given the above, it is useful to model HSE concentrations for a range of P_i and corresponding T_P. High degrees of melting applicable to cratonic lithosphere formation are not accessible to the lower-pressure melting paths (1–2 GPa) because decompressing mantle reaches the surface after $F < 0.2$. We will limit our discussion to $P \geq 3$ GPa, corresponding to a range from ambient to excess T_P according to the model of Korenaga (2008), but to excess T_P according to the model of Davies (2009). Pressure during adiabatic decompression is allowed to vary as a function of F, using the parameterization of Iwamori et al. (1995). The solidus temperature for dry melting and the adiabatic melting path of 50 ˚C/GPa were parameterized from Herzberg and O'Hara (2002). At these conditions, the decompressing mantle intersects the surface at $F = 0.6$ for $P_i = 7$ GPa, $F = 0.46$ for $P_i = 5$ GPa, and $F = 0.27$ for $P_i = 3$ GPa, although we note that the final pressures would be dictated by the thickness of the pre-existing lithosphere and the exhaustion of fusible components, which may limit melt production after melting intervals corresponding to 3–4 GPa (Herzberg et al. 2010).

Due to the siderophile and chalcophile character of the HSE, sulfides, PGE alloys and iron-nickel metals—if present—play dominant roles in determining the bulk distribution coefficient during partial melting. As described before, the sulfur solubility in the extracted silicate melt at sulfide saturation (sulfur concentration at sulfide saturation: SCSS) depends predominantly on pressure and FeO concentration in the silicate melt, and less on temperature (Wendlandt 1982; Mavrogenes and O'Neill 1999; Holzheid and Grove 2002; Liu et al. 2007). Given the dependence on FeO, there is an indirect control of f_{O_2} on SCSS in that it determines the ratio of FeO to Fe_2O_3. Thus, a term for Fe_2O_3 has been added to the calculation of SCSS in addition to constants parameterized from Wendlandt (1982) and Mavrogenes and O'Neill (1999). Finally, from the P–T dependence, it follows that the choice of T_P and corresponding pressure where the solidus is crossed (P_i) has implications for the S (and Se, Te?) capacity of partial melts extracted (e.g., Mavrogenes and O'Neill 1999).

Partition coefficients and alloy solubilities as a function of f_{O_2}, f_{S_2}, and P_i were parameterized from published experimental partition coefficients, following the approach outlined in Mungall and Brenan (2014). At the *P–T* conditions considered here, a parameterization of results in Rhyzenko and Kennedy (1973) and Hart and Gaetani (2006) shows that the sulfide phase is at all times well above its liquidus, which, for a starting composition of 250 ppm S (McDonough and Sun 1995), has a mass fraction ~0.07 wt% (assuming that all S resides in a sulfide with ~36 wt% S). As long as the silicate melt is saturated in sulfide, HSE partitioning into sulfide liquid and residual silicate minerals control residual concentrations. The distribution coefficients for sulfide melt-silicate melt were parameterized as a function of f_{O_2} and f_{S_2} and lie between 3.0×10^5 and 1.9×10^6 for the PGE. $D_{Re}^{\text{sulfide/silicate}}$ varies strongly as a function of f_{O_2} and f_{S_2} (Brenan 2008), ranging from 10^2 to 10^4 over the conditions addressed here. As a result, the PGE are little fractionated and effectively retained as long as sulfide melt is stable and Re remains chalcophile and little fractionated from Os under reducing conditions applicable to oceanic mantle melting (Fonseca et al. 2007; Brenan 2008; Mungall and Brenan 2014). After sulfide has been consumed by the melting reactions, bulk Ds reflect the relative compatibilities in silicate minerals as summarized by Mungall and Brenan (2014) and correspond well to those determined indirectly from peridotites having experienced low degrees of melt extraction (≤ 25%), i.e., $D_{Os} \sim D_{Ir} \sim D_{Ru} > D_{Pt} > D_{Pd} \geq D_S \sim D_{Re}$ (Pearson et al. 2004; Wang et al. 2013).

Alloy solubility in silicate melts is strongly dependent on f_{O_2} and f_{S_2} (Laurenz et al. 2013, 2014; Mungall and Brenan 2014; this work). Sulfur fugacity in the model is estimated using free energy data from Barin (1995) and Holzheid et al. (1997) to find an equilibrium constant for the mass action expression $FeO_{\text{silicate melt}} + 0.5\ S_2 = FeS_{\text{sulfide melt}} + 0.5\ O_2$ (see also Brenan 2008). The pressure-dependence for this reaction was estimated using a $\Delta_r V$ obtained by comparing the partial molar volume of FeO (Lange and Carmichael 1987) to that of γ_{FeS} (Balabin and Urusov 1995), adjusted for $\Delta_{\text{melting}} V$ of γ_{FeS} (Moretti and Baker 2008). After exhaustion of sulfide liquid from the restite, f_{S_2} is scaled linearly with S concentration in the silicate melt from its value at sulfide saturation (e.g., Mungall and Brenan 2014). Modern convecting mantle has a log f_{O_2} relative the fayalite–magnetite–quartz oxygen buffer (ΔFMQ) of approximately −2 to 0 at low pressure (Frost and McCammon 2008). There is some uncertainty regarding convecting mantle f_{O_2} in the Archean. It appears to have been constant since ca 3.5 Ga, i.e., since the stabilization of cratonic lithospheric mantle, based on investigations of continental mantle rocks (Canil 1997, 2002; Berry et al. 2008), but more reducing conditions prior to the oxygenation of the oceans are advocated by some authors (Kasting 1993; Foley 2011; Aulbach and Viljoen in press). Since abyssal peridotites form via melting at relatively low pressures (1–2 GPa) and since the mantle becomes more reducing with increasing pressure, at constant concentration (Frost and McCammon 2008), higher P_i during Archean melt generation in the convecting mantle implies correspondingly lower ΔFMQ (~ −4 at 200 km depth).

Though the evidence is controversial (e.g., Lee et al. 2010), the modern arc mantle may be more oxidizing than the convecting mantle due to the transfer of oxidized material from the slab during subduction (Wood et al. 1990; Mungall 2002), with arc xenoliths recording mean ΔFMQ of +0.5 (Foley 2011). If transfer of oxidized material does occur, H_2O-fluxed melting in the mantle wedge is expected to entail significantly different HSE behavior compared to decompression melting of convecting mantle (e.g., Brenan et al. 2003), which may be relevant to scenarios of craton formation and/or thickening in Archean subduction zones. In the absence of oxygenated seawater in the Archean, the flux of oxidized material from the wedge was probably small and the transfer of water alone is insufficient to increase mantle f_{O_2} at pressures <5 GPa (Frost and McCammon 2008), resulting in arc mantle that was likely more reducing than today (Foley 2011). We therefore confine our discussion to situations in which sulfur remains in its reduced state (c.f., Jugo et al. 2010) and do not consider the role of sulfate in the comportment of S.

The total solubility of each HSE in the silicate melt is calculated as the sum of its solubility as metal oxide and as metal sulfide as a function of f_{S_2} and f_{O_2}. Metals are apportioned to the residual solid silicates according to mineral modal abundances and distribution coefficients, which were parameterized as a function of f_{O_2} (Mungall and Brenan 2014), with the remainder assumed to reside in PGE alloy phases after saturation. Palladium does not form alloys and is assumed to be perfectly incompatible in olivine. As a monovalent element with a similar ionic radius, Pd may partition into opx with a *D* similar to Na, taken from Bédard (2007), although its slightly smaller cation size may imply slightly larger *D* (Dygert et al. 2014).

The model approximates columnar fractional melting by step-wise extraction of 1.1% partial melt, of which 1% is retained in and combined with the residue as the "starting composition" for the next melting increment (Mungall and Brenan 2014). The effect of the modelled melt retention is to retard the exhaustion of incompatible elements, such as S, Pd and Re, and of Pt. Concentrations of major elements and silicate mineral modes in the residue were parameterized from isobaric batch melting experiments of Walter (1998) as a function of *F* in order to approximate how much pyroxene ± garnet vs olivine remain in the restite, which control the partitioning of HSE between solid and melt. For example, for melting beginning at 70 kbar, the initial mode is 0.453 olivine, 0.323 pyroxenes (opx + cpx combined) and 0.223 garnet, for that beginning at 30 kbar, the initial mode is 0.537 olivine and 0.463 pyroxenes (no garnet). These modes are not very sensitive to the nature of melt extraction (fractional vs. batch) or to changes in the melting reaction.

A comparison not only of the modelled residues to cratonic mantle, but also of the modelled melts to picrites and komatiites (Mungall and Brenan 2014), provides an additional control of the quality of the models and assumptions—in particular with regard to the starting composition (ACM)—as poor choices can produce reasonable matches for the restite while magnifying the mismatch from the melts. Although a discussion of the modelled versus natural melts is beyond the scope of this work, such checks were carried out as part of the quality control process.

On a final note, cratonic mantle formation at higher Archean T_P implies deeper onset of partial melting, including at depths where metal saturation in the mantle is potentially reached. This would lead to stabilization of solid Fe–Ni metal that partitions and fractionates the HSE and is progressively diluted by less noble siderophiles, such as Ni and Co (Ballhaus 1995; Woodland and Koch 2003; Rohrbach et al. 2007; Rohrbach and Schmidt 2011; Stagno et al. 2013). Exploration of the effect of iron-nickel metal in the modelling presented here is precluded by the lack of appropriate partitioning and solubility data.

Effects of Partial Melt Extraction on HSE based on Modelling

We describe here the modelled HSE relationships as a function of F and P_i, and then compare natural samples against these modelled residues. The data and modelling form a combined perspective that, though not providing unique constraints, help distinguish primary depletion-related signatures from those that must have been inherited during subsequent processes, provided the model is an accurate reflection of nature. In the model results, Al_2O_3 is extracted increasingly efficiently with decreasing P_i (<1 wt% Al_2O_3 at $F = 0.20$ and 3 GPa, or at $F = 0.31$ at 7 GPa). The change in residual S concentration is initially small but then asymptotically approaches zero when sulfide is practically exhausted, concurrent with PGE alloy stabilization. Due to increased S solubility, this occurs at lower melt fractions for more oxidizing conditions ($F = 0.20$ for $\Delta FMQ = -2$, $F = 0.16$ at $\Delta FMQ = 0$). In contrast, the pressure-sensitivity is small because the increased SCSS at higher T_P and FeO in the melt are balanced by decreased SCSS at higher P_i. Trends of modelled HSE concentrations as a function of melt fraction (*F*) are shown in Figure 11A–F.

The IPGE are compatible in sulfide liquid, and both experiments and natural samples indicate that extraction of picrite and komatiite melts at high pressure lead to saturation in Ru-

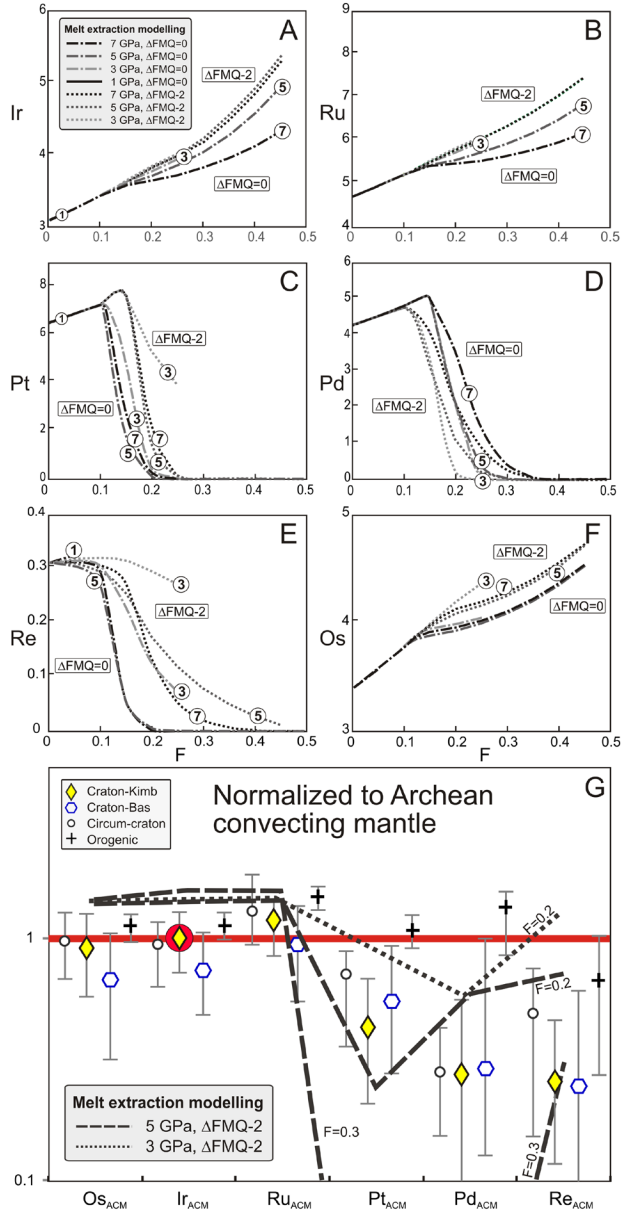

Figure 11. (A–F) Contours for peridotite HSE concentrations against melt fraction F, after melt extraction from model Archean convecting mantle (Table 2) at different pressures (3, 5, 7 GPa—numbers in circles) determined from melt extraction modelling at oxygen fugacities relative to the fayalite–magnetite–quartz buffer (ΔFMQ) of −2 (stippled lines) and 0 (dot–dash lines), following the rationale and using parameterization as outlined in the text. (G) Median concentrations of various peridotite classes shown in Figure 3, normalized to the concentrations of Archean Convecting Mantle (ACM) described in the text and given in Table 2, as well as modelled residues for partial melting at ΔFMQ = −2 and P_i of 3 GPa after 20% partial melting (F = 0.2) and P_i of 5 GPa after 20 and 30% partial melting. The bars encompass the upper and lower interquartile range.

Os–Ir alloys at some time around sulfide exhaustion, and that neither Rh or Pd are concentrated in alloy minerals (Barnes and Fiorentini 2008; Fonseca et al. 2012; Mungall and Brenan 2014). The concentrations of Ru, Ir, and Os increase continuously throughout the melting interval, but mostly at a slower rate after alloy saturation, in particular under higher f_{O_2} (Fig. 11A,B,F). The highest concentrations are, of course, reached for the longest melting columns (highest melt fraction F), corresponding to the highest P_i. After apportioning the appropriate amount of HSE to olivine, the calculated weight fraction of alloy in the residue is minute and in the ppb range, and yet in some instances it dominates the HSE budget. Because of the combination of very low alloy abundances with $^{\text{alloy–silicate liquid}}D_{\text{IPGE}}$ on the order of 10^6, the choice of $^{\text{alloy–silicate liquid}}D_{\text{IPGE}}$ has only a weak effect on bulk D if conventional modelling approaches are used.

At S concentrations of ~20–30 ppm in the residual mantle, maximum concentrations are reached for Pt and Pd, which are ~20% higher than starting concentrations for ΔFMQ = −2 and ~15% higher for ΔFMQ = 0, after which the concentrations of both start to decrease relatively sharply over small melting intervals as they are liberated into the silicate melt from a rapidly diminishing amount of sulfide. Platinum concentrations show a notable exception at ΔFMQ = −2 and 3 GPa, as they decrease much more slowly than at higher f_{O2} or pressures, owing to saturation of the silicate melt in Pt alloy. As outlined above, Pd does not saturate under any of the modelled conditions and becomes strongly incompatible after sulfide is exhausted. Rhenium also does not form an alloy and its concentration increases by at most a few percent while sulfide is stable. After sulfide exhaustion, Re concentration decreases quickly at ΔFMQ = 0 and more slowly at lower f_{O_2}, showing the greatest relative dependence on f_{O_2} of all HSE considered here. At low P_i (3 GPa), Re is retained in the residue more efficiently than at higher pressures (Fig. 11E).

Effects of Partial Melt Extraction on HSE—Comparison of Model and Nature

The effects of partial melting on modelled HSE concentrations are summarized in chondrite-normalized diagrams (Fig. 11G), with the median concentrations of various sample classes from Figure 3 shown for comparison. The modelled residues are useful in highlighting processes that are not consistent with decompression melting of dry primitive mantle under the chosen pressure (7–3 GPa) and redox conditions (ΔFMQ = −2 to 0).

IPGE. Kimberlite-borne cratonic peridotites have highly variable IPGE concentrations at a given Al_2O_3 (Figs. 4A–C). In contrast, over the range of f_{O_2} considered, the concentrations in the modelled residues vary by less than a factor 2 and show little sensitivity to pressure of melt extraction, as they are effectively retained first by sulfide and then by PGE alloys together with olivine, in which they are compatible or only mildly incompatible, depending on f_{O_2}. Although the modelled range of ΔFMQ has been chosen to be small (−2 to 0) and consistent with conditions expected in convecting mantle during MORB extraction at ~3 GPa (Frost and McCammon 2008), the results show that at increasing f_{O2}, alloy solubility is enhanced. For example, at ΔFMQ of +2, which is reached by the most oxidized of modern arc lavas, but not by arc xenoliths (Frost and McCammon 2008; Foley 2011), Ir and Ru become mildly incompatible. Thus, strongly depleted IPGE concentrations—by failure of IPGE alloys to saturate or by secondary dissolution—could only be achieved at very high f_{O_2} and either flux melting or metasomatism by oxidized small-volume melts, such as carbonatites and kimberlites, at high melt-rock ratios (Frost and McCammon 2008; Foley 2011). Alternatively, IPGE alloys may be physically entrained, leading to heterogeneity (Lorand et al. 2013).

Samples from the part of the North American craton sampled in Greenland (G-NAC; Wittig et al. 2010a) show IPGE depletions relative to the modelled residues at high F (low Al_2O_3; Figs. 4A–C) that mimic the behavior of incompatible HSE, such as Pd and Re (Figs. 4D,F). Barring nugget effects, this begs the question whether these depletions were generated during melt extraction under high-f_{O_2} conditions with significantly enhanced IPGE solubilities. Accretionary processes may have been involved in the NeoArchean amalgamation of the G-NAC (Wittig et al.

2008, 2010a; Tappe et al. 2011), and, if Archean (or modern) subduction zone mantle did form under higher f_{O_2} than convecting mantle, variable flushing with putative oxidizing melts and fluids might explain some of the variability of Os concentrations at the low-Al_2O_3 end.

In the partial melting model, Os and Ir are mildly fractionated at high melt fractions where Os concentrations increase more slowly than Ir concentrations with increasing F (Fig. 11). The effect of increasing f_{O_2} is to increase PGE solubility in silicate melts, leading to lower concentrations in the residue, but it will not sufficiently fractionate Os from Ir to account for the observed deviation from reasonable starting compositions because of the similar solubilities. Thus, low Os concentrations over a range of Al_2O_3, such as those observed for other cratonic mantle suites (Fig. 4A), were possibly imposed during secondary processes, such as metasomatic interaction with high-f_{O_2} melts or fluids that would lead to destabilization of (resulfidized) PGE alloys and loss of HSE. The particularly pervasive Os depletions shown by both on- and off-craton basalt-borne xenoliths (Fig. 4A; median concentrations of 2.2 and 1.9 ppb, respectively) relative to kimberlite-borne cratonic and circum-cratonic xenoliths (median concentrations of 3.1 and 3.3 ppb, respectively; Table 1) suggest a relationship to the nature of the host magma and may be related to Os volatility during degassing of the slowly cooling host basalts, with perhaps greater susceptibility to loss occurring when Os is still hosted in sulfides. In contrast, kimberlites, as fast-rising, volatile-rich magmas, are emplaced during explosive volcanism, with little time for devolatilization of mantle-derived xenoliths (e.g., Sparks et al. 2006).

If Ru and Ir behave congruently during partial melting, the observed suprachondritic Ru/Ir in various peridotitic materials could be taken to indicate that the mantle's HSE systematics do not derive from carbonaceous chondrite, but from a different or unknown meteoritic component (Rehkämper et al. 1997; Snow and Schmidt 1998; Becker et al. 2006; Liu et al. 2009). Alternatively, they could reflect earlier Ru alloy saturation compared to Ir, secondary processes, such as chromite accumulation, or analytical artefacts related to Cr-based polyatomic interferences, as mentioned above.

Platinum and palladium. Once sulfide is exhausted, the concentrations of elements that do not form alloys—Pt under oxidizing conditions or at high P, Pd and Re under any conditions)—are dictated by their low compatibilities in the residual silicate mineral assemblage and their variable sensitivity to f_{O_2}. They are efficiently depleted at large melt fractions or high pressures of melt extraction or a combination of both (Figs. 4D–F). One of the most striking differences between cratonic/circum-cratonic and off-cratonic or orogenic peridotites is the strongly Pt- and Pd-depleted character of the former, with median concentrations of 2.8 and 1.2 ppb, respectively in cratonic peridotites (Table 1). The drastic drop in Pt and in Pt/Ir over small ranges of Al_2O_3 (1–2 wt%; Figs. 4D and 10B) in cratonic peridotites—with variations spanning more than two orders of magnitude at a given Al_2O_3 concentration—contrasts with the near-constant or slightly decreasing Pt concentrations in orogenic peridotites over the same Al_2O_3 interval.

It has been suggested that high-temperature PGE alloys are Pt-poor and that during high-pressure melting, Os–Ir–Ru alloy is stabilized, whereas Pt alloy is too soluble in the melt to be stable (Brenan and Andrews 2001; Mungall and Brenan 2014), allowing Pt to behave as an incompatible element. However, at lower pressures and under reducing conditions (ΔFMQ = −2; Fig. 11C), Pt may saturate at a much lower concentration in silicate melt than at higher P_i or f_{O_2}. In theory, therefore, Pt can serve as a pressure sensor if the sensitivity of Pt alloy solubility to f_{O_2} and f_{S_2} is sufficiently tightly constrained. For example, the modelled Pt concentrations at 5 and 7 GPa drop to < 0.1 ppb much faster than Pd concentrations, implying $D_{Pt} < D_{Pd}$ due to incorporation of Pd in pyroxene at high pressure. However, from a consideration of natural high-degree melts at low pressure (picrites, komatiites) and of residual mantle, a stronger incompatibility of Pd is evident (e.g., Barnes et al. 1985; Puchtel and Humayun 2000; Pearson et al. 2004; Fischer-Gödde et al. 2012; Lorand et al. 2013). Hence the stronger depletion of cratonic peridotite samples in Pd than in Pt is consistent with the relative partitioning inferred from partial melts.

Because Pd does not partition into alloys, there are no uncertainties related to alloy solubility, and the concentration of this element is controlled by its incompatibility in the silicate residue and f_{O_2} once sulfide is exhausted. Modelled melt residues are sensitive to P_i (Fig. 4E), with stronger depletions at a given Al_2O_3 content with increasing pressure. The FeO content of the melt has recently been shown to be an important parameter, as the solubility of Pd increases with increasing FeO in the melt (Laurenz et al. 2010). Because the FeO content of the melt increases with increasing pressure (e.g., Kinzler and Grove 1992), deep P_i enables strong Pd depletion of the residue. Indeed, Pd concentrations and Pd/Ir in both cratonic and orogenic peridotites generally start to decrease rapidly at about 1.2% Al_2O_3 (Figs. 4E, 10C).

Significant scatter in Pd concentrations and Pd/Ir is evident both for kimberlite- and basalt-borne peridotite xenoliths. This may be related to gains due to metasomatic sulfide or melt addition. In the Kaapvaal craton, the conspicuously S-enriched mantle xenoliths entrained in the older Group II kimberlites have markedly higher median Pd concentrations (1.8 ppb) compared to those from Group I kimberlites (0.53 ppb), suggestive of co-enrichment of S and Pd, and implying that their P_i of 3–5 GPa that could be inferred from Figure 4E is underestimated. Distinguishing between P_i of 5 and 7 GPa is not possible at the low Al_2O_3 end of the compositional array, but a large number of samples from Kalahari and G-NAC appear to have been depleted at $P_i \geq 5$ GPa. In contrast, samples from the Rae craton form a comparatively tight array consistent with P_i of 3–5 GPa, which probably also applies to the Karelian craton, whereas the few samples from China and the Slave craton apparently require $P_i > 7$ GPa. As mentioned above, it is possible that the incompatibility of Pd in the residue is underestimated and new experiments to constrain this better are needed. Hence, although Pd shows promise as a pressure sensor due to its P_i-sensitivity, which is not complicated by alloy saturation and solubility, it is not currently possible to confidently distinguish between primary and secondary Pd–Al_2O_3 relationships and to use them as a measure of P_i and, by implication, as an indicator of the tectonic setting where melt extraction occurred (ambient or excess T_P).

The Pt/Pd ratio in natural cratonic peridotites does not co-vary with Pt concentrations, but shows a broad negative co-variation with Pd concentration (Fig. 12A.B), falling between modelled melt depletion trends at P_i of 3 and 5 GPa, seemingly indicating control by Pd depletion while Pt alloy is stable. On the other hand, there is a complete lack of the expected covariation of Pt/Pd with Al_2O_3 (a melt depletion index), and the large scatter of Pt/Pd at a given Al_2O_3 together with high Pt/Pd spread over a range of Al_2O_3 may indicate the influence of secondary processes (Fig. 12C). Alternatively, the scatter may result from a nugget effect related to the tendency for Pt and Pd to be hosted by different phases after sulfide has been removed (e.g., Pt alloy, Pd in silicates?) with consequent loss of the correlated behavior observed when both are hosted by the same phase prior to sulfide exhaustion. In the basalt-borne xenoliths, higher than initial Pt/Pd are observed for an even larger range of Al_2O_3 (Fig. 12C). It is possible that Pt alloy solubility in the model is overestimated, especially given that the f_{S_2} model, on which Pt solubility depends, is currently constrained by an extremely limited experimental database. It is also possible that the assumption of moderate Pd incorporation into pyroxene is not true. Thus, Pt values and Pt/Pd rations in residues cannot yet be used to infer the conditions of melting with confidence, but they are consistent with controls by f_{O_2} and P. Given current uncertainty, the most that can be said is that the appearance of compatible behavior by Pt is highly suggestive of low-pressure melting.

Re/Os and $^{187}Os/^{188}Os$. Kimberlite-borne cratonic mantle xenoliths are conspicuously enriched in Re at low Al_2O_3 contents (Fig. 4F) compared to orogenic peridotites. This is a well-known feature for xenoliths in this type of host rock, which can be explained by infiltration of Re-rich kimberlite melt, and is visualized by sub-horizontal arrays in Re–Os isochron diagrams, at least for Phanerozoic kimberlites (e.g., Carlson et al. 2005). It is also evident in extended chondrite-normalized PGE plots, with normalized values plotted in the order of

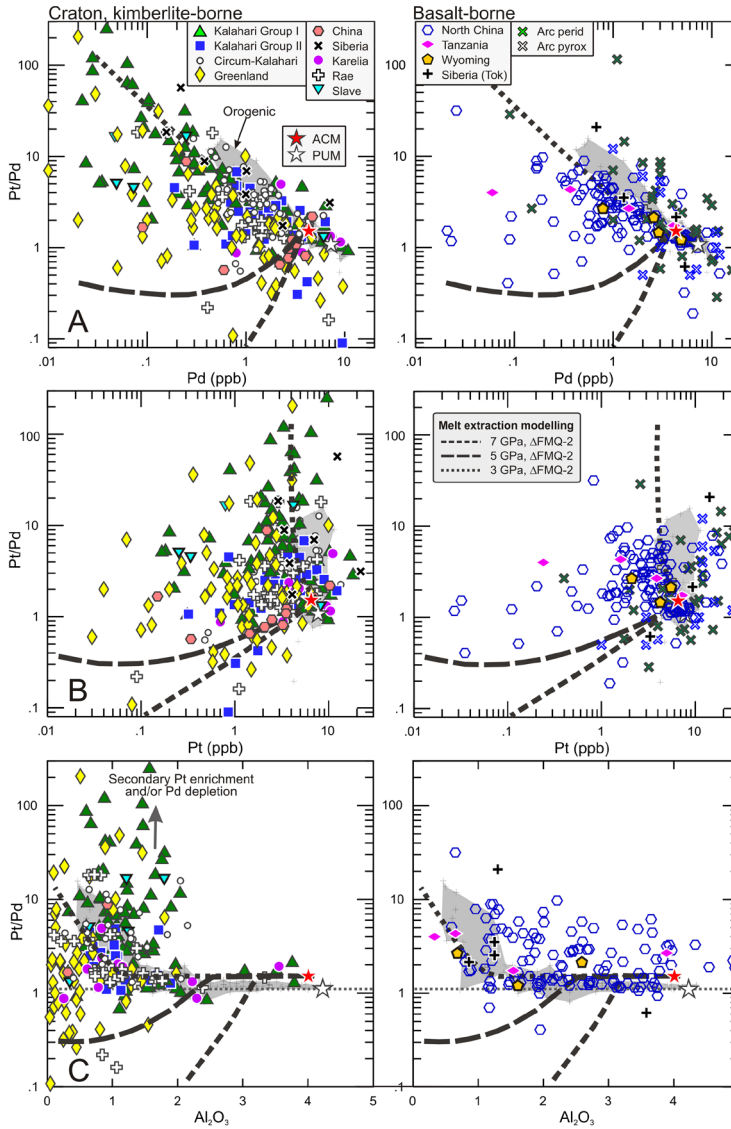

Figure 12. Whole-rock Pt/Pd in various peridotite classes against (A) Pd concentrations (ppb), (B) Pt concentrations (ppb) and (C) Al_2O_3 (wt%). Shown for comparison are melting contours as described in the text and displayed in Figure 11. Other information as in Figures 3 and 5.

decreasing compatibility, where Re is often enriched relative to less incompatible HSE, such as Pd and Pt. In contrast, the effects of the infiltration of more viscous basaltic melts are largely limited to the xenolith rinds (e.g., Chesley et al. 1999). Basalt-borne xenoliths generally have Re concentrations similar to or lower than orogenic peridotites, but show large scatter, with a range of Re depletions at a given Al_2O_3, which suggests secondary volatility-related Re-loss. Thus, the use of Re to constrain conditions of melt extraction is completely compromised

by its volatility and mobility in metasomatic agents (e.g., Li 2014). This decoupling of Re from the primary melting process also leads to geologically meaningless T_{MA} model ages being calculated for most cratonic peridotites, as discussed earlier. Meaningful T_{RD} can be obtained if (1) sufficient Re extraction has occurred during melt depletion, such that the initial $^{187}Os/^{188}Os$ is essentially frozen in and (2) if secondary Re addition (or loss) is so recent that no significant increase of ^{187}Os ingrowth has occurred.

Melt modelling shows that Re/Os decreases with increasing P_i and that residues with <20 ppt Re—below which decay to ^{187}Os is too small to lead to resolvable change in the isotope ratio, and thus T_{RD}, with the currently attainable precision—can be generated for P_i of 5 and 7 GPa at $F \geq 0.17$ and ΔFMQ of 0. In contrast, higher F (≥0.30) is required at ΔFMQ of −2, and for P_i of 3 GPa, such low Re concentrations are not accessible at all (Fig. 11E). A comparison of modelled residual Re/Os–Al_2O_3 to measured samples shows that a large proportion of cratonic mantle peridotites have Re/Os that is too high for their degree of melt depletion and even higher than that of orogenic peridotites, which formed at lower average P_i and F, implying secondary Re addition and/or Os loss (Fig. 9A). Also, many basalt-borne cratonic peridotites have Re/Os that overlap with orogenic peridotites, even though cratonic peridotites formed by on average larger degrees of melt extraction and at higher pressures.

The disturbance of Re concentrations in peridotites of all types is evident in the large scatter in the Re–Os isochron diagram (Fig. 9B). While orogenic and basalt-borne peridotites show some coherence of $^{187}Os/^{188}Os$ with Al_2O_3 (Fig. 9C), as has been recognized early (Reisberg and Lorand 1995) and exemplified by the excellent correlation documented in Vitim peridotites (Pearson et al. 2004), such correlations are not observed in kimberlite-borne cratonic xenoliths (Pearson et al. 2004). The wide range of Al_2O_3 at $^{187}Os/^{188}Os \leq 0.11$ (i.e., giving ≥ 2.5 Ga T_{RD} ages) could be explained by variable melt extraction ages or degrees of Re depletion, later Re addition and/or Al_2O_3 addition. The addition of cpx and minor garnet is usually ascribed to interaction with kimberlite (e.g., Simon et al. 2003), whereas opx could be part of the mantle from which the Kaapvaal craton formed (Aulbach et al. 2011) or due to interaction with siliceous fluids (Pearson and Wittig 2008). As neither kimberlite nor fluids will add significant Al_2O_3, it requires interaction with silicate melt, which is rarely produced beneath thick cratonic lithosphere. Moreover, such interaction should have led to co-introduction of Re. This is not supported by the lack of co-variation of Re/Os with Al_2O_3. Rhenium addition for samples with $^{187}Os/^{188}Os \leq 0.11$ must have been relatively recent, as otherwise ingrowth of radiogenic Os would have obliterated the Archean signature.

Despite these complications from multi-stage metasomatic overprint, a striking feature of the database is that ancient Os isotope signatures are preserved in many cratonic mantle xenoliths and individual sulfide grains (Figs. 6, 9C). This resilience may be due to high Os abundances in sulfides where residual PGE alloys recording primary melting events were captured by metasomatic BMS. Although Re (and perhaps also Pt and Pd) appears to be too overprinted to be a useful indicator of melt depletion conditions, the persistence of unradiogenic Os—as record-keeper of time-integrated low Re/Os—allows some insights into the required conditions of partial melting. For cratonic mantle formed between 3.5 and 2.9 Ga to have present-day $^{187}Os/^{188}Os \leq 0.11$, time-integrated Re/Os must have been <0.025 and 0.012, respectively. Reproduction of the present-day $^{187}Os/^{188}Os$ of these samples using modelled Re/Os and assuming formation from primitive mantle 3.5 or 2.9 Ga ago, shows that in order to reach sufficiently low Re/Os to preserve $^{187}Os/^{188}Os$ of 0.11—as displayed by a sizable proportion of cratonic peridotites—$P_i \geq 5$ GPa appears to be required.

The origin of circum-cratonic mantle is controversial, as it may represent lithosphere formed in the Proterozoic (e.g., Pearson et al. 2004; Janney et al. 2010) or cratonic lithosphere that was reworked during Proterozoic collisions at the craton margins (e.g., Griffin et al.

2009). Although most circum-Kalahari kimberlite-borne mantle xenoliths also appear to have suffered a secondary increase in Re/Os, a subset of samples may have retained primary Re/Os (Fig. 9A). However, unambiguously Archean T_{RD} have not been determined for these samples (Pearson et al. 2004; Janney et al. 2010; Aulbach et al. 2014). This could be taken to indicate that this mantle did form in the Proterozoic, in keeping with their association with exclusively Proterozoic crust. On the other hand, Al_2O_3 and Re may have been re-introduced during strong reworking of cratonic margins. If Re addition was ancient, ingrowth of ^{187}Os may lead to a correlation of measured $^{187}Os/^{188}Os$ with Al_2O_3 and individual sample suites would lie on an apparent Proterozoic partial melting trend. This may also be the case for some on-craton samples that yield Proterozoic T_{RD} model ages. As noted above, it is not easy to pin-point the melt composition existing at the base of the lithospheric mantle that is capable of introducing Al in sufficient quantities. More strongly incompatible, minor elements such as TiO_2 are better suited to address this question, as partial melting will cause such elements to lie on curved melting trends with moderately incompatible elements, such as Al_2O_3 and Re (Niu 1997), compared to straight trends for bulk mixing, but such data are not often reported for cratonic peridotites and are also subject to nugget effects from accessory host minerals, such as TiO_2 in chromite.

Post-core formation, sluggish downward mixing of a late veneer

It has long been recognized that the abundances of the HSE in the terrestrial mantle are higher and their ratios more similar to undifferentiated chondrite meteorites than those expected from theoretical modelling of post-core formation mantle, during which the siderophile elements should have been near-quantitatively, but differentially extracted into the metallic core (Ringwood 1966; Jagoutz et al. 1979). A widely held view is that heterogeneous accretion and addition of the HSE from an oxidized "late veneer" remains the most viable explanation for the abundances and ratios of the HSE (Kimura et al. 1974; Chou 1978; Jagoutz et al. 1979; Morgan et al. 1981; Lodders and Palme 1991; Brenan and McDonough 2009; Siebert et al. 2011; Mann et al. 2012; Bennett et al. 2014). This veneer appears to have been spatially widespread and diachronous across the inner Solar System (Dale et al. 2012; Day et al. 2012, 2016, this volume). This hypothesis can be examined from the perspective of ancient high-volume melts, such as komatiites sampling deep mantle sources, and from cratonic peridotites that formed from Archean convecting mantle. Older (3.5–3.2 Ga) komatiites have been suggested to show PGE depletions relative to younger (2.9–2.7 Ga) komatiites, with the implication that this was related to slow downward mixing of a late accreted component into a lower mantle depleted by core formation, after accounting for, or discounting, effects of fractional crystallization, degree and depth of partial melting, sulfide saturation at source, or dilution by an eclogite component (Maier et al. 2009; Fiorentini et al. 2011).

Lower median Os and Ir concentrations in kimberlite-borne xenoliths than in modern mantle represented by orogenic peridotites (Fig. 3) are seemingly permissive of the idea that at least some mantle regions had not "seen" the late veneer (Maier et al. 2012). Although it is difficult to assess whether progressive homogenization with a late veneer occurred during the Archean owing to the inherent challenges to obtain precise and accurate ages from cratonic mantle xenoliths with multi-stage histories, the two radiogenic isotope systems embedded in the HSE—^{186}Os from the decay of ^{190}Pt and ^{187}Os from the decay of ^{187}Re—can provide some constraints on the time-integrated ratios of Pt/Os and Re/Os (e.g., Carlson et al. 2008; Puchtel et al. 2014). Core formation fractionates the HSE even under magma ocean conditions (Righter 2005) and should lead to suprachondritic Re/Os and Pt/Os in the silicate Earth (Walker et al. 1995, 1997; Cottrell and Walker 2006; Brenan and McDonough 2009; Bennett et al. 2014). If a late-added veneer was indeed incompletely mixed with the post-core formation mantle, one would expect to find supra-chondritic $^{186,187}Os$ isotope compositions of the deep sources of komatiites and cratonic mantle until homogenization

was reached. The record of initial $^{187}Os/^{188}Os$ of komatiites and mantle samples reveals that two types of sources were present since at least 3.8 Ga: One evolving at roughly chondritic parent-daughter ratios—and thus precluding global sluggish downward mixing of a late-accreted component—the other at supra-chondritic Os isotopic ratios and thus possibly indicative of the persistence of some mantle regions that did not equilibrate with the late veneer (Walker et al. 1997; Bennett et al. 2002; Walker and Nisbet 2002). Recent analyses of EoArchean ultramafic rocks, including chromitites, from western Greenland suggest sub-chondritic Pt/Os, likely generated in the Hadaean, at 4.1 Ga (Coggon et al. 2013).

There are a few examples of peridotite-derived age arrays, with geologically meaningful ages corresponding to events expressed in the overlying crust, that have indeed yielded radiogenic initial $^{187}Os/^{188}Os$: This is the case for the central Slave craton (Aulbach et al. 2004, 2009a, 2011; Westerlund et al. 2006) and potentially the Pilbara craton and SW Greenland (Graham et al. 1999; Bennett et al. 2002). While such data can be, and have been, explained by addition of crustal components to the mantle source, they are also permissive—from an isotopic perspective—of regions of post-core formation HSE-depleted mantle source that evolved for some time at elevated Re/Os prior to mixing with the late accreted component.

SUMMARY

Due to higher Archean T_P, partial melting during generation of cratonic lithospheric mantle is characterized by deep melting paths enabling unusually strong depletion observed only rarely in later-formed mantle. We reviewed the HSE and Re–Os isotope systematics of cratonic mantle samples in the context of partial melting and subsequent multi-stage metasomatic overprint. In addition, we use partial melting models to determine whether HSE systematics can be used as barometers for oxygen and sulfur partial pressures (f_{O_2} and f_{S_2}) as well as for pressures of onset of partial melting. We quantitatively compare published HSE systematics of natural samples to modelled melting residues in order to distinguish between those with potentially primary signatures and those that must have experienced secondary modification. A review of the literature combined with the modelling presented here lead us to the following general conclusions:

- Cratonic peridotites are the most PPGE depleted peridotites sampled from the Earth's mantle, showing consistently the most extreme fractionations of PPGE over IPGE. They also have the lowest average and median Os isotope ratios, as might be expected from their tectonic setting, and they have amongst the lowest Se and Te concentrations so far measured in mantle peridotites, although some depleted orogenic harzburgites have similar concentrations.
- Modelling of HSE behavior during mantle melting shows that the IPGE hold promise as redox sensors, whereas PPGE and Re can be employed as pressure sensors. The IPGE are compatible and at higher degrees of melting they form alloys under all conditions considered (P_i=3–7 GPa, ΔFMQ=−2 to 0). Their compatibility decreases sharply at higher f_{O_2}, which increases the solubilities of their alloys in silicate melts while also diminishing their partition coefficients in olivine. Platinum forms alloy only at the low-P and –f_{O_2} end of the melting environment, whereas Pd, Rh, Re, and Au never form alloys and behave incompatibly in residual silicates once sulfide liquid is exhausted, whereupon they partition into the melt more strongly with increasing P and f_{O_2}.
- Kimberlite-borne cratonic xenoliths have median Ir concentrations of 3.1 ppb, Os=3.1 ppb, Pt=2.8 ppb, and Pd=1.2 ppb. Higher median Pt but similar Pd contents in circum-cratonic xenoliths may attest to formation at shallower pressures allowing Pt alloy stabilization and/or Pt-dominated overprint during reworking of cratonic margins. The exceptionally strong Pd and Pt depletions in kimberlite-borne samples compared to off-cratonic and orogenic mantle are consistent with their formation at elevated Archean

T_P and correspondingly higher P_i. Mantle xenoliths from the Greenland, Rae and Karelian cratons have HSE systematics suggestive of formation at lower P_i than those from the Kaapvaal and Slave cratons.

- All primary sulfide is expected to be exhausted at the depleted Al_2O_3 contents exhibited by the vast majority of cratonic mantle xenoliths (initial S = 250 ppm, melt fraction $F \leq 0.20$ for $\Delta FMQ = -2$ and $F \leq 0.16$ for $\Delta FMQ = 0$), yet significant S concentrations are measured in many of these samples, requiring secondary S addition from low-volume volatile-rich melts. If this process occurs while the peridotite resides in the deep lithosphere, this likely leads to "resulfidation" of residual PGE alloys or extraction into newly formed sulfide liquid of IPGE formerly hosted by residual olivine, and co-introduction of Pd, Pt and Re, leading to the false appearance of lower apparent melt extraction P. The pervasiveness of this signature in cratonic mantle peridotites means that PPGE and Re systematics cannot be reliably used at present to infer depths of partial melting.
- The extreme variability of IPGE concentrations in cratonic peridotites cannot be explained by decompression melting of convecting mantle. Instead, they appear to document partial melting under more oxidizing conditions or percolation of oxidizing melts. Concomitant loss of Pt alloy, if present, will lead to high apparent melt extraction P. The melts are consequently HSE enriched and can act as metasomatic agents in the cratonic lithosphere. Alternatively, the more oxidizing conditions required for IPGE and Pt alloy destabilization could be interpreted as being due to flux-melting in the presence of water. However, as with the PPGE, the signature is ambiguous and precludes drawing firm conclusions regarding melting environment.
- The lower median IPGE concentrations of kimberlite-borne cratonic mantle xenoliths compared to orogenic mantle is permissive of sluggish downward mixing of late-accreted components post-core formation, but may, alternatively, reflect the inadequacy of the currently used estimates of primitive upper mantle concentrations, which are based on heavily refertilized Phanerozoic samples that experienced enrichment in Pd, Pt, and Ru and possibly some IPGE. We therefore estimate the HSE concentrations of Archean convecting mantle based on median concentrations of Ir, a compatible, non-volatile element, in kimberlite-borne mantle xenoliths erupted through cratons, which, coming from intact lithospheric mantle, are the least-disturbed samples with respect to Ir. Using chondritic relative abundances to calculate other HSEs relative to Ir, yields concentrations of Ir = 3.1 ppb, Os = 3.4 ppb, Pd = 4.3 ppb, Pt = 6.5 ppb, and Re = 0.27 ppb.
- Re–Os isotopes combined with HSE systematics remain an unrivalled method to establish lithosphere stabilization ages. In using such ages, it is critical to assess whether the T_{RD} ages provide a meaningful record of the extraction age leading to lithosphere formation, as opposed to minimum ages that can severely underestimate true age due to metasomatic disturbance or incomplete removal of Re during melting. Careful interpretation requires additional constraints, such as the use of major oxide relationships to distinguish melt- vs. metasomatism-related effects, lithophile trace-element fingerprinting to unravel the nature of the metasomatic agents, conventional oxybarometry to quantify consequences for the mantle redox state, and thermobarometry to allow localization in the lithosphere column.
- A quantitative application of mantle HSE barometry will be possible once tighter constraints on the f_{S_2}-dependent alloy solubilities into silicate melts are established together with fully quantitative data on the partitioning into residual silicates (e.g., orthopyroxene and garnet). In addition, the use of P_i–f_{O_2} as an indicator of melting environment (ridge, plume, arc) must await resolution of the as yet uncertain secular T_P and redox evolution of the convecting and arc mantle.

ACKNOWLEDGMENTS

We thank the editors of this special publication—Jason Harvey and James Day—for their invitation to contribute. Jean-Pierre Lorand, John Pernet-Fisher and the editors provided detailed and constructive comments that significantly improved the manuscript. Illuminating discussions with Chris Ballhaus and Raúl Fonseca are greatly appreciated.

REFERENCES

Abbott DH, Drury R, Mooney WD (1997) Continents as lithological icebergs: The importance of buoyant lithospheric roots. Earth Planet Sci Lett 149:15–27

Ackerman L, Walker RJ, Puchtel IS, Pitcher L, Jelínek E, Strnad L (2009) Effects of melt percolation on highly siderophile elements and Os isotopes in subcontinental lithospheric mantle: A study of the upper mantle profile beneath Central Europe. Geochim Cosmochim Acta 73:2400–2414

Afonso JC, Schutt DL (2012) The effects of polybaric partial melting on density and seismic velocities of mantle restites. Lithos 134:289–303

Afonso JC, Fernandez M, Ranalli G, Griffin WL, Connolly JAD (2008) Integrated geophysical-petrological modeling of the lithosphere and sublithospheric upper mantle: Methodology and applications. Geochem Geophys Geosyst 9: Q05008, doi:10.1029/2007GC001834

Alard O, Griffin WL, Lorand JP, Jackson SE, O'Reilly SY (2000) Non-chondritic distribution of the highly siderophile elements in mantle sulfides. Nature 407:891–894

Alard O, Griffin WL, Pearson NJ, Lorand JP, O'Reilly SY (2002) New insights into the Re–Os systematics of sub-continental lithospheric mantle from in situ analysis of sulfides. Earth Planet Sci Lett 203:651–663

Alard O, Lorand JP, Reisberg L, Bodinier JL, Dautria JM, O'Reilly SY (2011) Volatile-rich Metasomatism in Montferrier Xenoliths (Southern France): Implications for the Abundances of Chalcophile and Highly Siderophile Elements in the Subcontinental Mantle. J Petrol 52:2009–2045

Allègre CJ, Poirier JP, Humler E, Hofmann AW (1995) The chemical composition of the Earth. Earth Planet Sci Lett 134:515–526

Armytage RMG, Brandon AD, Peslier AH, Lapen TJ (2014) Osmium isotope evidence for Early to Middle Proterozoic mantle lithosphere stabilization and concomitant production of juvenile crust in Dish Hill, CA peridotite xenoliths. Geochim Cosmochim Acta 137:113–133

Arndt NT, Lewin E, Albarède F (2002) Strange partners: formation and survival of continental crust and lithospheric mantle. Early Earth: Phys Chem Biol Dev 199:91–103

Arndt N, Lesher CM, Barnes SJ (2008) Komatiite. Cambridge University Press

Arndt NT, Coltice N, Helmstaedt H, Grégoire M (2009) Origin of Archean subcontinental lithospheric mantle: Some petrological constraints. Lithos 109:61–71

Artemieva IM, Mooney WD (2001) Thermal thickness and evolution of Precambrian lithosphere: A global study. J Geophys Res-Solid Earth 106(B8):16387–16414

Aulbach S (2012) Craton nucleation and formation of thick lithospheric roots. Lithos 149:16–30

Aulbach S, Viljoen KS (in press) Eclogite xenoliths from the Lace kimberlite, Kaapvaal craton: From convecting mantle source to palaeo-ocean floor and back. Earth Planet Sci Lett. doi:10.1016/j.epsl.2015.08.039

Aulbach S, Griffin WL, O'Reilly SY, McCandless TE (2004) Genesis and evolution of the lithospheric mantle beneath the Buffalo Head Terrane, Alberta (Canada). Lithos 77:413–451

Aulbach S, Griffin WL, Pearson NJ, O'Reilly SY, Doyle BJ (2007) Lithosphere formation in the central Slave Craton (Canada): plume subcretion or lithosphere accretion? Contrib Miner Petrol 154:409–427

Aulbach S, Stachel T, Creaser RA, Heaman LM, Shirey SB, Muehlenbachs K, Eichenberg D, Harris JW (2009a) Sulfide survival and diamond genesis during formation and evolution of Archean subcontinental lithosphere: A comparison between the Slave and Kaapvaal cratons. Lithos 112:747–757

Aulbach S, Creaser RA, Pearson NJ, Simonetti SS, Heaman LM, Griffin WL, Stachel T (2009b) Sulfide and whole rock Re–Os systematics of eclogite and pyroxenite xenoliths from the Slave Craton, Canada. Earth Planet Sci Lett 283:48–58

Aulbach S, Shirey SB, Stachel T, Creighton S, Muehlenbachs K, Harris JW (2009c) Diamond formation episodes at the southern margin of the Kaapvaal Craton: Re–Os systematics of sulfide inclusions from the Jagersfontein Mine. Contrib Miner Petrol 157:525–540

Aulbach S, Stachel T, Heaman LM, Creaser RA, Shirey SB (2011) Formation of cratonic subcontinental lithospheric mantle and complementary komatiite from hybrid plume sources. Contrib Miner Petrol 161:947–960

Aulbach S, Stachel T, Seitz HM, Brey GP (2012) Chalcophile and siderophile elements in sulfide inclusions in eclogitic diamonds and metal cycling in a Paleoproterozoic subduction zone. Geochim Cosmochim Acta 93:278–299

Aulbach S, Griffin WL, Pearson NJ, O'Reilly SY (2013) Nature and timing of metasomatism in the stratified mantle lithosphere beneath the central Slave craton (Canada). Chem Geol 352:153–169

Aulbach S, Luchs T, Brey GP (2014) Distribution and behavior during metasomatism of PGE-Re and Os isotopes in off-craton mantle xenoliths from Namibia. Lithos 184:478–490

Balabin AI, Urusov VS (1995) Recalibration of the sphalerite cosmobarometer—experimental and theoretical treatment. Geochim Cosmochim Acta 59:1401–1410

Ballhaus C (1995) Is the upper mantle metal-saturated? Earth Planet Sci Lett 132:75–86

Ballhaus C, Sylvester P (2000) Noble metal enrichment processes in the Merensky Reef, Bushveld Complex. J Petrol 41545–561

Ballhaus C, Tredoux M, Späth A (2001) Phase relations in the Fe–Ni–Cu–PGE–S system at magmatic temperature and application to massive sulfide ores of the Sudbury Igneous Complex. J Petrol 42:1911–1926

Ballhaus C, Bockrath C, Wohlgemuth-Ueberwasser C, Laurenz V, Berndt J (2006) Fractionation of the noble metals by physical processes. Contrib Miner Petrol 152:667–684

Barin I (1995) Thermochemical Data of Pure Substances. Wiley-VCH, New York

Barnes SJ, Picard CP (1993) The behavior of platinum-group elements during partial melting, crystal fractionation, and sulfide segregation—an example from the Cape-Smith fold belt, Northern Quebec. Geochim Cosmochim Acta 57:79–87

Barnes SJ, Fiorentini ML (2008) Iridium, ruthenium and rhodium in komatiites: Evidence for iridium alloy saturation. Chem Geol 257:44–58

Barnes SJ, Naldrett AJ, Gorton MP (1985) The origin of the fractionation of platinum-group elements in terrestrial magmas. Chem Geol 53:303–323

Barnes SJ, Makovicky E, Makovicky M, RoseHansen J, KarupMoller S (1997) Partition coefficients for Ni, Cu, Pd, Pt, Rh, and Ir between monosulfide solid solution and sulfide liquid and the formation of compositionally zoned Ni–Cu sulfide bodies by fractional crystallization of sulfide liquid. Can J Earth Sci 34:366–374

Barth MG, Rudnick RL, Horn I, McDonough WF, Spicuzza MJ, Valley JW, Haggerty SE (2001) Geochemistry of xenolithic eclogites from West Africa, Part I: A link between low MgO eclogites and Archean crust formation. Geochim Cosmochim Acta 65:1499–1527

Barth MG, Rudnick RL, Carlson RW, Horn I, McDonough WF (2002) Re–Os and U–Pb geochronological constraints on the eclogite-tonalite connection in the Archean Man Shield, West Africa. Precambr Res 118:267–283

Batanova VG, Brügmann GE, Bazylev BA, Sobolev AV, Kamenetsky VS, Hofmann AW (2008) Platinum-group element abundances and Os isotope composition of mantle peridotites from the Mamonia complex, Cyprus. Chem Geol 248:195–212

Becker H, Dale CW (2016) Re–Pt–Os isotopic and highly siderophile element behavior in oceanic and continental mantle tectonite. Rev Mineral Geochem 81:369–440

Becker M, Le Roex AP (2006) Geochemistry of South African on- and off-craton, Group I and Group II kimberlites: Petrogenesis and source region evolution. J Petrol 47:673–703

Becker H, Horan MF, Walker RJ, Gao S, Lorand J-P, Rudnick RL (2006) Highly siderophile element composition of the Earth's primitive upper mantle: Constraints from new data on peridotite massifs and xenoliths. Geochim Cosmochim Acta 70:4528–4550

Bédard JH (2007) Trace element partitioning coefficients between silicate melts and orthopyroxene: Parameterizations of D variations. Chem Geol 244:263–303

Bell DR, Grégoire M, Grove TL, Chatterjee N, Carlson RW, Buseck PR (2005) Silica and volatile-element metasomatism of Archean mantle: a xenolith-scale example from the Kaapvaal Craton. Contrib Miner Petrol 150:251–267

Bennett VC, Nutman AP, Esat TM (2002) Constraints on mantle evolution from Os−187/Os−188 isotopic compositions of Archean ultramafic rocks from southern West Greenland (3.8 Ga) and Western Australia (3.46 Ga). Geochim Cosmochim Acta 66:2615–2630

Bennett NR, Brenan JM, Koga KT (2014) The solubility of platinum in silicate melt under reducing conditions: Results from experiments without metal inclusions. Geochim Cosmochim Acta 133:422–442

Berry AJ, Danyushevsky LV, O'Neill HSC, Newville M, Sutton SR (2008) Oxidation state of iron in komatiitic melt inclusions indicates hot Archean mantle. Nature 455:960–963

Bizimis M, Griselin M, Lassiter JC, Salters VJM, Sen G (2007) Ancient recycled mantle lithosphere in the Hawaiian plume: Osmium-Hafnium isotopic evidence from peridotite mantle xenoliths. Earth Planet Sci Lett 257:259–273

Bleeker W (2003) The late Archean record: a puzzle in ca. 35 pieces. Lithos 71:99–134

Bockrath C, Ballhaus C, Holzheid A (2004a) Stabilities of laurite RuS_2 and monosulfide liquid solution at magmatic temperature. Chem Geol 208:265–271

Bockrath C, Ballhaus C, Holzheid A (2004b) Fractionation of the platinum-group elements during mantle melting. Science 305:1951–1953

Botcharnikov RE, Holtz F, Mungall JE, Beermann O, Linnen RL, Garbe-Schoenberg D (2013) Behavior of gold in a magma at sulfide-sulfate transition: Revisited. Am Miner 98:1459–1464

Boyd FR (1987) High- and low-temperature garnet peridotite xenoliths and their possible relation to the lithosphere-asthenosphere boundary beneath southern Africa. *In:* Mantle Xenoliths, Nixon PH (ed), J. Wiley and Sons, New York, p 403–412

Boyd FR (1989) Compositional distinction between oceanic and cratonic lithosphere. Earth Planet Sci Lett 96:15–26

Boyd FR, Pokhilenko NP, Pearson DG, Mertzman SA, Sobolev NV, Finger LW (1997) Composition of the Siberian cratonic mantle: evidence from Udachnaya peridotite xenoliths. Contrib Miner Petrol 128:228–246

Bragagni A, Luguet A, Pearson DG, Fonseca ROC, Kjarsgaard BA (2014) Re–Os in single sulfides vs. whole rock: mantle melting, metasomatism and kimberlitic overprinting in Somerset (Rae Craton, Canada). 6th Orogenic Lherzolite Conference. Marrakech, Morocco. Not paginated

Brandon AD, Creaser RA, Shirey SB, Carlson RW (1996) Osmium recycling in subduction zones. Nature 272:861–864

Brandon AD, Becker H, Carlson RW, Shirey SB (1999) Isotopic constraints on time scales and mechanisms of slab material transport in the mantle wedge: evidence from the Simcoe mantle xenoliths, Washington, USA. Chem Geol 160:387–407

Brandon AD, Snow JE, Walker RJ, Morgan JW, Mock TD (2000) Pt-190-Os−186 and Re-187-Os−187 systematics of abyssal peridotites. Earth Planet Sci Lett 177:319–335

Brenan JM (2008) Re–Os fractionation by sulfide melt-silicate melt partitioning: A new spin. Chem Geol 248:140–165

Brenan JM, Andrews D (2001) High-temperature stability of laurite and Ru-Os–Ir alloy and their role in PGE fractionation in mafic magmas. Can Miner 39:341–360

Brenan JM, McDonough WF (2009) Core formation and metal-silicate fractionation of osmium and iridium from gold. Nature Geosci 2:798–801

Brenan JM, McDonough WF, Dalpé C (2003) Experimental constraints on the partitioning of rhenium and some platinum-group elements between olivine and silicate melt. Earth Planet Sci Lett 212:135–150

Brenan JM, McDonough WF, Ash R (2005) An experimental study of the solubility and partitioning of iridium, osmium and gold between olivine and silicate melt. Earth Planet Sci Lett 237:855–872

Brenan JM, Finnigan CF, McDonough WF, Homolova V (2012) Experimental constraints on the partitioning of Ru, Rh, Ir, Pt and Pd between chromite and silicate melt: The importance of ferric iron. Chem Geol 302:16–32

Brenan JM, Bennett NR, Zajacz Z (2016) Experimental results on fractionation of the highly siderophile elements (HSE) at variable pressures and temperatures during planetary and magmatic differentiation. Rev Mineral Geochem 81:1–87

Brügmann GE, Arndt NT, Hofmann AW, Tobschall H-J (1987) Precious metal abundances in komatiite suites from Alexo, Ontario, and Gorgona Island, Colombia. Geochim Cosmochim Acta 51:2159–2169

Büchl A, Brügmann G, Batanova VG, Münker C, Hofmann AW (2002) Melt percolation monitored by Os isotopes and HSE abundances: a case study from the mantle section of the Troodos Ophiolite. Earth Planet Sci Lett 204:385–402

Büchl A, Brügmann GE, Batanova VG, Hofmann AW (2004) Os mobilization during melt percolation: The evolution of Os isotope heterogeneities in the mantle sequence of the Troodos ophiolite, Cyprus. Geochim Cosmochim Acta 68:3397–3408

Burnham OM, Rogers NW, Pearson DG, van Calsteren PW, Hawkesworth CJ (1998) The petrogenesis of the eastern Pyrenean peridotites: An integrated study of their whole-rock geochemistry and Re–Os isotope composition. Geochim Cosmochim Acta 62:2293–2310

Burton KW, Schiano P, Birck JL, Allègre CJ (1999) Osmium isotope disequilibrium between mantle minerals in a spinel-lherzolite. Earth Planet Sci Lett 172:311–322

Burton KW, Schiano P, Birck J-L, Allègre CJ, Rehkämper M, Halliday AN, Dawson JB (2000) The distribution and behavior of rhenium and osmium amongst mantle minerals and the age of the lithospheric mantle beneath Tanzania. Earth Planet Sci Lett 183:93–106

Burton KW, Gannoun A, Birck JL, Allègre CJ, Schiano P, Clocchiatti R, Alard O (2002) The compatibility of rhenium and osmium in natural olivine and their behavior during mantle melting and basalt genesis. Earth Planet Sci Lett 198:63–76

Canil D (1991) Experimental evidence for the exsolution of cratonic peridotite from high-temperature harzburgite. Earth Planet Sci Lett 106:64–72

Canil D (1997) Vanadium partitioning and the oxidation state of Archean komatiite magmas. Nature 389:842–845

Canil D (2002) Vanadium in peridotites, mantle redox and tectonic environments: Archean to present. Earth Planet Sci Lett 195:75–90

Canil D (2004) Mildly incompatible elements in peridotites and the origins of mantle lithosphere. Lithos 77:375–393

Canil D, Fedortchouk Y (1999) Garnet dissolution and the emplacement of kimberlites. Earth Planet Sci Lett 167:227–237

Capobianco CJ, Drake MJ (1990) Partitioning of ruthenium, rhodium, and palladium between spinel and silicate melt and implications for platinum group element fractionation trends. Geochim Cosmochim Acta 54:869–874

Carlson RW, Irving AJ (1994) Depletion and enrichment history of subcontinental lithospheric mantle—an Os, Sr, Nd and Pb isotopic study of ultramafic xenoliths from the Northwestern Wyoming Craton. Earth Planet Sci Lett 126:457–472

Carlson RW, Moore RO (2004) Age of the Eastern Kaapvaal mantle: Re–Os isotope data for peridotite xenoliths from the Monastery kimberlite. S Afr J Geol 107:81–90

Carlson RW, Irving AJ, Hearn BCJ (1999a) Chemical and isotopic systematics of peridotite xenoliths from the Williams kimberlite, Montana: clues to processes of lithospheric formation, modification and destruction. Proc 7th Inter Kimberlite Conf:90–98

Carlson RW, Pearson DG, Boyd FR, Shirey SB, Irvine G, Menzies AH, Gurney JJ (1999b) Regional age variation of the southern African mantle: Significance for models of lithospheric mantle formation. Proc 7th Inter Kimberlite Conf:99–108

Carlson RW, Pearson DG, James DE (2005) Physical, chemical, and chronological characteristics of continental mantle. Rev Geophys 43:RG1001

Carlson RW, Shirey SB, Schönbächler M (2008) Applications of PGE radioisotope systems in geo- and cosmochemistry. Elements 4:239–245

Chalapathi Rao NV, Lehmann B, Balaram V (2014) Platinum-group element (PGE) geochemistry of Deccan orangeites, Bastar craton, central India: implication for a non-terrestrial origin for iridium enrichment at the K–Pg boundary. J Asian Earth Sci 84:24–33

Chesley JT, Rudnick RL, Lee CT (1999) Re–Os systematics of mantle xenoliths from the East African Rift: Age, structure, and history of the Tanzanian craton. Geochim Cosmochim Acta 63:1203–1217

Chesley J, Righter K, Ruiz J (2004) Large-scale mantle metasomatism: a Re–Os perspective. Earth Planet Sci Lett 219:49–60

Chou C-L (1978) Fractionation of Siderophile Elements in the Earth's Upper Mantle. 9th Lunar Planet Sci Conf. Lunar and Planetary Institute, p 219–230

Chu ZY, Wu FY, Walker RJ, Rudnick RL, Pitcher L, Puchtel IS, Yang YH, Wilde SA (2009) Temporal Evolution of the Lithospheric Mantle beneath the Eastern North China Craton. J Petrol 50:1857–1898

Chung H-Y, Mungall JE (2009) Physical constraints on the migration of immiscible fluids through partially molten silicates, with special reference to magmatic sulfide ores. Earth Planet Sci Lett 286:14–22

Coggon JA, Luguet A, Nowell GM, Appel PWU (2013) Hadean mantle melting recorded by southwest Greenland chromitite Os−186 signatures. Nature Geosci 6:871–874

Cottrell E, Walker D (2006) Constraints on core formation from Pt partitioning in mafic silicate liquids at high temperatures. Geochim Cosmochim Acta 70:1565–1580

Cox KG, Smith MR, Beswetherick S (1987) Textural studies of garnet lherzolites: evidence of exsolution origin from high temperature harzburgites. *In:* Mantle Xenoliths. Nixon PH (ed), Wiley, London, p 537–550

Creaser RA, Papanastassiou DA, Wasserburg GJ (1991) Negative thermal ion mass-spectrometry of osmium, rhenium, and iridium. Geochim Cosmochim Acta 55:397–401

Creighton S, Stachel T, McLean H, Muehlenbachs K, Simonetti A, Eichenberg D, Luth R (2008) Diamondiferous peridotitic microxenoliths from the Diavik Diamond Mine, NT. Contrib Mineral Petrol 155:541–554

Dale CW, Burton KW, Pearson DG, Gannoun A, Alard O, Argles TW, Parkinson IJ (2009) Highly siderophile element behavior accompanying subduction of oceanic crust: Whole rock and mineral-scale insights from a high-pressure terrain. Geochim Cosmochim Acta 73:1394–1416

Dale CW, Macpherson CG, Pearson DG, Hammond SJ, Arculus RJ (2012) Inter-element fractionation of highly siderophile elements in the Tonga Arc due to flux melting of a depleted source. Geochim Cosmochim Acta 89:202–225

Dalton JA, Presnall DC (1998) The continuum of primary carbonatitic–kimberlitic melt compositions in equilibrium with lherzolite: Data from the system CaO-MgO-Al_2O_3-SiO_2-CO_2 at 6 GPa. J Petrol 39:1953–1964

Dalton CA, Langmuir CH, Gale A (2014) Geophysical and Geochemical Evidence for Deep Temperature Variations Beneath Mid-Ocean Ridges. Science 344:80–83

Dasgupta R, Mallik A, Tsuno K, Withers AC, Hirth G, Hirschmann MM (2013) Carbon-dioxide-rich silicate melt in the Earth's upper mantle. Nature 493:211-222

Davies GF (2009) Effect of plate bending on the Urey ratio and the thermal evolution of the mantle. Earth Planet Sci Lett 287:513–518

Dawson JB (1984) Contrasting types of upper-mantle metasomatism? *In:* Kimberlites II: The Mantle and Crust–Mantle Relationships. Kornprobst J (ed), Elsevier, Amsterdam, p 282–331

Dawson JB (2002) Metasomatism and partial melting in upper-mantle peridotite xenoliths from the Lashaine volcano, northern Tanzania. J Petrol 43:1749–1777

Day JMD (2013) Hotspot volcanism and highly siderophile elements. Chemi Geol 341:50–74

Day JMD, Pearson DG, Nowell GM (2003) High precision rhenium and platinum isotope dilution analyses by plasma ionisation multicollector mass spectrometry. *In*: Plasma Source Mass Spectrometry: Applications and Emerging Technologies. Holland JG, Tanner SD (eds), R Soc Chem Spec Publ, London, p 374–390

Day JMD, Walker RJ, Qin LP, Rumble D (2012) Late accretion as a natural consequence of planetary growth. Nature Geosci 5:614–617

Day JMD, Brandon AD, Walker RJ (2016) Highly siderophile elements in Earth, Mars, the Moon, and asteroids. Rev Mineral Geochem 81:161–238
De Wit M, Thiart C (2005) Metallogenic fingerprints of Archean cratons. Miner Deposits Earth Evol 248:59–70
Delpech G, Lorand JP, Grégoire M, Cottin JY, O'Reilly SY (2012) In-situ geochemistry of sulfides in highly metasomatized mantle xenoliths from Kerguelen, southern Indian Ocean. Lithos 154:296–314
Dijkstra AH, Sergeev DS, Spandler C, Pettke T, Meisel T, Cawood PA (2010) Highly Refractory Peridotites on Macquarie Island and the Case for Anciently Depleted Domains in the Earth's Mantle. J Petrol 51:469–493
Dilek Y, Furnes H (2011) Ophiolite genesis and global tectonics: geochemical and tectonic fingerprinting of ancient oceanic lithosphere. Geol Soc Amer Bull 123:387–411
Drury MR, van Roermund HLM (1989) Fluid assisted recrystallization in upper mantle peridotite xenoliths from kimberlites. J Petrol 30:133–152
Dygert N, Liang Y, Sun C, Hess P (2014) An experimental study of trace element partitioning between augite and Fe-rich basalts. Geochim Cosmochim Acta 132:170–186
Erlank AJ, Waters FG, Hawkesworth CJ, Haggerty SE, Allsopp HL, Rickard RS, Menzies MA (1987) Evidence for mantle metasomatism in peridotite nodules from the Kimberley pipes, South Africa. *In:* Mantle Metasomatism. Hawkesworth CJ, Menzies MA (eds). Academic Press, London, p 221–311
Ernst WG, Liou JG (2008) High- and ultrahigh-pressure metamorphism: Past results and future prospects. Am Mineral 93:1771–1786
Fan WM, Zhang HF, Baker J, Jarvis KE, Mason PRD, Menzies MA (2000) On and off the North China Craton: Where is the Archean keel? J Petrol 41:933–950
Fedortchouk Y, Canil D (2004) Intensive variables in kimberlite magmas, Lac de Gras, Canada and implications for diamond survival. J Petrol 45:1725–1745
Finnerty AA, Boyd FR (1987) Thermobarometry for garnet peridotite xenoliths: a basis for upper mantle stratigraphy. *In:* Mantle Xenoliths. Nixon PH (ed) Wiley, Chichester, p 381–402
Finnigan CS, Brenan JM, Mungall JE, McDonough WF (2008) Experiments and models bearing on the role of chromite as a collector of platinum group minerals by local reduction. J Petrol 49:1647–1665
Fiorentini ML, Barnes SJ, Maier WD, Burnham OM, Heggie G (2011) Global Variability in the Platinum-group Element Contents of Komatiites. J Petrol 52:83–112
Fischer-Gödde M, Becker H, Wombacher F (2010) Rhodium, gold and other highly siderophile element abundances in chondritic meteorites. Geochim Cosmochim Acta 74:356–379
Fischer-Gödde M, Becker H, Wombacher F (2011) Rhodium, gold and other highly siderophile elements in orogenic peridotites and peridotite xenoliths. Chem Geol 280:365–383
Fischer-Gödde M, Becker H (2012) Osmium isotope and highly siderophile element constraints on ages and nature of meteoritic components in ancient lunar impact rocks. Geochim Cosmochim Acta 77:135–156
Fleet ME, Stone WE (1990) Nickeliferous sulfides in xenoliths, olivine megacrysts and basaltic glass. Contrib Mineral Petrol 105:629–636
Fleet ME, Crocket JH, Stone WE (1996) Partitioning of platinum-group elements (Os, Ir, Ru, Pt, Pd) and gold between sulfide liquid and basalt melt. Geochim Cosmochim Acta 60:2397–2412
Fleet ME, Liu MH, Crocket JH (1999) Partitioning of trace amounts of highly siderophile elements in the Fe–Ni–S system and their fractionation in nature. Geochim Cosmochim Acta 63:2611–2622
Foley SF (2011) A Reappraisal of Redox Melting in the Earth's Mantle as a Function of Tectonic Setting and Time. J Petrol 52:1363–1391
Fonseca ROC, Mallmann G, O'Neill HSC, Campbell IH (2007) How chalcophile is rhenium? An experimental study of the solubility of Re in sulfide mattes. Earth Planet Sci Lett 260:537–548
Fonseca ROC, Mallmann G, O'Neill HS, Campbell IH, Laurenz V (2011) Solubility of Os and Ir in sulfide melt: Implications for Re/Os fractionation during mantle melting. Earth Planet Sci Lett 311:339–350
Fonseca ROC, Laurenz V, Mallmann G, Luguet A, Hoehne N, Jochum KP (2012) New constraints on the genesis and long-term stability of Os-rich alloys in the Earth's mantle. Geochim Cosmochim Acta 87:227–242
Frey F, Green D (1974) The mineralogy, geochemistry and origin of lherzolite inclusions in Victorian basanites. Geochim Cosmochim Acta 38:1023–1059
Frick C (1973) Sulfides in griquaite and garnet-peridotite xenoiths in kimberlite. Contrib Mineral Petrol 39:1–16
Frost DJ, McCammon CA (2008) The redox state of Earth's mantle. Ann Rev Earth Planet Sci 36:389–420
Gannoun A, Burton KW, Thomas LE, Parkinson IJ, van Calsteren P, Schiano P (2004) Osmium Isotope Heterogeneity in the Constituent Phases of Mid-Ocean Ridge Basalts. Science 303:70–72
Gannoun A, Burton KW, Parkinson IJ, Alard O, Schiano P, Thomas LE (2007) The scale and origin of the osmium isotope variations in mid-ocean ridge basalts. Earth Planet Sci Lett 259:541–556
Gannoun A, Burton KW, Day JMD, Harvey J, Schiano P, Parkinson I (2016) Highly siderophile element and Os isotope systematics of volcanic rocks at divergent and convergent plate boundaries and in intraplate settings. Rev Mineral Geochem 81:651–724
Gao S, Rudnick RL, Carlson RW, McDonough WF, Liu YS (2002) Re–Os evidence for replacement of ancient mantle lithosphere beneath the North China craton. Earth Planet Sci Lett 198:307–322

Gao S, Zhang J, Xu W, Liu Y (2009) Delamination and destruction of the North China Craton. Chinese Science Bulletin 54:3367–3378

Garuti G, Oddone M, Torres-Ruiz J (1997) Platinum-group-element distribution in subcontinental mantle: Evidence from the Ivrea zone (Italy) and the Betic-Rifean cordillera (Spain and Morocco). Can J Earth Sci 34:444–463

Godel B, Barnes SJ, Barnes S-J, Maier WD (2010) Platinum ore in three dimensions: Insights from high-resolution X-ray computed tomography. Geology 38:1127–1130

González-Jiménez JM, Villaseca C, Griffin WL, O'Reilly SY, Belousova E, Ancochea E, Pearson NJ (2014) Significance of ancient sulfide PGE and Re–Os signatures in the mantle beneath Calatrava, Central Spain. Contrib Mineral Petrol 168:1047

Graham S, Lambert DD, Shee SR, Smith CB, Reeves S (1999) Re–Os isotopic evidence for Archean lithospheric mantle beneath the Kimberley block, Western Australia. Geol 27:431–434

Graham S, Lambert D, Shee S (2004) The petrogenesis of carbonatite, melnoite and kimberlite from the Eastern Goldfields Province, Yilgarn Craton. Lithos 76:519–533

Gréau Y, Alard O, Griffin WL, Huang J-X, O'Reilly SY (2013) Sulfides and chalcophile elements in Roberts Victor eclogites: unravelling a sulfide-rich metasomatic event. Chem Geol 354:73–92

Grégoire M, Bell DR, Le Roex AP (2002) Trace element geochemistry of phlogopite-rich mafic mantle xenoliths: their classification and their relationship to phlogopite-bearing peridotites and kimberlites revisited. Contrib Mineral Petrol 142:603–625

Grégoire M, Bell DR, Le Roex AP (2003) Garnet lherzolites from the Kaapvaal craton (South Africa): Trace element evidence for a metasomatic history. J Petrol 44:629–657

Griffin WL, Kaminsky FV, Ryan CG, Oreilly SY, Win TT, Ilupin IP (1996) Thermal state and composition of the lithospheric mantle beneath the Daldyn kimberlite field, Yakutia. Tectonophys 262:19–33

Griffin WL, Andi Z, O'Reilly SY, Ryan CG (1998) Phanerozoic evolution of the lithosphere beneath the Sino-Korean Craton. Mantle Dynamics and Plate Interactions in East Asia 27:107–126

Griffin WL, Spetsius ZV, Pearson NJ, O'Reilly SY (2002) In situ Re–Os analysis of sulfide inclusions in kimberlitic olivine: New constraints on depletion events in the Siberian lithospheric mantle. Geochem Geophys Geosyst 3:1069, doi:10.1029/2001GC000287

Griffin WL, O'Reilly SY, Abe N, Aulbach S, Davies RM, Pearson NJ, Doyle BJ, Kivi K (2003a) The origin and evolution of Archean lithospheric mantle. Precambr Res 127:19–41

Griffin WL, O'Reilly SY, Natapov LM, Ryan CG (2003b) The evolution of lithospheric mantle beneath the Kalahari Craton and its margins. Lithos 71:215–241

Griffin WL, Graham S, O'Reilly SY, Pearson NJ (2004) Lithosphere evolution beneath the Kaapvaal Craton: Re–Os systematics of sulfides in mantle-derived peridotites. Chem Geol 208:89–118

Griffin WL, O'Reilly SY, Afonso JC, Begg GC (2009) The composition and evolution of lithospheric mantle: a re-evaluation and its tectonic implications. J Petrol 50:1185–1204

Griffin WL, Belousova EA, O'Neill C, O'Reilly SY, Malkovets V, Pearson NJ, Spetsius S, Wilde SA (2014) The world turns over: Hadean–Archean crust-mantle evolution. Lithos 189:2–15

Gros M, Lorand JP, Luguet A (2002) Analysis of platinum group elements and gold in geological materials using NiS fire assay and Te co-precipitation; the NiS dissolution step revisited. Chem Geol 185:179–190

Giuliani A, Kamenetsky VS, Kendrick MA, Phillips D, Goemann K (2013) Nickel-rich metasomatism of the lithospheric mantle by pre-kimberlitic alkali-S–Cl-rich C–O–H fluids. Contrib Mineral Petrol 165:155–171

Gurney JJ, Helmstaedt HH, Richardson SH, Shirey SB (2010) Diamonds through Time. Econ Geol 105:689–712

Handler MR, Bennett VC (1999) Behavior of Platinum-group elements in the subcontinental mantle of eastern Australia during variable metasomatism and melt depletion. Geochim Cosmochim Acta 63:3597–3618

Handler MR, Bennett VC, Esat TM (1997) The persistence of off-cratonic lithospheric mantle: Os isotopic systematics of variably metasomatized southeast Australian xenoliths. Earth Planet Sci Lett 151:61–75

Handler MR, Wysoczanski RJ, Gamble JA (2003) Proterozoic lithosphere in Marie Byrd Land, West Antarctica: Re–Os systematics of spinel peridotite xenoliths. Chem Geol 196:131–145

Hanghøj K, Kelemen P, Bernstein S, Blusztajn J, Frei R (2001) Osmium isotopes in the Wiedemann Fjord mantle xenoliths: A unique record of cratonic mantle formation by melt depletion in the Archean. Geochem Geophys Geosyst 2:2000GC000085

Hanghøj K, Kelemen PB, Hassler D, Godard M (2010) Composition and genesis of depleted mantle peridotites from the Wadi Tayin Massif, Oman Ophiolite; Major and trace element geochemistry, and Os isotope and PGE systematics. J Petrol 51:201–227

Hart SR, Gaetani GA (2006) Mantle Pb paradoxes: the sulfide solution. Contrib Mineral Petrol 152:295–308

Hart SR, Ravizza G (1996) Osmium partitioning between phases in lherzolite and basalt. *In*: Earth Processes: Reading the Isotopic Code. Basu A, Hart SR (eds). AGU Geophys Monogr Ser, p 123–134

Hart SR, Zindler A (1986) In search of a bulk-earth composition. Chem Geol 57:247–267

Harte B (1983) Mantle peridotites and processes: The kimberlite sample. *In*: Continental Basalts and Mantle Xenoliths. Hawkesworth CJ, Norry MJ (eds) Shiva. Cheshire, UK, p 46–91

Harvey J, Gannoun A, Burton KW, Rogers NW, Alard O, Parkinson IJ (2006) Ancient melt extraction from the oceanic upper mantle revealed by Re–Os isotopes in abyssal peridotites from the Mid-Atlantic ridge. Earth Planet Sci Lett 244:606–621

Harvey J, Gannoun A, Burton KW, Schiano P, Rogers NW, Alard O (2010) Unravelling the effects of melt depletion and secondary infiltration on mantle Re–Os isotopes beneath the French Massif Central. Geochim Cosmochim Acta 74:293–320

Harvey J, Dale CW, Gannoun A, Burton KW (2011) Osmium mass balance in peridotite and the effects of mantle-derived sulfides on basalt petrogenesis. Geochim Cosmochim Acta 75:5574–5596

Harvey J, Warren J, Shirey S (2016) Mantle sulfides and their role in Re–Os–Pb geochronology. Rev Mineral Geochem 81:579–649

Hassler DR, Peucker-Ehrenbrink B, Ravizza GE (2000) Rapid determination of Os isotopic composition by sparging OsO4 into a magnetic-sector ICP-MS. Chem Geol 166:1–14

Hattori KH, Arai S, Clarke DB (2002) Selenium, tellurium, arsenic and antimony contents of primary mantle sulfides. Can Miner 40:637–650

Heaman LM, Kjarsgaard BA, Creaser RA (2004) The temporal evolution of North American kimberlites. Lithos 76:377–397

Helmstaedt HH, Schulze DJ (1989) Southern African kimberlites and their mantle sample: implications for Archean tectonics and lithosphere evolution. *In:* Kimberlites and related rocks. Proc 4th Intl Kimb Conf, Perth 1986, Vol 1, Geol Soc Australia, Spec Publ 14, p 358–368

Herzberg C (2004) Geodynamic information in peridotite petrology. J Petrol 45:2507–2530

Herzberg C, O'Hara MJ (1998) Phase equilibrium constraints on the origin of basalts, picrites, and komatiites. Earth-Sci Rev 44:39–79

Herzberg C, O'Hara MJ (2002) Plume-associated ultramafic magmas of Phanerozoic age. J Petrol 43:1857–1883

Herzberg C, Rudnick R (2012) Formation of cratonic lithosphere: An integrated thermal and petrological model. Lithos 149:4–15

Herzberg C, Asimow PD, Arndt N, Niu YL, Lesher CM, Fitton JG, Cheadle MJ, Saunders AD (2007) Temperatures in ambient mantle and plumes: Constraints from basalts, picrites, and komatiites. Geochem Geophys Geosyst 8:Q02006, doi:10.1029/2006GC001390

Herzberg C, Condie K, Korenaga J (2010) Thermal history of the Earth and its petrological expression. Earth Planet Sci Lett 292:79–88

Holzheid A, Grove TL (2002) Sulfur saturation limits in silicate melts and their implications for core formation scenarios for terrestrial planets. Am Miner 87:227–237

Holzheid A, Palme H, Chakraborty S. 1997. The activities of NiO, CoO and FeO in silicate melts. Chem Geol 139:21–38

Horan MF, Walker RJ, Morgan JW, Grossman JN, Rubin AE (2003) Highly siderophile elements in chondrites. Chem Geol 196:5–20

Hughes HSR, McDonald I, Goodenough KM, Ciborowski TJR, Kerr AC, Davies J, Selby D (2014) Enriched lithospheric mantle keel below the Scottish margin of the North Atlantic Craton: Evidence from the Paleoproterozoic Scourie Dyke Swarm and mantle xenoliths. Precambr Res 250:97–126

Ionov DA, Chanefo I, Bodinier JL (2005a) Origin of Fe-rich lherzolites and wehrlites from Tok, SE Siberia by reactive melt percolation in refractory mantle peridotites. Contrib Miner Petrol 150:335–353

Ionov DA, Prikhodko VS, Bodinier JL, Sobolev AV, Weis D (2005b) Lithospheric mantle beneath the south-eastern Siberian craton: petrology of peridotite xenoliths in basalts from the Tokinsky Stanovik. Contrib Miner Petrol 149:647–665

Ionov DA, Shirey SB, Weis D, Brügmann G (2006) Os–Hf–Sr–Nd isotope and PGE systematics of spinel peridotite xenoliths from Tok, SE Siberian craton: Effects of pervasive metasomatism in shallow refractory mantle. Earth Planet Sci Lett 241:47–64

Irvine GJ, Pearson DG, Carlson RW (2001) Lithospheric mantle evolution of the Kaapvaal Craton: A Re–Os isotope study of peridotite xenoliths from Lesotho kimberlites. Geophys Res Lett 28:2505–2508

Irvine GJ, Pearson DG, Kjarsgaard BA, Carlson RW, Kopylova MG, Dreibus G (2003) A Re–Os isotope and PGE study of kimberlite-derived peridotite xenoliths from Somerset Island and a comparison to the Slave and Kaapvaal cratons. Lithos 71:461–488

Ishikawa A, Pearson DG, Dale CW (2011) Ancient Os isotope signatures from the Ontong Java Plateau lithosphere: Tracing lithospheric accretion history. Earth Planet Sci Lett 301:159–170

Iwamori H, McKenzie D, Takahashi E (1995) Melt generation by isentropic mantle upwelling. Earth Planet Sci Lett 134:253–266

Jacob DE (2004) Nature and origin of eclogite xenoliths from kimberlites. Lithos 77:295–316

Jagoutz E, Palme H, Baddenhausen H, Blum K, Cendales M, Dreibus G, Spettel B, Lorenz V, Wänke H (1979) The abundances of major, minor, and trace elements in the Earth's mantle as derived from ultramafic nodules. 10th Lunar Planet Sci Conf, Lunar and Planetary Institute, p 2031–2050

Janney PE, Shirey SB, Carlson RW, Pearson DG, Bell DR, Le Roex AP, Ishikawa A, Nixon PH, Boyd FR (2010) Age, composition and thermal characteristics of South African off-craton mantle lithosphere: Evidence for a multi-stage history. J Petrol 51:1849–1890

Jégo S, Dasgupta R (2014) The fate of sulfur during fluid—Present melting of subducting basaltic crust at variable oxygen fugacity. J Petrol 55:1019–1050

Jordan TH (1975) Lateral heterogeneity and mantle dynamics. Nature 257:745–750

Jordan TH (1988) Structure and formation of the continental tectosphere. J Petrol, Spec Vol 1:11–38

Jugo PJ, Wilke M, Botcharnikov RE (2010) Sulfur K-edge XANES analysis of natural and synthetic basaltic glasses: Implications for S speciation and S content as function of oxygen fugacity. Geochim Cosmochim Acta 74:5926–5938

Kaislaniemi L, van Hunen J (2014) Dynamics of lithospheric thinning and mantle melting by edge-driven convection: Application to Moroccan Atlas mountains. Geochem Geophys Geosyst 15:3175–3189

Kasting JF 1993. Earth's early atmosphere. Science 259:920–926

Keays RR (1995) The role of komatiitic and picritic magmatism and S-saturation in the formation of ore deposits: Lithos 34:1–18

Kelemen PB, Hart SR, Bernstein S (1998) Silica enrichment in the continental upper mantle via melt/rock reaction. Earth Planet Sci Lett 164:387–406

Kepezhinskas P, Defant MJ, Widom E (2002) Abundance and distribution of PGE and Au in the island-arc mantle: implications for sub-arc metasomatism. Lithos 60:113–128

Kesson SE, Ringwood AE (1989) Slab mantle interactions 1. sheared and refertilized garnet peridotite xenoliths—samples of Wadati-Benioff-zones. Chem Geol 78:83–96

Khatun S, Mondal SK, Zhou M-F, Balaram V, Prichard HM (2014) Platinum-group element (PGE) geochemistry of Mesoarchean ultramafic-mafic cumulate rocks and chromitites from the Nuasahi Massif, Singhbhum Craton (India). Lithos 205:322–340

Kimura K, Lewis RS, Anders E (1974) Distribution of gold and rhenium between nickel-iron and silicate melts—implications for abundance of siderophile elements on earth and moon. Geochim Cosmochim Acta 38:683–701

Kinzler RJ, Grove TL (1992) Primary magmas of midocean ridge basalts. 2. Applications. J Geophys Res-Solid Earth 97(B5):6907–6926

Kobussen AF, Griffin WL, O'Reilly SY, Shee SR (2008) Ghosts of lithospheres past: Imaging an evolving lithospheric mantle in southern Africa. Geol 36:515–518

Kogarko LN, Henderson CMB, Pacheco H (1995) Primary Ca-rich carbonatite magma and carbonatite-silicate-sulfide liquid immiscibility in the upper mantle. Contrib Miner Petrol 121:267–274

Kogiso T, Suzuki K, Suzuki T, Shinotsuka K, Uesugi K, Takeuchi A, Suzuki Y (2008) Detecting micrometer-scale platinum-group minerals in mantle peridotite with microbeam synchrotron radiation X-ray fluorescence analysis. Geochem Geophys Geosyst 9:Q03018, doi:10.1029/2007GC001888

König S, Luguet A, Lorand JP, Wombacher F, Lissner M (2012) Selenium and tellurium systematics of the Earth's mantle from high precision analyses of ultra-depleted orogenic peridotites. Geochim Cosmochim Acta 86:354–366

König S, Lorand JP, Luguet A, Pearson DG (2014) A non-primitive origin of near-chondritic S-Se-Te ratios in mantle peridotites; implications for the Earth's late accretionary history. Earth Planet Sci Lett 385:110–121

König S, Lissner M, Lorand J-P, Bragagni A, Luguet A (2015) Mineralogical control of selenium, tellurium and highly siderophile elements in the Earth's mantle: Evidence from mineral separates of ultra-depleted mantle residues. Chem Geol 396:16–24

Kopylova MG, Matveev S, Raudsepp M (2007) Searching for parental kimberlite melt. Geochim Cosmochim Acta 71:3616–3629

Korenaga J (2008) Urey ratio and the structure and evolution of Earth's mantle. Rev Geophys 46: RG2007, RG2007, doi:10.1029/2007RG000241

Kusky TM, Windley BF, Wang L, Wang ZS, Li XY, Zhu PM (2014) Flat slab subduction, trench suction, and craton destruction: Comparison of the North China, Wyoming, and Brazilian cratons. Tectonophysics 630:208–221

Lange RA, Carmichael ISE. 1987. Densities of Na_2O-K_2O-CaO-MgO-FeO-Fe_2O_3-Al_2O_3-TiO_2-SiO_2 liquids—new measurements and derived partial molar properties. Geochim Cosmochim Acta 51:2931–2946

Laurenz V, Fonseca ROC, Ballhaus C, Sylvester PJ (2010) Solubility of palladium in picritic melts: 1. The effect of iron. Geochim Cosmochim Acta 74:2989–2998

Laurenz V, Fonseca ROC, Ballhaus C, Jochum KP, Heuser A, Sylvester PJ (2013) The solubility of palladium and ruthenium in picritic melts: 2. The effect of sulfur. Geochim Cosmochim Acta 108:172–18

Laurenz V, Rubie DC, Frost DJ (2014) Metal-silicate partitioning of HSE in S-bearing systems- Implications for Earth's accretion and core formation. V.M. Goldschmidt Conference. Sacramento, CA. p 1368

Le Roex AP, Bell DR, Davis P (2003) Petrogenesis of group I kimberlites from Kimberley, South Africa: Evidence from bulk-rock geochemistry. J Petrol 44:2261–2286

Le Roux V, Bodinier J-L, Tommasi A, Alard O, Dautria J-M, Vauchez A, Riches AJV (2007) The Lherz spinel lherzolite: Refertilized rather than pristine mantle. Earth Planet Sci Lett 259:599–612

Lee CTA (2002) Platinum-group element geochemistry of peridotite xenoliths from the Sierra Nevada and the Basin and Range, California. Geochim Cosmochim Acta 66:3987–4005
Lee CTA (2005) Trace element evidence for hydrous metasomatism at the base of the North American lithosphere and possible association with Laramide low-angle subduction. J Geol 113:673–685
Lee CTA (2006) Geochemical/petrologic constraints on the origin of cratonic mantle. *In:* Archean Geodynamics and Environments. Vol 164. Benn K, Mareschal JC, Condie KC (eds), Geophys Monogr Ser, AGU, p 89–114
Lee C-T, Rudnick RL (1999) Compositionally stratified cratonic lithosphere: Petrology and geochemistry of peridotite xenoliths from the Labait Voclcano, Tanzania. Proc 7th Inter Kimberlite Conf, p 503–521
Lee SR, Walker RJ (2006) Re–Os isotope systematics of mantle xenoliths from South Korea: Evidence for complex growth and loss of lithospheric mantle beneath East Asia. Chem Geol 231:90–101
Lee CT, Yin QZ, Rudnick RL, Chesley JT, Jacobsen SB (2000) Osmium isotopic evidence for mesozoic removal of lithospheric mantle beneath the Sierra Nevada, California. Science 289:1912–1916
Lee CT, Yin QZ, Rudnick RL, Jacobsen SB (2001) Preservation of ancient and fertile lithospheric mantle beneath the southwestern United States. Nature 411:69–73
Lee CTA, Luffi P, Le Roux V, Dasgupta R, Albarede F, Leeman WP (2010) The redox state of arc mantle using Zn/Fe systematics. Nature 468:681–685
Lee CTA, Luffi P, Chin EJ (2011) Building and Destroying Continental Mantle. Ann Rev Earth Planet Sci 39:59–90
Lenardic A, Moresi L, Muhlhaus H (2000) The role of mobile belts for the longevity of deep cratonic lithosphere: The crumple zone model. Geophys Res Lett 27:1235–1238
Lenardic A, Moresi LN, Muhlhaus H (2003) Longevity and stability of cratonic lithosphere: Insights from numerical simulations of coupled mantle convection and continental tectonics. J Geophys Res-Solid Earth 108(B6)
Li C, Barnes SJ, Makovicky E, RoseHansen J, Makovicky M (1996) Partitioning of nickel, copper, iridium, rhenium, platinum, and palladium between monosulfide solid solution and sulfide liquid: Effects of composition and temperature. Geochim Cosmochim Acta 60:1231–1238
Li Y (2014) Comparative geochemistry of rhenium in oxidized arc magmas and MORB and rhenium partitioning during magmatic differentiation. Chem Geol 386:101–114
Li ZXA, Lee CTA, Peslier AH, Lenardic A, Mackwell SJ (2008) Water contents in mantle xenoliths from the Colorado Plateau and vicinity: Implications for the mantle rheology and hydration-induced thinning of continental lithosphere. J Geophys Res-Solid Earth 113(B9):B09210, doi:10.1029/2007JB005540
Liu YN, Samaha NT, Baker DR (2007) Sulfur concentration at sulfide saturation (SCSS) in magmatic silicate melts. Geochim Cosmochim Acta 71:1783–1799
Liu CZ, Snow JE, Brügmann G, Hellebrand E, Hofmann AW (2009) Non-chondritic HSE budget in Earth's upper mantle evidenced by abyssal peridotites from Gakkel ridge (Arctic Ocean). Earth Planet Sci Lett 283:122–132
Liu JG, Rudnick RL, Walker RJ, Gao S, Wu FY, Piccoli PM (2010) Processes controlling highly siderophile element fractionations in xenolithic peridotites and their influence on Os isotopes. Earth Planet Sci Lett 297:287–297
Liu J, Rudnick RL, Walker RJ, Gao S, Wu F-y, Piccoli PM, Yuan H, Xu W-l, Xu Y-G (2011) Mapping lithospheric boundaries using Os isotopes of mantle xenoliths: An example from the North China Craton. Geochim Cosmochim Acta 75:3881–3902
Lodders K, Palme H (1991) The role of sulfur in planetary core formation. Meteoritics 26:366–366
Lorand JP (1989) Sulfide petrology of spinel and garnet pyroxenite layers from mantle-derived spinel lherzolite massifs of Ariège, Northeastern Pyrenees, France. J Petrol 30:987–1015
Lorand JP, Alard O (2001) Platinum-group element abundances in the upper mantle: New constraints from in situ and whole-rock analyses of Massif Central xenoliths (France). Geochim Cosmochim Acta 65:2789–2806
Lorand JP, Alard O (2010) Determination of selenium and tellurium concentrations in Pyrenean peridotites (Ariege, France): New insight into S/Se/Te systematics of the upper in mantle samples. Chem Geol 278:120–130
Lorand JP, Conquéré F (1983) Contribution to the study of sulfide parageneses in spinel lherzolite xenoliths from alkali basalts (Massif Central and Languedoc, France). Bull Minéral 106:585–605
Lorand JP, Grégoire M (2006) Petrogenesis of base metal sulfide assemblages of some peridotites from the Kaapvaal craton (South Africa). Contrib Miner Petrol 151:521–538
Lorand J-P, Luguet A (2016) Chalcophile and siderophile elements in mantle rocks: Trace elements controlled by trace minerals. Rev Mineral Geochem 81:441–488
Lorand JP, Alard O, Luguet A, Keays RR (2003a) Sulfur and selenium systematics of the subcontinental lithospheric mantle: Inferences from the Massif Central xenolith suite (France). Geochim Cosmochim Acta 67:4137–4151
Lorand JP, Reisberg L, Bedini RM (2003b) Platinum-group elements and melt percolation processes in Sidamo spinel peridotite xenoliths, Ethiopia, East African Rift. Chem Geol 196:57–75
Lorand JP, Luguet A, Alard O (2008) Platinum-group elements: A new set of key tracers for the earth's interior. Elements 4:247–252

Lorand JP, Alard O, Godard M (2009) Platinum-group element signature of the primitive mantle rejuvenated by melt-rock reactions: evidence from Sumail peridotites (Oman Ophiolite). Terra Nova 21:35–40
Lorand JP, Alard O, Luguet A (2010) Platinum-group element micronuggets and refertilization process in Lherz orogenic peridotite (northeastern Pyrenees, France). Earth Planet Sci Lett 289:298–310
Lorand JP, Luguet A, Alard O (2013) Platinum-group element systematics and petrogenetic processing of the continental upper mantle: A review. Lithos 164:2–21
Luchs T, Brey GP, Gerdes A, Höfer HE (2013) The lithospheric mantle underneath the Gibeon Kimberlite field (Namibia):A mix of old and young components—Evidence from Lu–Hf and Sm–Nd isotope systematics. Precambr Res 231:263–276
Luguet A, Reisberg L (2016) Highly siderophile element and ^{187}Os signatures in non–cratonic basalt–hosted peridotite xenoliths: Unravelling the origin and evolution of the post-Archean lithospheric mantle. Rev Mineral Geochem 81:305–367
Luguet A, Alard O, Lorand JP, Pearson NJ, Ryan C, O'Reilly SY (2001) Laser-ablation microprobe (LAM)-ICPMS unravels the highly siderophile element geochemistry of the oceanic mantle. Earth Planet Sci Lett 189:285–294
Luguet A, Lorand JP, Seyler M (2003) Sulfide petrology and highly siderophile element geochemistry of abyssal peridotites: A coupled study of samples from the Kane Fracture Zone (45 degrees W 23 degrees 20N, MARK Area, Atlantic Ocean). Geochim Cosmochim Acta 67:1553–1570
Luguet A, Lorand JP, Alard O, Cottin JY (2004) A multi-technique study of platinum group element systematic in some Ligurian ophiolitic peridotites, Italy. Chem Geol 208:175–194
Luguet A, Shirey SB, Lorand JP, Horan MF, Carlson RW (2007) Residual platinum-group minerals from highly depleted harzburgites of the Lherz massif (France) and their role in HSE fractionation of the mantle. Geochim Cosmochim Acta 71:3082–3097
Luguet A, Pearson DG, Nowell GM, Dreher ST, Coggon JA, Spetsius ZV, Parman SW (2008) Enriched Pt-Re–Os isotope systematics in plume lavas explained by metasomatic sulfides. Science 319:453–456
Luguet A, Jaques AL, Pearson DG, Smith CB, Bulanova GP, Roffey SL, Rayner MJ, Lorand JP (2009) An integrated petrological, geochemical and Re–Os isotope study of peridotite xenoliths from the Argyle lamproite, Western Australia and implications for cratonic diamond occurrences. Lithos 112:1096–1108
Luguet A, Behrens M, Pearson DG, König S, Herwartz D (2015) Significance of the whole rock Re–Os ages in cryptically and modally metasomatized cratonic peridotites: Constraints from HSE–Se–Te systematics. Geochim Cosmochim Acta 164:441–463
Luth RW, Stachel T (2014) The buffering capacity of lithospheric mantle: implications for diamond formation. Contrib Mineral Petrol 168:1083
MacGregor ID, Manton WI. 1986. Roberts Victor eclogites: ancient oceanic crust. J Geophys Res 91:14063– 14079
Maier WD, Barnes SJ, Campbell IH, Fiorentini ML, Peltonen P, Smithies RH (2009) Progressive mixing of meteoritic veneer into the early Earth's deep mantle. Nature 460:620–623
Maier WD, Peltonen P, McDonald I, Barnes SJ, Hatton C, Viljoen F (2012) The concentration of platinum-group elements and gold in southern African and Karelian kimberlite-hosted mantle xenoliths: Implications for the noble metal content of the Earth's mantle. Chem Geol 302:119–135
Mallmann G, O'Neill HSC (2007) The effect of oxygen fugacity on the partitioning of Re between crystals and silicate melt during mantle melting. Geochim Cosmochim Acta 71:2837–285
Mann U, Frost DJ, Rubie DC, Becker H, Audetat A (2012) Partitioning of Ru, Rh, Pd, Re, Ir and Pt between liquid metal and silicate at high pressures and high temperatures—implications for the origin of highly siderophile element concentrations in the Earth's mantle. Geochim Cosmochim Acta 84:593–613
Marchesi C, Griffin WL, Garrido CJ, Bodinier JL, Pearson NJ (2010) Persistence of mantle lithospheric Re–Os signature during asthenospherization of the subcontinental lithospheric mantle: insights from in situ isotopic analysis of sulfides from the Ronda peridotite (Southern Spain). Contrib Miner Petrol 159:315–330
Martin H, Smithies RH, Rapp R, Moyen JF, Champion D (2005) An overview of adakite, tonalite-trondhjemite-granodiorite (TTG), and sanukitoid: relationships and some implications for crustal evolution. Lithos 79:1–24
Mavrogenes JA, O'Neill HSC (1999) The relative effects of pressure, temperature and oxygen fugacity on the solubility of sulfide in mafic magmas. Geochim Cosmochim Acta 63:1173–1180
McBride JS, Lambert DD, Greig A, Nicholls IA. 1996. Multistage evolution of Australian subcontinental mantle: Re–Os isotopic constraints from Victorian mantle xenoliths. Geol 24:631–634
McCoy-West AJ, Bennett VC, Puchtel IS, Walker RJ (2013) Extreme persistence of cratonic lithosphere in the southwest Pacific: Paleoproterozoic Os isotopic signatures in Zealandia. Geol 41:231–234
McCulloch MT, Wasserburg GJ. 1978. Sm-Nd and Rb-Sr chronology of continental crust formation. Science 200:1003–1011
McDonald I, de Wit MJ, Smith CB, Bizzi LA, Viljoen KS (1995) The geochemistry of the platinum-group elements in Brazilian and Southern African kimberlites. Geochim Cosmochim Acta 59:2883–2903
McDonough WF, Sun SS (1995) The composition of the Earth. Chem Geol 120:223–253
McInnes BIA, McBride JS, Evans NJ, Lambert DD, Andrew AS (1999) Osmium isotope constraints on ore metal recycling in subduction zones. Science 286:512–516

Meibom A, Sleep NH, Chamberlain CP, Coleman RG, Frei R, Hren MT, Wooden JL (2002) Re–Os isotopic evidence for long-lived heterogeneity and equilibration processes in the Earth's upper mantle. Nature 419:705–708

Meisel T, Biino GG, Nagler TF (1996) Re–Os, Sm-Nd, and rare earth element evidence for Proterozoic oceanic and possible subcontinental lithosphere in tectonized ultramafic lenses from the Swiss Alps. Geochim Cosmochim Acta 60:2583–2593

Meisel T, Moser J, Fellner N, Wegscheider W, Schoenberg R (2001) Simplified method for the determination of Ru, Pd, Re, Os, Ir and Pt in chromitites and other geological materials by isotope dilution ICP-MS and acid digestion. Analyst 126:322–328

Meisel T, Horan MF (2016) Analytical methods for the highly siderophile elements. Rev Mineral Geochem 81:89–106

Melcher F, Meisel T (2004) A metamorphosed early Cambrian crust-mantle transition in the Eastern Alps, Austria. J Petrol 45:1689–1723

Menzies AH, Carlson RW, Shirey SB, Gurney JJ (2003) Re–Os systematics of diamond-bearing eclogites from the Newlands kimberlite. Lithos 71:323–336

Menzies MA, Hawkesworth CJ (1987) Upper mantle processes and composition. *In:* Mantle Xenoliths. Nixon PH (ed), John Wiley & Sons, Chichester, p 725–738

Menzies MA, Fan W-M, Zhang M. 1993. Paleozoic and Cenozoic lithoprobes and the loss of >120 km of lithosphere, Sino-Korean craton, China. *In*: Magmatic Processes and Plate Tectonics. Prichard HM, Alabaster HM, Harris T, Neary CR (eds) London: Geol Soc. p 71–81

Menzies AH, Shirey SB, Carlson RW, Gurney JJ (1999) Re–Os systematics of Newlands peridotite xenoliths: implications for diamond and lithosphere formation. *In*: Proc 7th Inter Kimberlite Conf 1999, p 566–583

Mitchell RH (1995) Melting experiments on a sanidine phlogopite lamproite at 4–7 GPa and their bearing on the sources of lamproitic magmas. J Petrol 36:1455–1474

Mitchell RH, Keays RR. 1981. Abundance and distribution of gold, palladium and iridium in some spinel and garnet lherzolites—implications for the nature and origin of precious metal-rich intergranular components in the upper mantle. Geochim Cosmochim Acta 45:2425–2442

Moretti R, Baker DR (2008) Modeling the interplay of fO(2) and fS(2) along the FeS-silicate melt equilibrium. Chem Geol 256:286–298

Morgan JW, Wandless GA, Petrie RK, Irving AJ. 1981. Composition of the Earth's upper mantle. 1. Siderophile trace elements in ultramafic nodules. Tectonophys 75:47–67

Mungall JE (2002) Roasting the mantle: Slab melting and the genesis of major Au and Au-rich Cu deposits. Geol 30:915–918

Mungall JE, Brenan JM (2014) Partitioning of platinum-group elements and Au between sulfide liquid and basalt and the origins of mantle-crust fractionation of the chalcophile elements. Geochim Cosmochim Acta 125:265–289

Mungall JE, Andrews DRA, Cabri LJ, Sylvester PJ, Tubrett M (2005) Partitioning of Cu, Ni, An, and platinum-group elements between monosulfide solid solution and sulfide melt under controlled oxygen and sulfur fugacities. Geochim Cosmochim Acta 69:4349–4360

Mungall JE, Hanley JJ, Arndt NT, Debecdelievre A (2006) Evidence from meimechites and other low-degree mantle melts for redox controls on mantle-crust fractionation of platinum-group elements. PNAS 103:12695–12700

Niu YL (1997) Mantle melting and melt extraction processes beneath ocean ridges: Evidence from abyssal peridotites. J Petrol 38:1047–1074

Nixon PH (1987) Mantle Xenoliths. Chichester: Wiley & Sons

Nowell GM, Luguet A, Pearson DG, Horstwood MSA (2008) Precise and accurate Os−186/Os−188 and Os−187/Os−188 measurements by multi-collector plasma ionisation mass spectrometry (MC-ICP-MS) part I: Solution analyses. Chem Geol 248:363–393

O'Driscoll B, González-Jiménez J (2016) Petrogenesis of the platinum-group minerals. Rev Mineral Geochem 81:489–578

O'Driscoll B, Day JMD, Daly JS, Walker RJ, McDonough WF (2009) Rhenium–osmium isotopes and platinum-group elements in the Rum Layered Suite, Scotland: Implications for Cr-spinel seam formation and the composition of the Iceland mantle anomaly. Earth Planet Sci Lett 286:41–51

O'Reilly SY, Griffin WL (2010) The continental lithosphere-asthenosphere boundary. Can we sample it? Lithos 120:1–13

O'Reilly SY, Griffin WL (2013) Moho vs crust-mantle boundary: Evolution of an idea. Tectonophys 609:535–546

O'Reilly SY, Griffin WL, Poudjom Djomani Y, Morgan P (2001) Are lithospheres forever? Tracking changes in subcontinental lithspheric mantle through time. GSA Today 11:4–9

Olive V, Ellam RM, Harte B (1997) A Re–Os isotope study of ultramafic xenoliths from the Matsoku kimberlite. Earth Planet Sci Lett 150:129–140

Park J-W, Campbell IH, Arculus RJ (2013) Platinum-alloy and sulfur saturation in an arc-related basalt to rhyolite suite: Evidence from the Pual Ridge lavas, the Eastern Manus Basin. Geochim Cosmochim Acta 101:76–95

Parkinson IJ, Hawkesworth CJ, Cohen AS. 1998. Ancient mantle in a modern arc: Osmium isotopes in Izu-Bonin-Mariana forearc peridotites. Science 281:2011–2013

Patten C, Barnes SJ, Mathez EA, Jenner FE (2013) Partition coefficients of chalcophile elements between sulfide and silicate melts and the early crystallization history of sulfide liquid: LA-ICP-MS analysis of MORB sulfide droplets. Chem Geol 358:170–188

Pattou L, Lorand JP, Gros M (1996) Non-chondritic platinum-group element ratios in the Earth's mantle. Nature 379:712–715

Peach CL, Mathez EA, Keays RR (1990) Sulfide melt silicate melt distribution coefficients for noble-metals and other chalcophile elements as deduced from MORB—implications for partial melting. Geochim Cosmochim Acta 54:3379–3389

Pearson DG (1999) The age of continental roots. Lithos 48:171–194

Pearson DG, Wittig N (2008) Formation of Archean continental lithosphere and its diamonds: the root of the problem. Journal of the Geological Society 165:895–914

Pearson DG, Wittig N (2014) The Formation and Evolution of Cratonic Mantle Lithosphere—Evidence from Mantle Xenoliths. *In*: Treatise on Geochemistry, 2nd Edition. Holland H, Turekian K (eds) Amsterdam: Elsevier. p 255–292

Pearson DG, Woodland SJ (2000) Solvent extraction/anion exchange separation and determination of PGEs (Os, Ir, Pt, Pd, Ru) and Re–Os isotopes in geological samples by isotope dilution ICP-MS. Chem Geol 165:87–107

Pearson DG, Snyder GA, Shirey SB, Taylor LA, Carlson RW, Sobolev NV (1995a) Re–Os age for Siberian eclogites and constraints on tectonics. Nature 374:711–713

Pearson DG, Carlson RW, Shirey SB, Boyd FR, Nixon PH (1995b) Stabilization of lithospheric mantle—A Re–Os isotope study of peridotite xenoliths from the Kaapvaal craton. Earth Planet Sci Lett 134:341–357

Pearson DG, Shirey SB, Carlson RW, Boyd FR, Pokhilenko NP, Shimizu N (1995c) Re–Os, Sm-Nd, Rb-Sr isotope evidence for thick lithospheric mantle beneath the Siberian craton modified by multistage metasomatism. Geochim Cosmochim Acta 59:959–977

Pearson DG, Shirey SB, Harris JW, Carlson RW (1998) Sulfide inclusions in diamonds from the Koffiefontein kimberlite, S Africa: constraints on diamond ages and mantle Re–Os systematics. Earth Planet Sci Lett 160:311–326

Pearson DG, Shirey SB, Bulanova GP, Carlson RW, Milledge HJ (1999) Re–Os isotope measurements of single sulfide inclusions in a Siberian diamond and its nitrogen aggregation systematics. Geochim Cosmochim Acta 63:703–711

Pearson DG, Irvine GJ, Carlson RW, Kopylova MG, Ionov DA (2002) The development of lithospheric keels beneath the earliest continents: time constraints using PGE and Re–Os isotope systematics. Early Earth: Physical, Chemical and Biological Development 199:65–90

Pearson DG, Irvine GJ, Ionov DA, Boyd FR, Dreibus GE (2004) Re–Os isotope systematics and platinum group element fractionation during mantle melt extraction: a study of massif and xenolith peridotite suites. Chem Geol 208:29–59

Pearson DG, Canil D, Shirey SB (2005) Mantle samples included in volcanic rocks: Xenoliths and diamonds. *In*: Treatise on Geochemistry: The Mantle and the Core. Holland HD, Turekian KK, Carlson RW (eds) Elsevier Pergamon, Amsterdam, p 175–275

Pearson DG, Parman SW, Nowell GM (2007) A link between large mantle melting events and continent growth seen in osmium isotopes. Nature 449:202–205

Pearson DG, Brenker FE, Nestola F, McNeill J, Nasdala L, Hutchison MT, Matveev S, Mather K, Silversmit G, Schmitz S et al (2014) Hydrous mantle transition zone indicated by ringwoodite included within diamond. Nature 507:221–224

Pearson NJ, Alard O, Griffin WL, Jackson SE, O'Reilly SY (2002) In situ measurement of Re–Os isotopes in mantle sulfides by laser ablation multicollector-inductively coupled plasma mass spectrometry: Analytical methods and preliminary results. Geochim Cosmochim Acta 66:1037–1050

Peltonen P, Brügmann G (2006) Origin of layered continental mantle (Karelian craton, Finland): Geochemical and Re–Os isotope constraints. Lithos 89:405–423

Pernet-Fisher JF, Howarth GH, Pearson DG, Woodland S, Barry PH, Pokhilenko NP, Pokhilenko LN, Agashev AM, Taylor LA (2015) Plume impingement on the Siberian SCLM: Evidence from Re–Os isotope systematics. Lithos 218–219:141–154

Peslier AH, Reisberg L, Ludden J, Francis D (2000a) Os isotopic systematics in mantle xenoliths; age constraints on the Canadian Cordillera lithosphere. Chem Geol 166:85–101

Peslier AH, Reisberg L, Ludden J, Francis D (2000b) Re–Os constraints on harzburgite and lherzolite formation in the lithospheric mantle: A study of Northern Canadian Cordillera xenoliths. Geochim Cosmochim Acta 64:3061–3071

Polat A, Kerrich R (2001) Geodynamic processes, continental growth, and mantle evolution recorded in late greenstone belts of the southern Superior Province, Canada. Precambr Res 112:5–25

Polat A, Hofmann AW, Rosing MT (2002) Boninite-like volcanic rocks in the 3.7–3.8 Ga Isua greenstone belt, West Greenland: geochemical evidence for intra-oceanic subduction zone processes in the early Earth. Chem Geol 184:231–254

Polat A, Kusky T, Li JH, Fryer B, Kerrich R, Patrick K (2005) Geochemistry of Neoarchean (ca. 2.55–2.50 Ga) volcanic and ophiolitic rocks in the Wutaishan greenstone belt, central orogenic belt, North China craton: Implications for geodynamic setting and continental growth. Geol Soc Amer Bull 117:1387–1399

Poudjom-Djomani YH, Griffin WL, O'Reilly SY, Doyle BJ (2005) Lithospheric domains and controls on kimberlite emplacement, Slave Province, Canada: Evidence from elastic thickness and upper mantle composition. Geochem Geophys Geosyst 6

Powell W, O'Reilly S (2007) Metasomatism and sulfide mobility in lithospheric mantle beneath eastern Australia: Implications for mantle Re–Os chronology. Lithos 94:132–147

Priestley K, McKenzie D (2006) The thermal structure of the lithosphere from shear wave velocities. Earth Planet Sci Lett 244:285–301

Puchtel I, Humayun M (2000) Platinum group elements in Kostomuksha komatiites and basalts: Implications for oceanic crust recycling and core-mantle interaction. Geochim Cosmochim Acta 64:4227–4242

Puchtel IS, Walker RJ, Touboul M, Nisbet EG, Byerly GR (2014) Insights into early Earth from the Pt–Re–Os isotope and highly siderophile element abundance systematics of Barberton komatiites. Geochim Cosmochim Acta 125:394–413

Rapp RP, Norman MD, Laporte D, Yaxley GM, Martin H, Foley SF (2010) Continent Formation in the Archean and Chemical Evolution of the Cratonic Lithosphere: Melt-Rock Reaction Experiments at 3–4 GPa and Petrogenesis of Archean Mg-Diorites (Sanukitoids). J Petrol 51:1237–1266

Ravizza G, Pyle D (1997) PGE and Os isotopic analyses of single sample aliquots with NiS fire assay preconcentration. Chem Geol 141:251–268

Rehkämper M, Halliday AN, Barfod D, Fitton JG (1997) Platinum-group element abundance patterns in different mantle environments. Science 278:1595–1598

Rehkämper M, Halliday AN, Alt J, Fitton JG, Zipfel J, Takazawa E (1999) Non-chondritic platinum-group element ratios in oceanic mantle lithosphere: petrogenetic signature of melt percolation? Earth Planet Sci Lett 172:65–81

Reisberg L, Lorand JP (1995) Longevity of sub-continental mantle lithospehre from osmium isotope systmatics in orogenic peridotite massifs. Nature 376:159–162

Reisberg L, Meisel T (2002) The Re–Os isotopic system: A review of analytical techniques. Geostand Newsl J Geostand Geoanal 26:249–267

Reisberg LC, Allègre CJ, Luck JM (1991) The Re–Os systematics of the Ronda ultramafic complex of southern Spain. Earth Planet Sci Lett 105:196–213

Reisberg L, Zhi XC, Lorand JP, Wagner C, Peng ZC, Zimmermann C (2005) Re–Os and S systematics of spinel peridotite xenoliths from east central China: Evidence for contrasting effects of melt percolation. Earth Planet Sci Lett 239:286–308

Rhyzenko B, Kennedy GC (1973) The effect of pressure on the eutectic in the system Fe–FeS. Am J Sci 273:803–810

Richardson SH, Shirey SB, Harris JW, Carlson RW (2001) Archean subduction recorded by Re–Os isotopes in eclogitic sulfide inclusions in Kimberley diamonds. Earth Planet Sci Lett 191:257–266

Richardson SH, Shirey SB, Harris JW (2004) Episodic diamond genesis at Jwaneng, Botswana, and implications for Kaapvaal craton evolution. Lithos 77:143–154

Righter K (2005) Highly siderophile elements: Constraints on Earth accretion and early differentiation. *In:*Earth's Deep Mantle: Structure, Composition, and Evolution. AGU Monogr Ser 160:201–218, doi:10.1029/160GM13

Righter K, Hauri EH (1998) Compatibility of rhenium in garnet during mantle melting and magma genesis. Science 280:1737–1741

Righter K, Campbell AJ, Humayun M, Hervig RL (2004) Partitioning of Ru, Rh, Pd, Re, Ir, and Au between Cr-bearing spinel, olivine, pyroxene and silicate melts. Geochim Cosmochim Acta 68:867–880

Righter K, Chesley JT, Calazza CM, Gibson EK, Jr., Ruiz J (2008) Re and Os concentrations in arc basalts: The roles of volatility and source region fO(2) variations. Geochim Cosmochim Acta 72:926–947

Ringwood AE (1966) Chemical evolution of terrestrial planets. Geochim Cosmochim Acta 30:41–104

Ritsema J, Nyblade AA, Owens TJ, Langston CA, VanDecar JC (1998) Upper mantle seismic velocity structure beneath Tanzania, east Africa: Implications for the stability of cratonic lithosphere. J Geophys Res-Solid Earth 103(B9):21201–21213

Rohrbach A, Schmidt MW (2011) Redox freezing and melting in the Earth's deep mantle resulting from carbon-iron redox coupling. Nature 472:209–212

Rohrbach A, Ballhaus C, Golla-Schindler U, Ulmer P, Kamenetsky VS, Kuzmin DV (2007) Metal saturation in the upper mantle. Nature 449:456–458

Rose-Weston L, Brenan JM, Fei YW, Secco RA, Frost DJ (2009) Effect of pressure, temperature, and oxygen fugacity on the metal-silicate partitioning of Te, Se, and S: Implications for earth differentiation. Geochim Cosmochim Acta 73:4598–4615

Roy-Barman M, Allègre CJ (1994) $^{187}Os/^{188}Os$ ratios of mid-ocean ridge basalts and abyssal peridotites. Geochim Cosmochim Acta 58:5043–5054
Roy-Barman M, Luck JM, Allègre CJ. (1996) Os isotopes in orogenic lherzolite massifs and mantle heterogeneities. Chem Geol 130:55–64
Roy-Barman M, Wasserburg GJ, Papanastassiou DA, Chaussidon M (1998) Osmium isotopic compositions and Re–Os concentrations in sulfide globules from basaltic glasses. Earth Planet Sci Lett 154:331–347
Rudnick RL, Walker RJ (2009) Interpreting ages from Re–Os isotopes in peridotites. Lithos 112:1083–1095
Rudnick RL, McDonough WF, Chappell BW (1993) Carbonatite metasomatism in the northern Tanzanian mantle—petrographic and geochemical characteristics. Earth Planet Sci Lett 114:463–475
Rudnick RL, Donough WL, Orpin A (1994) Northern Tanzanian peridotite xenoliths: a comparison with Kaapvaal peridotites and inferences on metasomatic interactions. *In*: Kimberlites, Related Rocks and Mantle Xenoliths. Brasilia: CPRM Special Publication. Meyer HOA (ed), p 336–353
Saal AE, Takazawa E, Frey FA, Shimizu N, Hart SR (2001) Re–Os isotopes in the Horoman peridotite: Evidence for refertilization? J Petrol 42:25–37
Saha A, Basu AR, Jacobsen SB, Poreda RJ, Yin QZ, Yogodzinski GM (2005) Slab devolatilization and Os and Pb mobility in the mantle wedge of the Kamchatka arc. Earth Planet Sci Lett 236:182–194
Salters VJM, Stracke A (2004) Composition of the depleted mantle. Geochem Geophys Geosyst 5:Q05B07, doi:10.1029/2003GC000597
Santosh M (2013) Evolution of continents, cratons and supercontinents: building the habitable Earth. Curr Sci 104:871–879
Sarkar C, Heaman LM, Pearson DG (2015) Duration and periodicity of kimberlite volcanic activity in the Lac de Gras kimberlite field, Canada and some recommendations for kimberlite geochronology. Lithos 218–219:155–166
Sattari P, Brenan JM, Horn I, McDonough WF (2002) Experimental constraints on the sulfide- and chromite-silicate melt partitioning behavior of rhenium and platinum-group elements. Econ Geol Bull Soc Econ Geol 97:385–398
Schmidberger SS, Francis D (2001) Constraints on the trace element composition of the Archean mantle root beneath Somerset Island, Arctic Canada. J Petrol 42:1095–1117
Schmidt G, Palme H, Kratz KL, Kurat G (2000) Are highly siderophile elements (PGE, Re and Au) fractionated in the upper mantle of the earth? New results on peridotites from Zabargad. Chem Geol 163:167–188
Schmidt G, Witt-Eickschen G, Palme H, Seck H, Spettel B, Kratz KL (2003) Highly siderophile elements (PGE, Re and Au) in mantle xenoliths from the West Eifel volcanic field (Germany). Chem Geol 196:77–105
Schoenberg R, Nagler TF, Kramers JD (2000) Precise Os isotope ratio and Re–Os isotope dilution measurements down to the picogram level using multicollector inductively coupled plasma mass spectrometry. Inter J Mass Spectr 197:85–94
Schulte RF, Schilling M, Anma R, Farquhar J, Horan MF, Komiya T, Piccoli PM, Pitcher L, Walker RJ (2009) Chemical and chronologic complexity in the convecting upper mantle: Evidence from the Taitao ophiolite, southern Chile. Geochim Cosmochim Acta 73:5793–5819
Schulze DJ (1989) Constraints on the abundance of eclogite in the upper mantle. J Geophys Res-Solid Earth Planets 94(B4):4205–4212
Sen G, Yang HJ, Ducea M (2003) Anomalous isotopes and trace element zoning in plagioclase peridotite xenoliths of Oahu (Hawaii): implications for the Hawaiian plume. Earth Planet Sci Lett 207:23–38
Sen IS, Bizimis M, Sen G, Huang S (2011) A radiogenic Os component in the oceanic lithosphere? Constraints from Hawaiian pyroxenite xenoliths. Geochim Cosmochim Acta 75:4899–4916
Shervais JW (2006) The significance of subduction-related accretionary complexes in early Earth processes. Proc Early Earth:173–192
Shirey SB, Richardson SH (2011) Start of the Wilson Cycle at 3 Ga shown by diamonds from subcontinental mantle. Science 333:434–436
Shirey SB, Walker RJ (1995) Carius tube digestion for low-blank rhenium-osmium analysis. Anal Chem 67(13)
Shirey SB, Walker RJ (1998) The Re–Os isotope system in cosmochemistry and high-temperature geochemistry. Ann Rev Earth Planet Sci 26:423–500
Shirey SB, Carlson RW, Richardson SH, Menzies A, Gurney JJ, Pearson DG, Harris JW, Wiechert U (2001) Archean emplacement of eclogitic components into the lithospheric mantle during formation of the Kaapvaal Craton. Geophys Res Lett 28:2509–2512
Shirey SB, Harris JW, Richardson SH, Fouch MJ, James DE, Cartigny P, Deines P, Viljoen F (2002) Diamond genesis, seismic structure, and evolution of the Kaapvaal-Zimbabwe craton. Science 297:1683–1686
Siebert J, Corgne A, Ryerson FJ (2011) Systematics of metal-silicate partitioning for many siderophile elements applied to Earth's core formation. Geochim Cosmochim Acta 75:1451–1489
Simon NSC, Irvine GJ, Davies GR, Pearson DG, Carlson RW (2003) The origin of garnet and clinopyroxene in "depleted" Kaapvaal peridotites. Lithos 71:289–322
Simon NSC, Carlson RW, Pearson DG, Davies GR (2007) The origin and evolution of the Kaapvaal cratonic lithospheric mantle. J Petrol 48:589–625
Smit KV, Pearson DG, Stachel T, Seller M (2014a) Peridotites from Attawapiskat, Canada: Mesoproterozoic Reworking of PaleoArchean Lithospheric Mantle beneath the Northern Superior Superterrane. J Petrol 55:1829–1863

Smit KV, Stachel T, Creaser RA, Ickert RB, DuFrane SA, Stern RA, Seller M (2014b) Origin of eclogite and pyroxenite xenoliths from the Victor kimberlite, Canada, and implications for Superior craton formation. Geochim Cosmochim Acta 125:308–337

Smith CB (1983) Pb, Sr and Nd isotopic evidence for sources of southern African creataceous kimberlites. Nature 304:51–54

Smith D, Boyd FR (1987) Compositional heterogeneities in a high- temperature lherzolite nodule and implications for mantle processes. *In:* Mantle Xenoliths. Nixon PH (ed). John Wiley and Sons, Chichester, p 551–561

Smith D, Boyd FR (1992) Compositional zonation in garnets of peridotite xenoliths. Contrib Mineral Petrol 112:134–147

Smith CB, Pearson DG, Bulanova GP, Beard AD, Carlson RW, Wittig N, Sims K, Chimuka L, Muchemwa E (2009) Extremely depleted lithospheric mantle and diamonds beneath the southern Zimbabwe Craton. Lithos 112:1120–1132

Snow JE, Reisberg L (1995) Os isotopic systematics of the MORB mantle: Results from altered abyssal peridotites (vol 133, pg 411, 1995). Earth Planet Sci Lett 136:723–733

Snow JE, Schmidt G (1998) Constraints on Earth accretion deduced from noble metals in the oceanic mantle. Nature 391:166–169

Sobolev AV, Hofmann AW, Kuzmin DV, Yaxley GM, Arndt NT, Chung SL, Danyushevsky LV, Elliott T, Frey FA, Garcia MO et al. (2007) The amount of recycled crust in sources of mantle-derived melts. Science 316:412–417

Sparks RSJ, Baker L, Brown RJ, Field M, Schumacher J, Stripp G, Walters A (2006) Dynamical constraints on kimberlite volcanism. J Volc Geotherm Res 155:18–48

Stagno V, Ojwang DO, McCammon CA, Frost DJ (2013) The oxidation state of the mantle and the extraction of carbon from Earth's interior. Nature 493:84–88

Sun J, Liu C-Z, Wu F-Y, Y Y-H, C Z-Y (2012) Metasomatic origin of clinopyroxene in Archean mantle xenoliths from Hebi, North China Craton: Trace-element and Sr-isotope constraints. Chem Geol 328:123–136

Tainton KM, McKenzie D. 1994. The generation of kimberlites, lamproites, and their source rocks. J Petrol 35:787–817

Tang Y-J, Zhang H-F, Santosh M, Ying J-F (2013) Differential destruction of the North China Craton: A tectonic perspective. J Asian Earth Sci 78:71–82

Tappe S, Foley SF, Jenner GA, Heaman LM, Kjarsgaard BA, Romer RL, Stracke A, Joyce N, Hoefs J (2006) Genesis of ultramafic lamprophyres and carbonatites at Aillik Bay, Labrador: A consequence of incipient lithospheric thinning beneath the North Atlantic craton. J Petrol 47:1261–1315

Tappe S, Smart KA, Pearson DG, Steenfelt A, Simonetti A (2011) Craton formation in Late Archean subduction zones revealed by first Greenland eclogites. Geology 39:1103–1106

Tappe S, Kjarsgaard BA, Kurszlaukis S, Nowell GM, Phillips D (2014) Petrology and Nd-Hf Isotope Geochemistry of the Neoproterozoic Amon Kimberlite Sills, Baffin Island (Canada): Evidence for Deep Mantle Magmatic Activity Linked to Supercontinent Cycles. J Petrol 55:2003–2042

Thakurta J, Ripley EM, Li C (2008) Geochemical constraints on the origin of sulfide mineralization in the Duke Island Complex, southeastern Alaska. Geochem Geophys Geosyst 9:Q07003, doi:10.1029/2008GC001982

van Acken D, Becker H, Hammerschmidt K, Walker RJ, Wombacher F (2010) Highly siderophile elements and Sr–Nd isotopes in refertilized mantle peridotites—A case study from the Totalp ultramafic body, Swiss Alps. Chem Geol 276:257–268

Van Kranendonk MJ, Smithies RH, Hickman AH, Wingate MTD, Bodorkos S (2010) Evidence for Meso (similar to 3.2 Ga) rifting of the Pilbara Craton: The missing link in an early Precambrian Wilson cycle. Precambr Res 177:145–161

Vernières J, Godard M, Bodinier JL (1997) A plate model for the simulation of trace element fractionation during partial melting and magma transport in the Earth's upper mantle. J Geophys Res-Solid Earth 102(B11):24771–24784

Völkening J, Walczyk T, Heumann KG (1991) Osmium isotope ratio determinations by negative thermal ionization mass spectrometry. Int J Mass Spectrom Ion Process 151:147–159

Wainwright AN, Luguet A, Fonseca ROC, Pearson DG (2015) Investigating metasomatic effects on the ^{187}Os isotopic signature: A case study on micrometric base metal sulfides in metasomatized peridotite from the Letlhakane kimberlite (Botswana). Lithos 232:35–48

Walker RJ, Nisbet E (2002) Os−187 isotopic constraints on Archean mantle dynamics. Geochim Cosmochim Acta 66:3317–3325

Walker RJ, Carlson RW, Shirey SB, F. R B (1989) Os, Sr, Nd, and Pb isotope systematics of southern African peridotite xenoliths: Implications for the chemical evolution of subcontinental mantle. Geochim Cosmochim Acta 53:1583–1595

Walker RJ, Morgan JW, Naldrett AJ, Li C, Fassett JD (1991) Re–Os isotope systematics of Ni-Cu sulfide ores, Sudbury igneous comples, Ontario—evidence for a major crustal component. Earth Planet Sci Lett 105:416–429

Walker RJ, Morgan JW, Horan MF (1995) Os−187 enrichment in some plumes—evidence for core-mantle interaction. Science 269:819–822

Walker RJ, Morgan JW, Hanski EJ, Smolkin VF (1997) Re–Os systematics of Early Proterozoic ferropicrites, Pechenga Complex, northwestern Russia: Evidence for ancient Os-187-enriched plumes. Geochim Cosmochim Acta 61:3145–3160

Walker RJ, Prichard HM, Ishiwatari A, Pimentel M (2002) The osmium isotopic composition of convecting upper mantle deduced from ophiolite chromites. Geochim Cosmochim Acta 66:329–345

Walter MJ (1998) Melting of garnet peridotite and the origin of komatiite and depleted lithosphere. J Petrol 39:29–60

Walter MJ (2005) Melt extraction and compositional variability in mantle lithosphere. *In:* Treatise on Geochemistry. Vol 2. Holland HD, Turekian KK, Carlson RW (eds), Elsevier Pergamon, Amsterdam, p 363–394

Wang HL, van Hunen J, Pearson DG, Allen MB (2014) Craton stability and longevity: The roles of composition-dependent rheology and buoyancy. Earth Planet Sci Lett 391:224–233

Wang HL, van Hunen J, Pearson DG (2015) The thinning of subcontinental lithosphere: The roles of plume impact and metasomatic weakening, Geochem Geophys Geosyst 16:1156–1171

Wang ZC, Becker H (2013) Ratios of S, Se and Te in the silicate Earth require a volatile-rich late veneer. Nature 499:328–331

Wang ZC, Becker H, Gawronski T (2013) Partial re-equilibration of highly siderophile elements and the chalcogens in the mantle: A case study on the Baldissero and Balmuccia peridotite massifs (Ivrea Zone, Italian Alps). Geochim Cosmochim Acta 108:21–44

Warren JM, Shirey SB (2012) Lead and osmium isotopic constraints on the oceanic mantle from single abyssal peridotite sulfides. Earth Planet Sci Lett 359:279–293

Wendlandt RF (1982) Sulfide saturation of basalt and andesite melts at high pressures and temperatures. Am Miner 67:877–885

Westerlund KJ, Gurney JJ, Carlson RW, Shirey SB, Hauri EH, Richardson SH (2004) A metasomatic origin for late Archean eclogitic diamonds: Implications from internal morphology of diamonds and Re–Os and S isotope characteristics of their sulfide inclusions from the late Jurassic Klipspringer kimberlites. S Afr J Geol 107:119–130

Westerlund KJ, Shirey SB, Richardson SH, Carlson RW, Gurney JJ, Harris JW (2006) A subduction wedge origin for Paleoarchean peridotitic diamonds and harzburgites from the Panda kimberlite, Slave craton: evidence from Re–Os isotope systematics. Contrib Miner Petrol 152:275–294

Widom E, Hoernle KA, Shirey SB, Schmincke HU (1999) Os isotope systematics in the Canary Islands and Madeira: Lithospheric contamination and mantle plume signatures. J Petrol 40:279–296

Widom E, Kepezhinskas P, Defant M (2003) The nature of metasomatism in the sub-arc mantle wedge: evidence from Re–Os isotopes in Kamchatka peridotite xenoliths. Chem Geol 196:283–306

Wiggers de Vries DF, Pearson DG, Bulanova GP, Smelov AP, Pavlushin AD, Davies GR (2013) Re–Os dating of sulfide inclusions zonally distributed in single Yakutian diamonds: Evidence for multiple episodes of Proterozoic formation and protracted timescales of diamond growth. Geochim Cosmochim Acta 120:363–394

Windley BF, Maruyama S, Xiao WJ (2010) Delamination/thinning of sub-continental lithospheric mantle under Eastern China: The role of water and multiple subduction. American Journal of Science 310:1250–1293

Wittig N, Pearson DG, Webb M, Ottley CJ, Irvine GJ, Kopylova M, Jensen SM, Nowell GM (2008) Origin of cratonic lithospheric mantle roots: A geochemical study of peridotites from the North Atlantic Craton, West Greenland. Earth Planet Sci Lett 274:24–33

Wittig N, Pearson DG, Baker JA, Duggen S, Hoernle K (2010a) A major element, PGE and Re–Os isotope study of Middle Atlas (Morocco) peridotite xenoliths: Evidence for coupled introduction of metasomatic sulfides and clinopyroxene. Lithos 115:15–26

Wittig N, Webb M, Pearson DG, Dale CW, Ottley CJ, Hutchison M, Jensen SM, Luguet A (2010b) Formation of the North Atlantic Craton: Timing and mechanisms constrained from Re–Os isotope and PGE data of peridotite xenoliths from SW Greenland. Chem Geol 276:166–187

Wood BJ, Bryndzia LT, Johnson KE (1990) Mantle oxidation-state and its relationship to tectonic environment and fluid speciation. Science 248:337–345

Woodland AB, Koch M (2003) Variation in oxygen fugacity with depth in the upper mantle beneath the Kaapvaal craton, Southern Africa. Earth Planet Sci Lett 214:295–310

Workman RK, Hart SR (2005) Major and trace element composition of the depleted MORB mantle (DMM). Earth Planet Sci Lett 231:53–72

Wu FY, Walker RJ, Ren XW, Sun DY, Zhou XH (2003) Osmium isotopic constraints on the age of lithospheric mantle beneath northeastern China. Chem Geol 196:107–129

Wu F-Y, Walker RJ, Yang Y-H, Yuan H-L, Yang J-H (2006) The chemical-temporal evolution of lithospheric mantle underlying the North China Craton. Geochim Cosmochim Acta 70:5013–5034

Xu XS, Griffin WL, O'Reilly SY, Pearson NJ, Geng HY, Zheng JP (2008) Re–Os isotopes of sulfides in mantle xenoliths from eastern China: Progressive modification of lithospheric mantle. Lithos 102:43–64

Yaxley GM, Green DH (1998) Reactions between eclogite and peridotite: mantle refertilization by subduction of oceanic crust. Schweiz Mineral Petrogr Mitt 78:243–255

Yongbin J, Xiachen Z, Meng Q, Gao T, Peng Z (2004) Re–Os dating of the Raobazhai ultra mafic massif in North Dabie. Chi Sci Bull 49:508–513

Zhang HF, Goldstein SL, Zhou XH, Sun M, Zheng JP, Cai Y (2008) Evolution of subcontinental lithospheric mantle beneath eastern China: Re–Os isotopic evidence from mantle xenoliths in Paleozoic kimberlites and Mesozoic basalts. Contrib Mineral Petrol 155:271–293

Zhang H-F, Goldstein SL, Zhou X-H, Sun M, Cai Y (2009) Comprehensive refertilization of lithospheric mantle beneath the North China Craton: further Os-Sr-Nd isotopic constraints. J Geol Soc 166:249–259

Zheng JP, Griffin WL, O'Reilly SY, Liou JG, Zhang RY, Lu FX (2005) Late mesozoic-eocene mantle replacement beneath the eastern North China craton: Evidence from the Paleozoic and Cenozoic peridotite xenoliths. Inter Geol Rev 47:457–472

Zheng JP, Griffin WL, O Reilly SY, Yu CM, Zhang HF, Pearson N, Zhang M (2007) Mechanism and timing of lithospheric modification and replacement beneath the eastern North China Craton: peridotitic xenoliths from the 100 Ma Fuxin basalts and a regional synthesis. Geochim Cosmochim Acta 71:5203–5225